N84-28089

# Advanced Gas Turbine

# AGT

# Technology Project

DOE/NASA/0168-7
NASA CR-174629
EDR 11577

## Seventh Semiannual Report
## For work performed from 1 January 1983-30 June 1983

Allison Gas Turbine Division
General Motors Corporation
Indianapolis, Indiana 46206-0420

June 1984

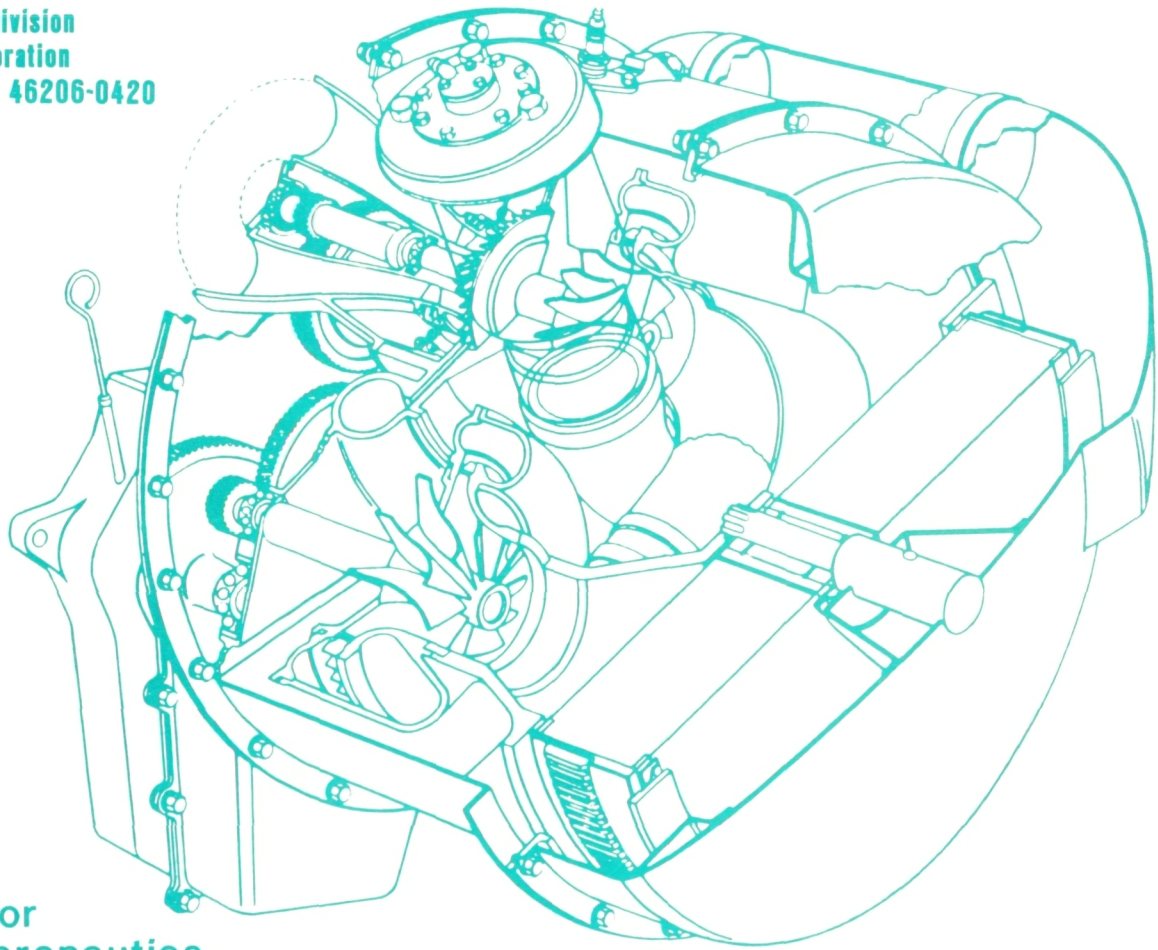

Prepared for
National Aeronautics
and Space Administration
Lewis Research Center
Cleveland, Ohio 44135
Contract DEN 3-168

For U.S. Department of Energy
Conservation and Renewable Energy
Office of Vehicle and Engine Research and Development

## NOTICE

DOE/NASA/0168-7
NASA CR-174629
EDR 11577

# Advanced Gas Turbine
# AGT
# Technology Project

## Seventh Semiannual Report
## For work performed from
## 1 January 1983-30 June 1983

Allison Gas Turbine Division
General Motors Corporation
Indianapolis, Indiana 46206-0420

**June 1984**

Prepared for
NATIONAL AERONAUTICS AND SPACE ADMINISTRATION
Lewis Research Center
Under Contract DEN 3-168

for
U. S. Department of Energy
Conservation and Renewable Energy
Office of Vehicle and Engine Research and Development

# FOREWORD

This report presents a technical summary of the Allison Gas Turbine project to develop an automotive gas turbine power-train system under NASA Contract DEN 3-168 (Department of Energy funding). The report covers the 6-month period 1 January 1983 through 30 June 1983.

The basic objective of this project is to develop and demonstrate, by November 1986, an advanced automotive gas turbine that will, when installed in a 1985 Pontiac Phoenix vehicle of 1360 kg (3000 lbm) inertia weight, achieve a fuel economy of 18.1 km/L (42.5 mpg), meet or exceed the 1985 emission requirements, and have alternate fuel capability.

Several General Motors Divisions and other companies are major contributors to this effort. They are as follows: Pontiac Motor Division—vehicle and cost studies, Delco Remy Division—starter/boost motor, Corning Glass Works—regenerator, and The Carborundum Company and GTE—ceramics.

The Allison Program Manager for the AGT 100 is H. E. (Gene) Helms; design effort is directed by Leonard Lindgren; materials effort is directed by Dr. Peter Heitman; and project effort is directed by Richard Johnson. The Pontiac effort is headed by Leighton Smith. The NASA AGT 100 Project Manager is Paul T. Kerwin.

# TABLE OF CONTENTS



*No activity this period

# TABLE OF CONTENTS (cont)



*No activity this period

# LIST OF ILLUSTRATIONS

# LIST OF ILLUSTRATIONS (cont)

# LIST OF TABLES

# SUMMARY


## ENGINE DEVELOPMENT

The goal of the first year of engine testing was to accomplish engine familiarization and shakedown of mechanical systems and to reach design speed (100%, 86,000 rpm). This reporting period completes the first year of engine testing, in which these goals were accomplished. Familiarization and shakedown were begun during the previous period when five engine buildups were evaluated and 2 hr 45 min of engine testing was completed.

During the current period, three engine buildups (6, 7, and 8) were evaluated, and 6 hr 13 min of engine testing was accomplished. Total test time on the engine stands at 8 hr 58 min. Builds 6 and 7 were operated at maximum gasifier rotor speeds of 70% and 90%, respectively, and were followed by planned inspections to determine parts condition and hot running clearance. Build 8 accumulated 3 hr 21 min of test time, culminating with successful operation at 100% gasifier rotor speed.

Engine testing was accomplished with realistic heat-up rates and with a 1080°C (1976°F) steady-state limit on turbine inlet temperature. Ceramic components included the combustor (silicon carbide), regenerator disk (aluminum silicate) and bulkhead (lithium aluminum silicate), and zirconia insulators and spacers. An improved method of retaining (holding down) the turbine scroll assemblies was successfully tested. The control system was modified, and successfully tested, to add automatic limiting of measured turbine inlet temperature and automatic scheduling of combustor variable geometry (BVG).

Teardown inspection of the last test indicated that design modifications were required to improve retention of the carbon ring seals used on the two turbine rotor shafts and also to improve the combustor-to-scroll interface system. These design modifications and parts fabrication have been completed.

## COMPONENT DEVELOPMENT

A special engine test indicated that compressor inlet temperature was higher than ambient by approximately 2.8°C (5°F). Methods of eliminating this inlet heating are being studied.

Analysis indicated that the gasifier turbine efficiency shortfall (versus RPD goal) was due to vane loss. A new vane design was defined that incorporates thinned trailing edge, cambered airfoil with reduced downstream turning, and increased vane width. Analysis also indicated that the power turbine, although meeting the RPD efficiency goal, is not optimally matched to the present 1080°C (1976°F) experimental engine. Reducing its flow capacity and operating rpm provides a significant efficiency at the engine operating point.

Combustor development addressed the isopressed silicon-carbide (SiC) dome that had previously cracked during hot proof-tests conducted on the combustor rig. A design modification was translated into parts that successfully completed not only rig proof-tests but also engine testing.

Regenerator development was active in several areas. Highlights of rig testing included evaluation of ceramic disks with low through-wall leakage, the implementation of various seal improvements (that collectively allowed meeting the experimental engine regenerator leakage goal), and initial testing of a silicone outboard seal.

## CERAMIC MATERIALS DEVELOPMENT

Rotor attachment/thermal barrier development continued at Carborundum Company (CBO) with mullite and at Allison with zircon. Mullite development focused on microstructure consistency and shrinkage variability. Zircon development focused on scaling up the powder process and characterizing microstructures.

Rotor development was conducted at CBO (SiC) and GTE (silicon nitride [$Si_3N_4$]). The CBO effort concentrated on developing the injection-molding process and parameters. Significant quantities of rotors were molded and are in process. Allison spin-tested eight SiC rotors. GTE continued molding experiments, and Allison spin-tested nine $Si_3N_4$ rotors.

CBO produced and delivered four SiC combustors. CBO also continued to identify and apply improvements to fabrication of the gasifier scroll assembly. Areas covered include powder, slurry mixture, and mold design.

# INTRODUCTION

This is one of a series of semiannual reports documenting work performed on an Advanced Gas Turbine (AGT) Technology Development Project for automotive applications. The work is being conducted by Allison Gas Turbine Operations of General Motors Corporation under NASA/DOE contract DEN-168.

The objectives of the project, as highlighted in Table I, are to develop an experimental power-train system that demonstrates the following: (1) the potential of a combined cycle fuel economy of 18.1 km/L (42.5 mpg) using diesel fuel No. 2 in a 1985 Pontiac Phoenix of 1361 kg (3000 lbm) weight on a 15°C (59°F) day; (2) emission levels less than federal standards; and (3) the ability to use a variety of fuels. It is intended that the technology demonstrated through this project would assist the automotive industry in making a go/no-go decision regarding the production engineering development of gas turbine power trains.

In meeting the project objectives, the engine will be designed to accomplish the following, also outlined in Table I: (1) achieve reliability and life comparable to conventional 1985 vehicles; (2) achieve initial and life-cycle power-train costs competitive with 1985 power trains; (3) demonstrate vehicle acceleration suitable for safety and maneuverability; and (4) meet 1985 federal vehicle noise and safety standards.

Initially, the project scope included the fabrication and chassis dynamometer testing of the engine, transmission, and electronic control system installed in a 1985 Pontiac Phoenix passenger car. However, Government funding constraints after the first year made it necessary to reduce program scope. Activities eliminated included fabrication and testing of the transmission and vehicle. The electronic control scope was narrowed from that of controlling the engine, transmission, and vehicle to controlling an engine on a dynamometer. Figure 1 depicts the activity areas and schedule for the revised project.

**Table I.**
**AGT 100 project and design objectives.**

| Project objectives | System design objectives |
|---|---|
| 18.1 kg/L (42.5 mpg) in 1985 Pontiac Phoenix | Comparable reliability and life |
| Alternate fuels capability | Competitive initial and life-cycle costs |
| Compliance with 1985 emission standards | Competitive accelerations |
| | Compliance with noise/safety standards |

The AGT 100 design has been matched to the Pontiac Phoenix X-body car, shown in Figure 2. A front-wheel drive car, the Phoenix represents the current generation of advanced passenger cars, emphasizing efficiency of space and weight to combine comfort and function with high fuel economy. The AGT 100 will also fit into the Pontiac A6000, an A-body car that is slightly larger than the Phoenix and is the latest GM front-wheel design with potential to replace the X-body car in the Pontiac future marketing of cars.

The AGT 100, shown in Figures 3 and 4, is a two-shaft, regenerative gas turbine engine. In all respects, this engine design is tailored for high-volume application to fuel-efficient passenger cars. Its two-shaft configuration allows (1) the use of conventional transmissions, manual or automatic, and (2) turbine tip speeds (approximately 502.9 m/s [1650 ft/sec]) commensurate with available ceramic material properties (strength and variability). Single-shaft configurations were rejected by Allison because of the corresponding requirement for a continuously variable transmission and for approximately 40% higher turbine rotor ceramic material strength (for equal reliability).

Careful attention was given to component arrangement for both vehicle installation and management of potentially high heat losses. All hot-section components are grouped together, bounded on one end by the regenerator, on the other end by the gearbox, and enclosed by a well-insulated cylindrical case. High-cycle temperature is possible through the use of ceramic hot-section parts. This, coupled with high aerodynamic component efficiencies, produces low fuel consumption and a 50% improvement in composite miles per gallon (30% energy efficiency improvement) in a Pontiac Phoenix. Most importantly, the AGT 100 uses existing technologies for shafts, bearings, cases, control system, accessories, etc, and thereby provides a reliable test device for evaluating ceramic and aerodynamic components.

The main development challenges in the program are in building small, high-performance gas turbine components and developing ceramic components for the required high engine cycle tempera-

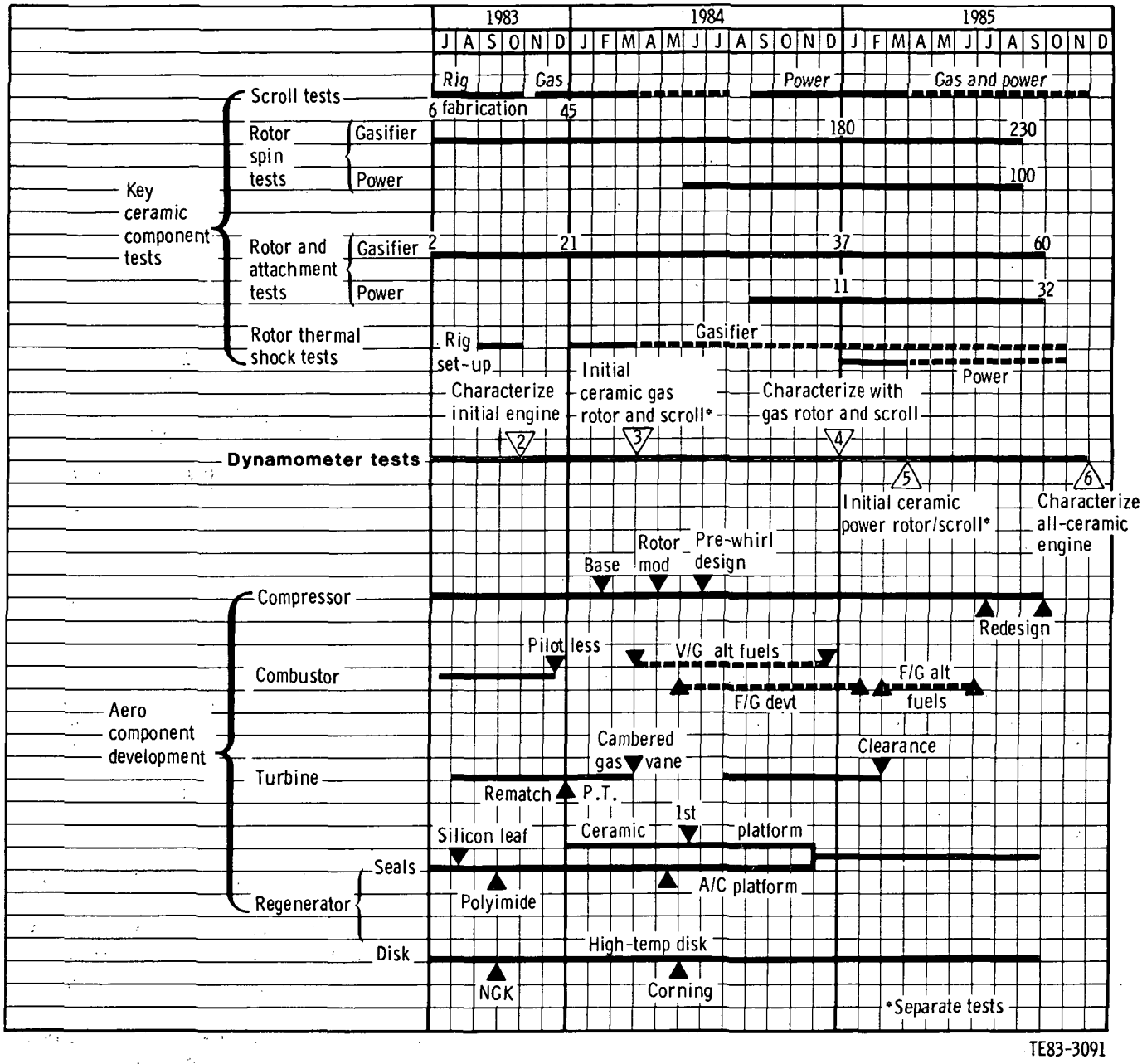


**Figure 1. AGT 100 project plan.**

tures that are price competitive and can be produced in an automotive production environment. The AGT 100 ceramic components are shown in Figure 5.

Because of the small-size engine (0.34 kg/s [0.76 lbm/sec] airflow), extensive rig testing, outlined in Table II, is being performed in component development. A major ceramic component development program is being pursued, and the ultimate success of the engine depends on the success of this activity.

Mechanical development of the engine is being conducted in two essential phases. The first incorporates early available ceramic components with metal substitutes for those components requiring further ceramics development. This phase includes metal turbine rotors and engine operation at 1079°C (1975°F) turbine inlet temperature. The second phase includes engine demonstration of all ceramic components at 1288°C (2350°F) turbine inlet tem-

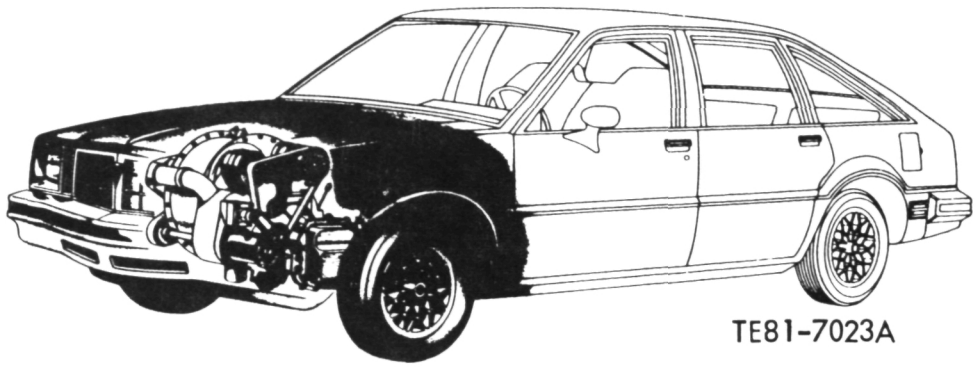


**Figure 2. AGT 100 engine in 1985 Pontiac Phoenix.**

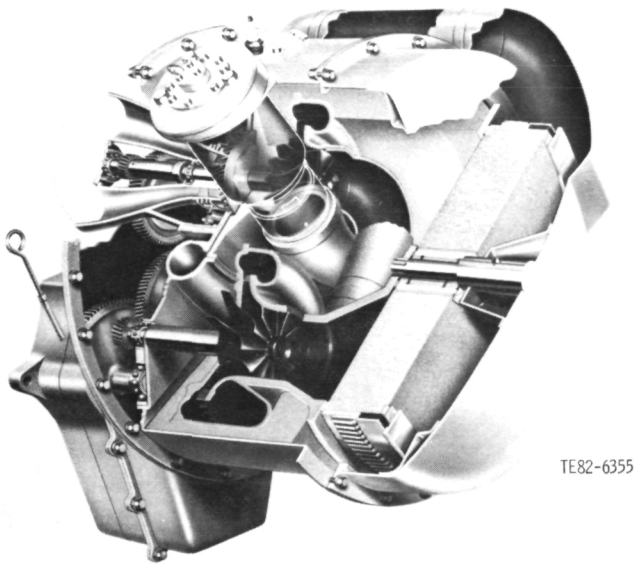


**Figure 3. AGT 100 advanced gas turbine engine.**

**Table II.**
**Aerodynamic component rigs.**

| Component | Builds | Hours |
|---|---|---|
| Compressor | 5 | 286 |
| Combustor | 10 | 153 |
| Turbines | | |
| Gasifier | 2 | 204 |
| Power | 1 | 26 |
| Interturbine duct | 3 | 239 |
| Regenerator | | |
| Cold side flow distribution | 8 | 110 |
| Hot side flow distribution | 1 | 72 |
| Seal leaf leakage | 5 | 55 |
| Hot simulator rig | 3 | 335 |
| Ceramic seal platform | Four units | 30 |
| | | 1510 |

perature. The transition from the first to second phase will occur in steps as the ceramic components become available.

A team concept is used in this project, with many of the team members being General Motors divisions. Allison is the prime contractor and team leader with responsibility for the overall power train and controls. Pontiac Motor Division (PMD) has vehicle design and cost analysis responsibility, and Delco Remy will develop the starter/boost system for the engine. The primary non-GM groups on the team are Carborundum Co. (CBO), Corning Glass Works (CGW), and GTE Laboratories, Inc., who are involved in the ceramic effort.

This report is structured on a component basis (e.g., all work relating to the gasifier turbine rotor, including rig work and ceramic rotor development, is discussed as a part of the gasifier turbine section). Exceptions to this are functional areas that are not peculiar to any one major component: engine subsystems, cover structures, gearbox and power transfer, rotor bearings, shafts/seals, and secondary flow. There are separate sections for materials development and controls development.

Certain sections are omitted in this report because no effort was expended in those areas. These sections are identified in the Table of Contents to preserve continuity.

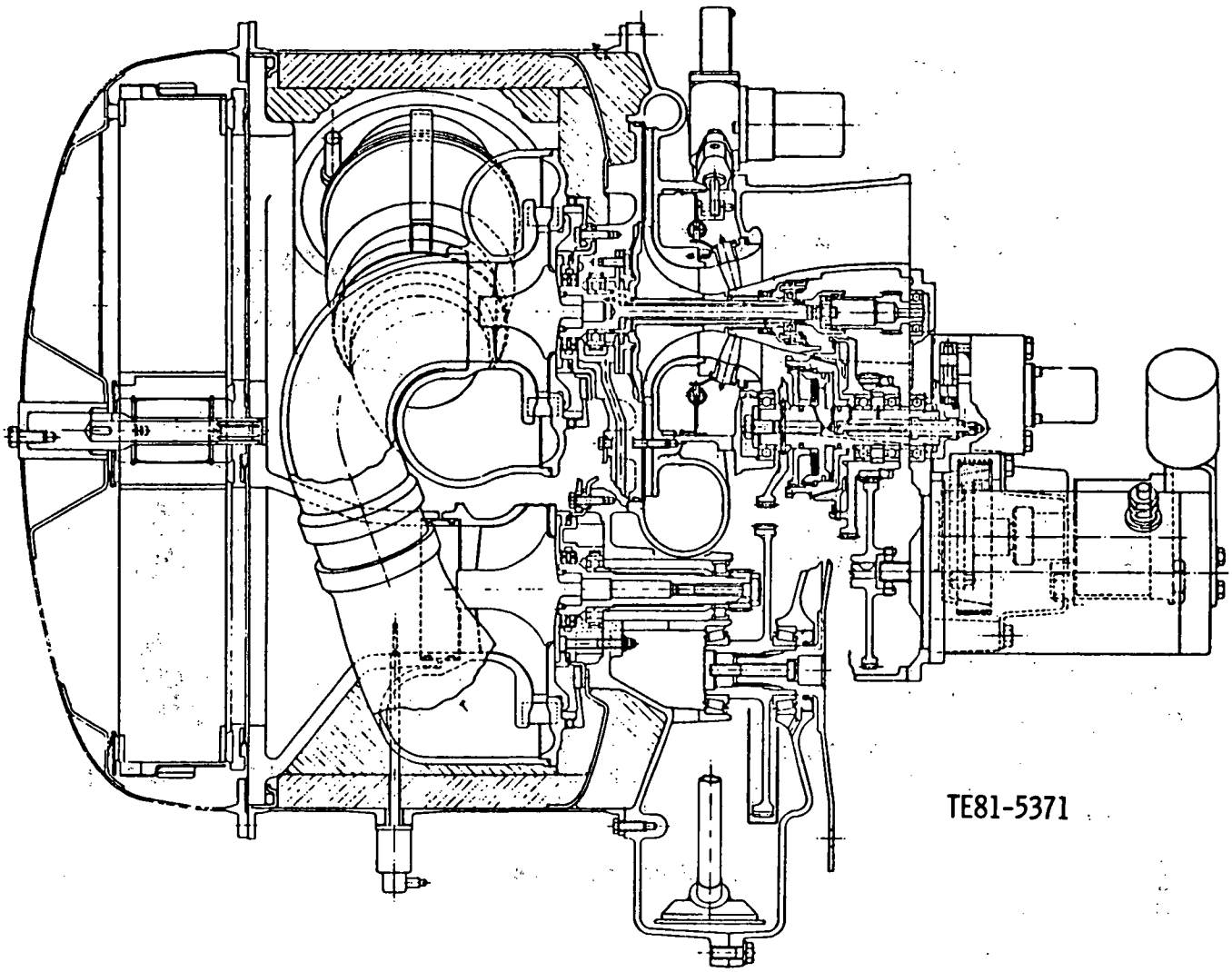


**Figure 4. Cross section of AGT 100 gas turbine engine.**

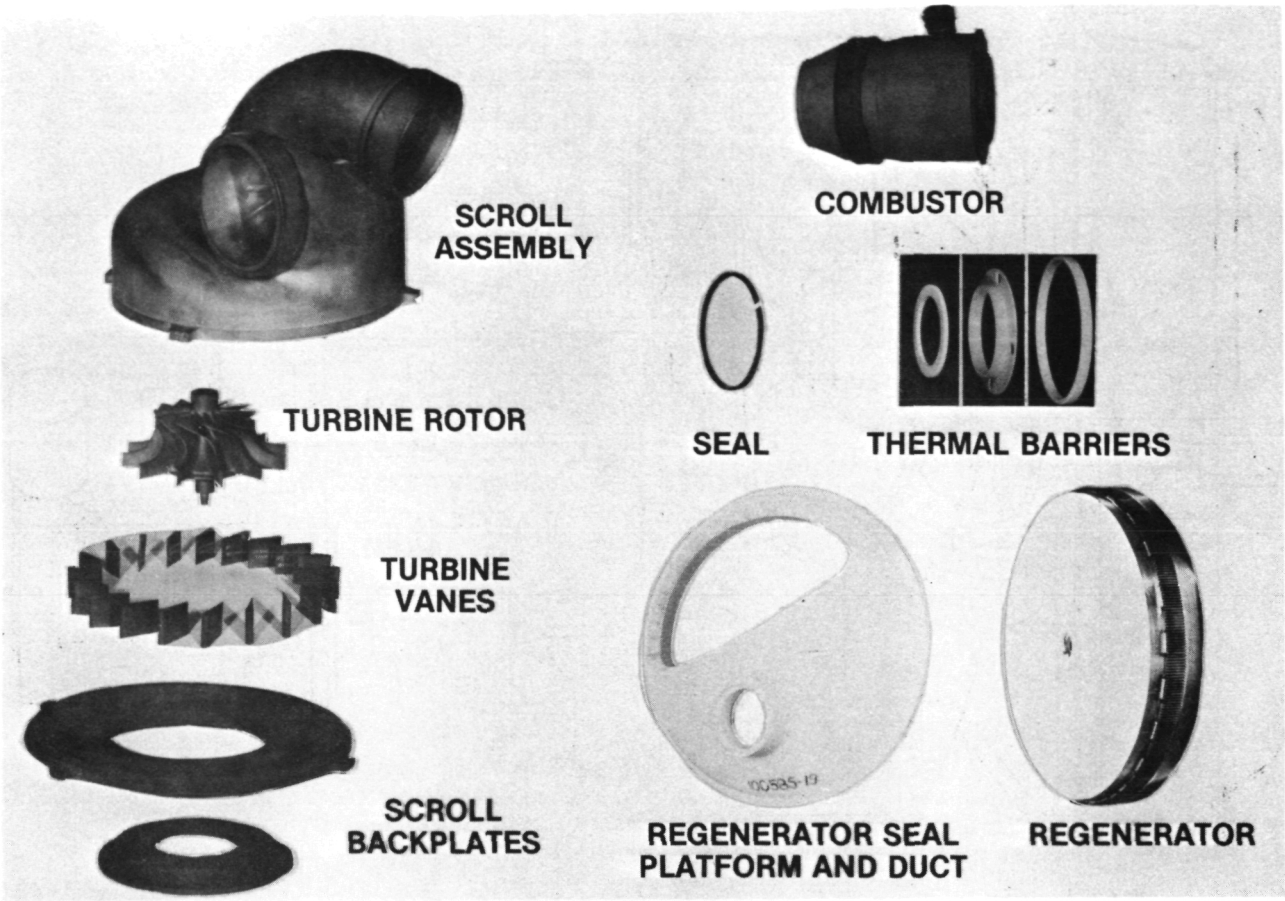


Figure 5. AGT 100 ceramic components.

# II. ENGINE DEVELOPMENT

The goal of experimental engine development in the first year of dynamometer testing was engine familiarization and shakedown of mechanical systems. This goal supports the establishment of the AGT 100 engine as a credible machine for evaluation of ceramic components and for identification of engine interaction of components. This process will yield early identification of engine-related mechanical and aerodynamic problems, define component performance to compare with rig results, suggest development emphasis for future rig work, identify engine-related ceramic component problems or improvements required, and demonstrate control system and instrumentation adequacy.

One engine was initially obtained to accomplish normal shakedown activity. This allowed a minimum of parts rework and was compatible with project funding. Most of the parts for a second engine were obtained with the initial engine, but many of them were not finish-machined until initial engine running revealed the important clearances and adjustments that needed to be made to geometries, lubrication, and instrumentation systems and until other normal engine shakedown development revealed further adjustments required. The goal of the experimental engine testing was to achieve 100% speed and 1080°C (1976°F) operating temperature by the end of the first year of testing, while demonstrating initial ceramic components.

Each experimental AGT 100 engine has been serialized. The first was designated S/N-1 and the second S/N-2. In this report, each assembly of an engine is referred to as a build or buildup (BU), and each subsequent disassembly is referred to as a teardown (TD). For example, the eighth assembly is BU8, and, when testing is completed, the corresponding teardown is TD8. A teardown is defined as having occurred when a major splitline of the engine is broken.

## 2.2 EXPERIMENTAL ENGINE

### Fabrication

Principal efforts during the first half of 1983 consisted of fabrication of the following items:

- redesigning of scroll supports and regenerator drive system
- reworking of components for engine S/N-2 to incorporate latest changes and instrumentation
- continuing development of ceramic processes and machining of a ceramic gasifier scroll

The scroll supports were redesigned to eliminate deflections occurring during engine transients. These parts were fabricated for both engines.

The regenerator drive was redesigned after bench testing of the gear train resulted in failure of the flexible ring gear in the harmonic drive system. The redesigned system incorporated a plan-o-centric gear drive that was successfully bench tested and incorporated in BU9 of engine S/N-1.

Components for engine S/N-2 were initially fabricated at the same time as the parts for engine S/N-1. However, since S/N-2 was not to be run until approximately one year after S/N-1, parts affecting flow capacity were left with machining stock to provide rematching capability. In addition, design changes to S/N-1 hardware were not incorporated into S/N-2 hardware, pending test results from S/N-1. All required reworks for S/N-2 (i.e., capacity, design changes, and instrumentation) were defined during February, and fabrication was completed in May. Additional changes defined from further S/N-1 testing were incorporated in June and July.

### Experimental Engine Testing

Assembly of the first engine was completed in July 1982. This first buildup was then installed on a motoring dynamometer test stand, and testing was initiated shortly thereafter. By December 1982, five buildups had been evaluated, as described in the sixth AGT semiannual report. Total accumulated engine running time through CY 1982 was 2 hr 45 min.

During the current reporting period, significant engine testing accomplishments were recorded. Three buildups (6, 7, and 8) were evaluated. Engine operating time for the period was 6 hr 13 min, bringing the total accumulated operating time to 8 hr 58 min. BU6 and BU7 achieved 70% and 90% gasifier speed, respectively. Teardowns 6 and 7 were scheduled so that turbine inspections could be performed as higher rotor speeds were reached. All previous teardowns had been mandated by some type of problem. BU8 was operated for 3 hr 21 min, culminating with successful operation to 100% gasifier speed for the first time on 7 June 1984.

**Engine BU6 and Test.** Buildup 6 of engine S/N-1 contained several important changes. These changes included an improved method for prevent-

ing unseating and cocking of turbine scrolls, zirconia coating of certain parts, changes in build clearance and turbine flow area, resizing of bulkhead coupling and piston ring, electronic control improvements, and the addition of a continuous-duty hydraulic starter. These changes are explained in more detail in the following paragraphs.

Redesigned parts were introduced in the seal area behind both turbines. These changes were made to produce increased air hold-down loads on the turbine scrolls and thus to prevent them from unseating and cocking. This approach is superior to earlier changes, which depended on high spring pressure. The turbine backplates were coated with zirconia for heat insulation. This coating was expected to reduce the thermal distortion of these parts during transient operation. The gasifier turbine shroud was coated with an abradable material, and assembly clearance was reduced between the gasifier turbine shroud, rotor, and backplate. The gasifier turbine flow area was reduced by 7% to decrease the steady-state turbine inlet temperature (TIT). No changes were made to the power turbine flow area or clearance.

The piston ring and coupling, which mate with the ceramic bulkhead, were reduced in diameter to accommodate the large difference in thermal expansion between the bulkhead, coupling, and piston ring. This was done to correct the cause of cracking a bulkhead in BU5. The electronic control was modified to accept a measurement of gasifier TIT and reprogrammed to limit TIT to a scheduled value. These control changes were made to more fully exploit the established temperature limit of the experimental engine (1080°C [1976°F]).

A continuous duty hydraulic motor was adapted to be used as a test equipment starter. This new starter provided increased time for the experimental engine to become self-sustaining. It also provided the flexibility of operating at any desired level of TIT without having to engage the power transfer clutch. The hydraulic motor drives through an overrunning clutch into the starter gear train, thus permitting the engine to overrun (i.e., operate independently from) the hydraulic motor.

Operationally, the engine was motored by the starter to a selected value of gasifier speed. Electronically controlled combustor light-off was then manually initiated. The engine accelerated, again electronically controlled, until the pre-set value of idle speed was reached. The electronic control then regulated fuel to that value required to maintain the selected gasifier speed. The flow rate of fuel (i.e., the energy input) required depends on the level of starter assistance. Thus TIT is effectively controlled by varying the torque input from the hydraulic starter motor.

Testing of BU6 quickly demonstrated satisfactory starting and operation with the hydraulic starter. After thermal stabilization at 70% gasifier speed, the hydraulic motor was shut off. The engine self-sustained at 71% $N_1$ and 854°C (1570°F) TIT. During operation, oil pressure started to decrease and the engine was manually shut down. Oil level in the sump was very low. Leakage appeared to be coming from several places, but most of the missing oil was believed to have come out of the fill pipe in which a breather was located. The engine was designed with an oil/air separator as part of the lubrication circuit, located in the region in which the gearbox is vented to the compressor inlet. This circuit was intentionally disabled for early runs to minimize the possibility of oil injection into the engine flow path. The absence of the separator explained the excessive oil loss.

This build of the engine had accomplished its goal of verifying the hydraulic starter system and of achieving self-sustained engine operation. The engine was removed from the test stand for a hot-end inspection prior to testing at higher speeds. The teardown was limited to removal of the regenerator assembly, combustor, and turbine scrolls to inspect for rub and to check operating clearances. No problem was discovered, and clearances were deemed adequate for continued running. Running time accumulated on this build was 1 hr 15 min. Total running time on the engine to date was 4 hr.

**Engine BU7 and Test.** After the hot section inspection, the engine was reassembled with no change in engine parts. The oil leakage evident on the previous test was addressed by a test stand plumbing change; the oil captured at the test stand breather-bottle was pumped back into the engine oil sump.

BU7 testing was scheduled to obtain data up to an intermediate gasifier speed of 90%. The engine was started by using the hydraulic motor for cranking. The motor was disconnected at 70% $N_1$ and the engine self-sustained. Testing was then accomplished at 60% and 70% $N_1$ speeds with the power turbine at 20% speed. The power turbine was increased in speed to 50% with the gasifier at 70%. The test sequence continued with operation at 80% gasifier and 20%, 40%, and 80% power turbine speeds. Final test operation was at 90% on both gasifier and power turbine speeds. This operation met the objectives of BU7, and a planned teardown

for inspection was implemented. Running time obtained on BU7 was 1 hr 37 min. Total engine running time accumulated was 5 hr 37 min.

Teardown inspection identified a cracked ceramic combustor body. Failure analysis of that body revealed a previously undetected flaw in the crack. The crack was "very tight" and thus had not been detected by borescope inspections conducted throughout engine testing. It is possible that builds previous to BU7 had operated with the combustor body cracked.

The power turbine shaft carbon ring seal showed oil coking, and other evidence indicated that oil had leaked into the turbine flow path. Data review revealed that no pressurizing air was available to the seal. Inspection of the power turbine support identified the misalignment of a connecting hole that supplies air pressure to the seal. The carbon ring seal at the gasifier turbine bearing location was also found cracked.

**Engine BU8 and Test.** Analysis of previous engine operation combined with physical evidence at engine teardown (TD7) and from subsequent inspection generated the following changes in the engine configuration for BU8:

- The ceramic combustor body was replaced.
- All carbon ring seals were replaced, and alignment of the seal air supply hole was corrected.
- Oil flow to the gasifier turbine bearing was increased to increase cooling.
- The vanes of the compressor impeller were thinned to increase high-speed airflow, as previously demonstrated on the compressor rig.
- Build clearances of both turbines were decreased.

Diagnostic instrumentation was added to the engine as follows:

- Thermocouples were added at the impeller inlet to investigate possible heating of the engine airflow before the airflow's entrance into the compressor.
- Pressure and temperature probes were added at the power turbine inlet, and pressure probes were added at the exit.
- A proximity pickup was added at the gasifier shaft to determine axial thrust direction during operation.

In an effort to keep the combustor cooler during operation using the start nozzle, the burner variable geometry (BVG) position and scheduling were modified to provide more air to the primary zone. A reduction in primary zone bulk temperature and burner outlet temperature was expected to minimize thermal stresses and reduce cracking potential.

The BVG movement was, for the first time, placed under the control of the electronic control unit (ECU). For starting, the BVG was scheduled to move to a less fuel-rich primary zone position immediately after ignition. Burner outlet temperature was automatically limited to 843°C (1550°F) by ECU authority. For the light-off regime (i.e., ignition), the BVG was positioned to obtain no more than 1649°C (3000°F) calculated bulk temperature in the primary zone.

With these parameters assigned, difficulties in starting BU8 were encountered. Control-to-engine interaction produced cycling, which led to automatic shutdowns at the 843°C (1550°F) limit. Several different adjustments were made to the control system, and the rate of manually applying the hydraulic starter torque was changed. Selection of a BVG position that produced a calculated primary zone temperature of 1982°C (3600°F) at light-off was required.

The first successful start was followed by a brief run to achieve a burner inlet temperature of 538°C (1000°F). Once this condition was reached, the engine was shut down to permit a borescope inspection of the ceramic combustor body. No problems were found.

Testing continued with the overall goal of obtaining performance data throughout the speed range—including 100% gasifier speed. Data were obtained by automatic recording from fire-up through 100% speed on the gasifier shaft. Thermal stability was achieved at speeds of (% $N_1$/% $N_2$) 67/20, 92/20, and 94/89. Data taken at 100% speed on the gasifier shaft with 90% speed on the power shaft were considered thermally stabilized, although the engine was shut down prematurely by a test stand safety device triggered by an erroneous exhaust gas temperature signal. Figures 6 through 9 indicate the time history of rotor speed and TIT as the 100% (86,000 rpm) condition was achieved.

Borescope inspection of the gas path after operation at 100% speed disclosed that approximately one-third of the compliant layer, which separates the ceramic combustor body and gasifier turbine scroll, was dislodged and hanging in the gas path. The remaining compliant layer was removed before proceeding with the test program.

During the testing, oil smoke was observed at the engine, apparently associated with the vent in the compartment between the hot and cold engine sections. At the next start, a camera was used to monitor the vent. Smoke could be seen jetting from

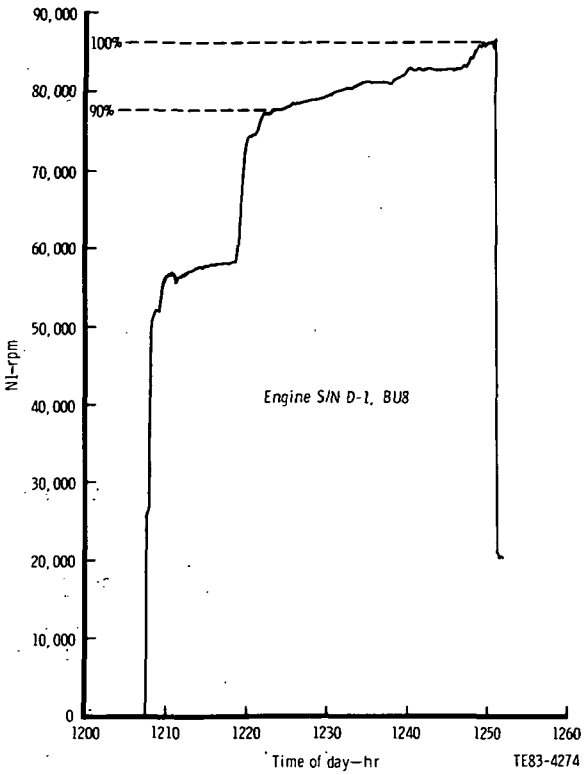


**Figure 6. Gasifier rotor speed, fire-up to 100% rpm.**

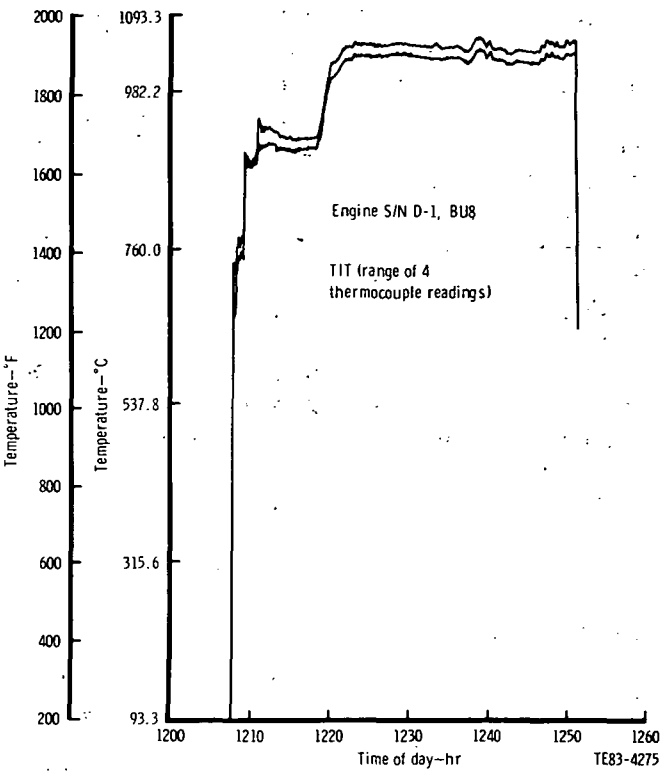


**Figure 7. Turbine inlet temperature, fire-up to 100% rpm.**

the vent, and the accumulation seemed to be heavier than previously observed. During an attempt to set the engine operating condition to 60% $N_1$, 50% $N_2$, to observe oil consumption, the engine speed decreased to eventual shutdown. While engine rpm was decaying after shutdown, a rapid rise in turbine outlet temperature indicated an apparent gas-path fire downstream of the power turbine. The engine was removed from the test stand for inspection. Test time obtained on BU8 was 3 hr 21 min. Total time on the engine was 8 hr 58 min.

Disassembly disclosed these conditions:

- failed carbon ring seals at the gasifier and power turbine locations (Both seal housings were also loose in their locations; a press fit is considered normal.)
- oil leakage from the gasifier turbine bearing cavity via a cracked instrumentation tube (This condition was judged to be the source of the smoke from the vent cavity.)
- chipped areas on the ceramic combustor body surface that butts against the gasifier scroll (This condition was caused by the absence of a separating compliant layer.)
- worn areas on the combustor body in the dilution band area (Inadequate clearance between the body and band was judged to explain the condition.)
- gasifier turbine rotor blade tips with minor damage from the ceramic combustor chips (The rotor was reusable.)

**Engine BU9 Preparation.** At the end of this reporting period, design modification and parts rework were being pursued to correct the problems found in TD8. New retention methods were designed for the carbon ring seals of both turbines. Increased radial clearance between the seals and turbine shafts was also deemed necessary. The combustor-to-scroll interface was redesigned to incorporate positive retention of the compliant material. All required parts fabrication is complete.

Additional preparation for BU9 includes proof-testing of a new combustor, resizing of combustor primary and dilution rings to reduce binding potential, reduced build clearances of compressor and power turbine, and higher compression of the compressor discharge O-ring seal.

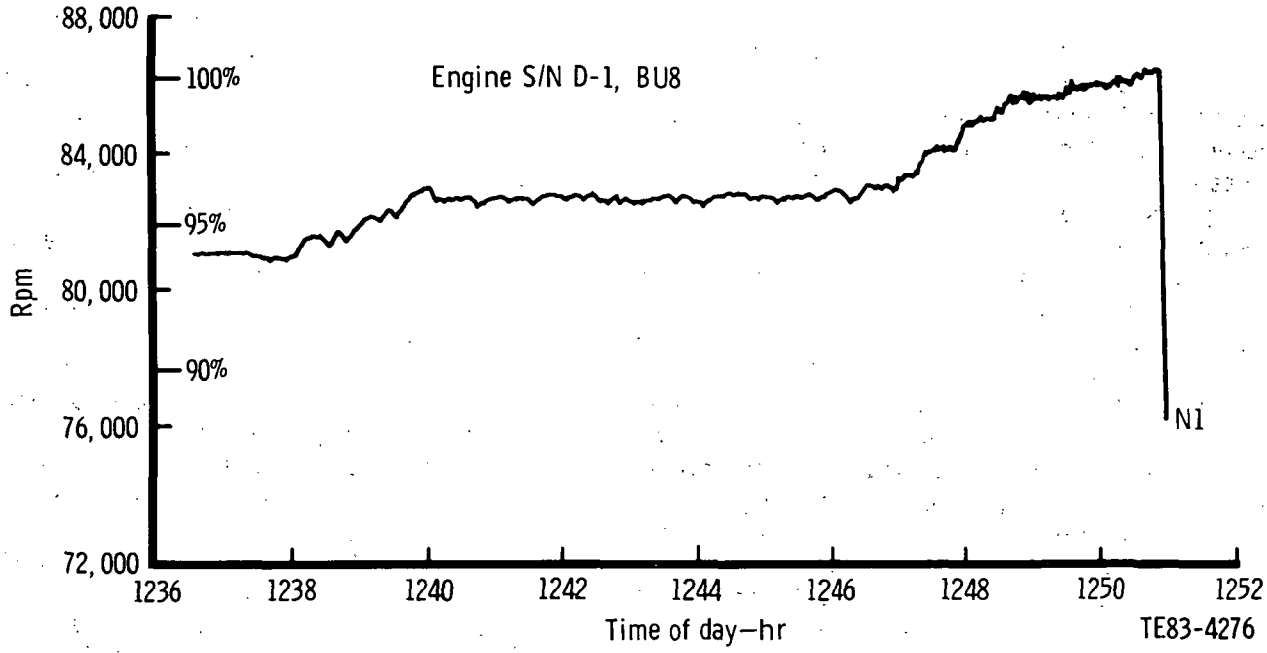


**Figure 8. Gasifier rotor speed, 94% to 100% rpm.**

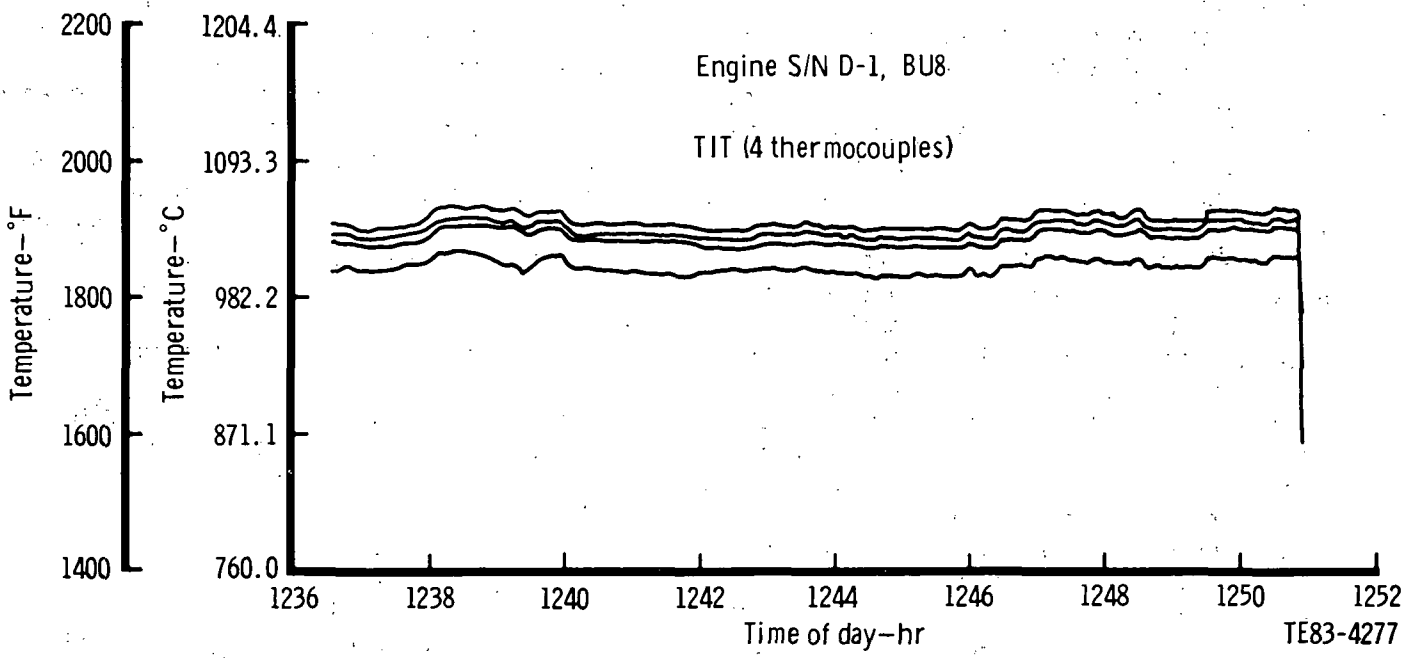


**Figure 9. Turbine inlet temperature, 94% to 100% rpm.**

## Performance Analysis

Performance testing during the reporting period was conducted on engine BU5 through BU8. This subsection discusses the performance characteristics measured and the analyses performed on the data.

Build 5 operation did not achieve self-sustaining status; therefore, stabilized data were not achieved and meaningful analysis could not be performed.

Engines BU6 through BU8 were equipped with a hydraulic starter capable of continuous operation.

Stabilized data were obtained for each of the three builds. Build 6 data were obtained at closed (40 deg) compressor inlet guide vane (IGV) setting, and BU7 data were obtained at open (0 deg) IGV setting. In BU8, the IGVs were replaced with temperature rakes to determine the magnitude of inlet air heating between the airflow measurement station and the compressor inlet. Build 8 data indicated inlet air heating of approximately 2.8°C (5°F).

Figure 10 shows corrected airflow and compressor pressure ratio data from engine BU5 through BU8 overplotted on the compressor performance map from compressor rig BU3. Figure 11 compares the corrected airflow with corrected speed characteristics of the engine and compressor rig. Engine test data points near the operating line (shown in Figure 10) are represented in Figure 11 by symbols. The rig is represented by lines. The comparison indicates that the engine flow is less than rig flow at constant speed by approximately 9% at open (0 deg) IGV setting and 6% at closed (40 deg reset) IGV setting. These flow reductions are attributed to running clearance and component dimensional differences between the rig and engine compressors.

Evaluation of BU6 data was inconclusive due to the low levels of achieved gasifier speed. This, in turn, caused the power turbine to operate at extremely low expansion ratio, a region in which the power turbine flow capacity and efficiency are highly sensitive to small changes of expansion ratio.

The test data of BU7 exhibited a high compressor operating line (Figure 10) at gasifier speeds greater than 70%. The subsequent engine teardown revealed that the cause was blockage of the gasifier turbine nozzles (vanes). The blockage was caused by the compliant layer, which is installed between the combustor and turbine scroll. A portion of this layer, a woven cloth of ceramic fibers, came loose and entered the primary flow path. It then was stopped by the gasifier turbine vane row and became a flow blockage. The resulting effect on turbine performance, beyond the obvious flow reduction, was unknown, and further data analysis was considered inconclusive.

A performance computer model was used to evaluate the data from testing engine BU8. The basic procedure followed will be briefly mentioned and followed by a discussion of the analysis results.

The computer model is one that determines overall engine performance based on the characteristics of all the engine components. Examples of characteristics used are compressor and turbine maps, leakage and secondary airflows, pressure drops, bearing loss, mechanical loss, heat rejection, etc. Through an iterative process, the computer matches a given set of component characteristics to determine the engine operating point and performance level. The term match is used to denote that airflow, rotor speed, and shaft work of the various components are appropriately matched.

The basic configuration of the performance computer model represents the 1080°C (1976°F) experimental engine goal performance. (The computer model was used to obtain the "Experimental adjusted goal" column of Table III.) Features of this basic model can be used to arrive at a modified model, which better matches test data (i.e., better than the goal model). Any of the component performance submodels can be modified or scaled, e.g., efficiency lowered, airflow scaled, etc. By combining mathematical technique and engineering experience, the basic model is transformed into an adjusted model that best fits the experimental engine data. The adjustments required to achieve the fit then describe the probable variance between the goal engine and the actual engine. The performance as calculated by the adjusted model is presented and compared with measured test data in Table IV. The adjusted model, which matches test data, was used to project experimental engine performance at maximum power and standard 29°C (85°F) day conditions, as shown in the "Adjusted model" column in Table III. This table also compares the projected BU8 maximum power with the experimental engine goal.

This comparison shows the major differences: engine BU8 had low airflow (-9%), high engine leakage (+5.4%), high mechanical loss (+9.5 kW [+12.8 hp]), and high heat rejection (+13.5 kW [+769 Btu/min]). The low airflow is a result of inlet air heating, compressor running clearance, and component dimensional differences between the rig and engine compressors. The leakage level is consistent with theoretical flow analysis of the experimental engine configurations and the seal clearances for engine BU8. The causes for high mechanical loss and high heat rejection will be investigated by analysis and further testing.

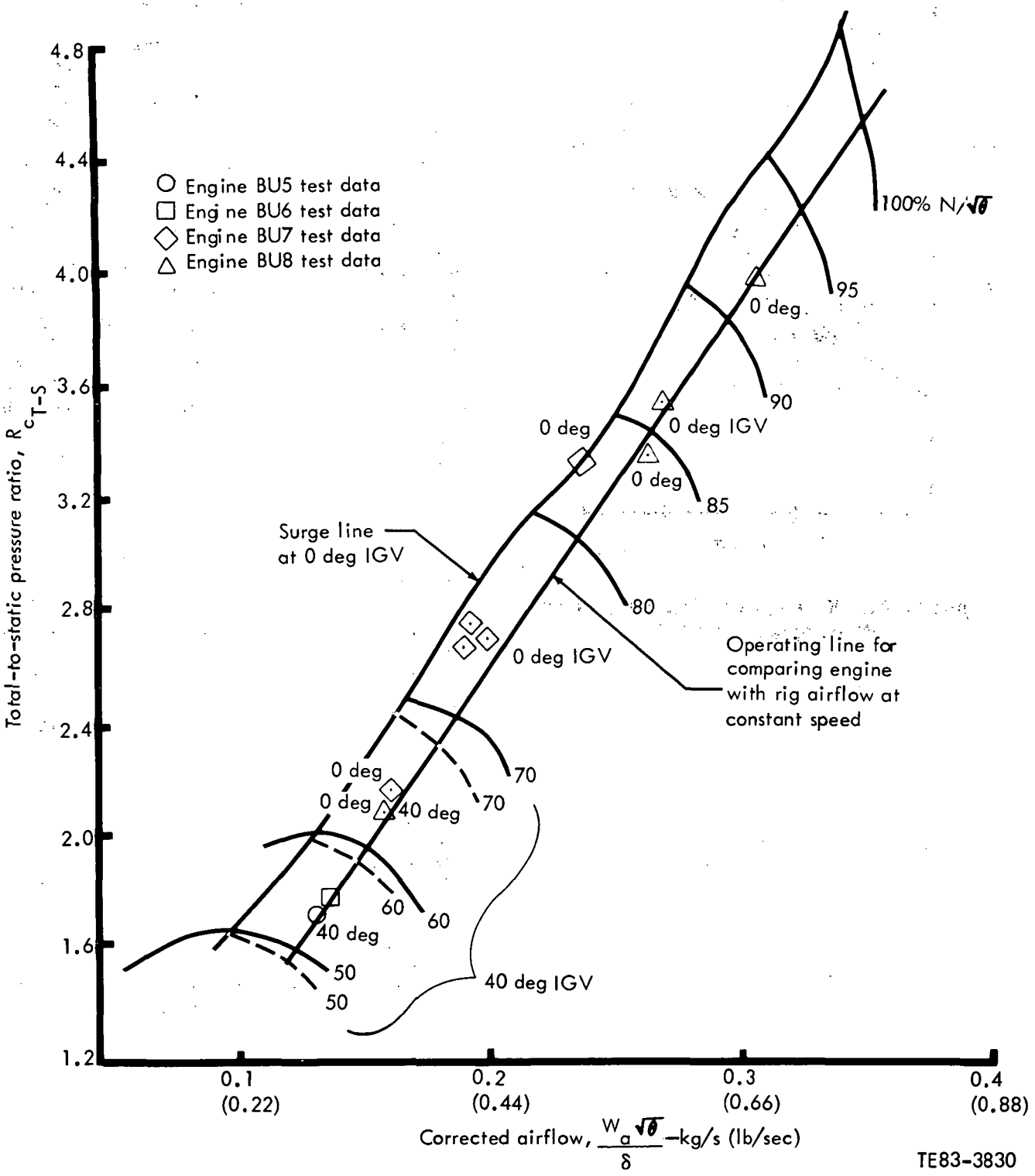


**Figure 10. AGT 100 rig and engine compressor performance.**

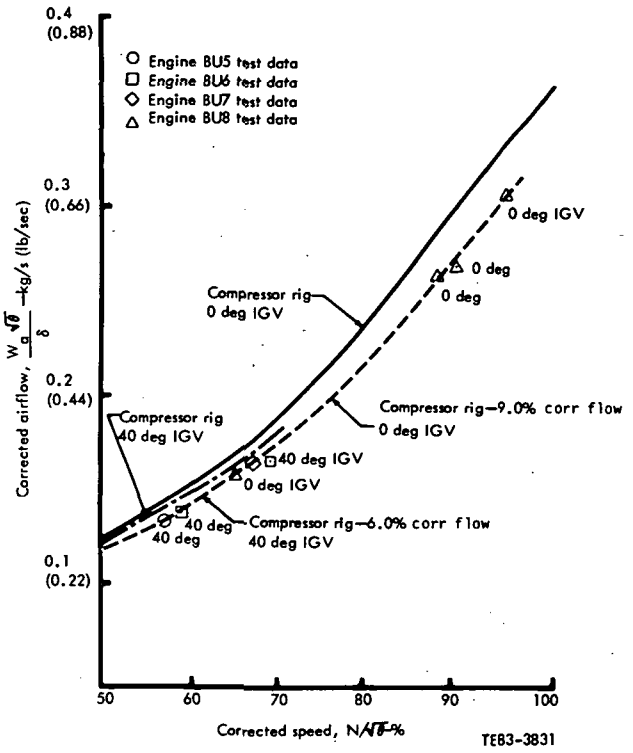


**Figure 11. AGT 100 engine airflow comparison with compressor rig BU3.**

**Table III.**
**AGT 100 S/N-1 performance analysis at rated condition.**

| | Experimental adjusted goal | Adjusted model |
|---|---|---|
| Record No.* | — | 11,163 |
| $T_1$—°C (°F) | 29.4 (85) | 29.4 (85) |
| $P_1$—kPa (psia) | 99.0 (14.36) | 97.9 (14.20) |
| $N_G$—% | 100 | 100 |
| $N_O$—% | 70*** | 70*** |
| $T_4$—°C (°F) | 1080 (1976) | 1080 (1976) |
| Dyne power—kW (hp) | 7.4 (50.1) | 24.0 (32.2) |
| Starter power—kW (hp) | 0 (0) | 5.9 (7.9) |
| $W_f$—kg/h (1b/hr) | 11.5 (25.4) | 10.3 (22.8) |
| $W_a$—kg/s (1lb/sec) | 0.328 (0.721) | 0.290 (0.639) |
| $R_c$ | 4.203 | 3.983 |
| $T_2$—°C (°F) | 232 (449) | 223 (434) |
| $T_5$—°C (°F) | 886 (1627) | 879 (1615) |
| $T_6$—°C (°F) | 777 (1431) | 784 (1444) |
| $\eta_c$—% | 74.8 | 75.0 |
| $\eta_{GT}$—% | 80.7 | 78.5 |
| $\eta_{PT}$—% | 88.1 | 86.2 |
| $\eta_{REGN}$—% | 91.7 | 92.4 |
| Engine leakage—% | 2.2 | 7.6 |
| Regenerator leakage—% | 6.8 | 6.6 |
| Mechanical loss—kW (hp) | 3.9 (5.2) | 13.4 (18.0) |
| Heat rejection—kW (Btu/min) | 2.2 (124) | 15.7 (893) |
| Rig to engine | | |
| $\Delta\eta_c$—% | 0 | − 1.2 |
| $\Delta\eta_{GT}$—% | − 2.2 | 0** |
| $\Delta\eta_{PT}$—% | − 1.2 | 0** |
| $\Delta\eta_{REGN}$—% | 0 | 0 |
| ΔGasifier turbine flow—% | − 15.8 | − 1.3** |
| ΔPower turbine flow—% | + 18.9 | + 4.4** |

*Engine build math model record No. projected to max power

**Engine relative to BU8 estimated maps

***Optimum output speed for max power

**Table IV.**
**AGT 100 S/N-1 BU8 performance analysis.**

| | Observed data | Adjusted math model | Observed data | Adjusted math model |
|---|---|---|---|---|
| Record No. | 11,163 | 11,163 | 12,788 | 12,788 |
| $T_1$—°C (°F) | 34.2 (93.6) | 34.2 (93.6) | 34.6 (94.3) | 34.6 (94.3) |
| $P_1$—kPa (psia) | 97.2 (14.10) | 97.2 (14.10) | 96.9 (14.05) | 97.1 (14.09) |
| $N_G$—% | 93.9 | 93.9 | 100.1 | 100.1 |
| $N_O$—% | 89.9 | 89.9 | 89.9 | 89.9 |
| $T_4$—°C (°F) | 1033 (1891) | 1033 (1891) | 1038 (1900) | 1052 (1925) |
| Dyne power—kW (hp) | 17.7 (23.8) | 17.4 (23.4) | 24.0 (32.2) | 22.6 (30.3) |
| Starter power—kW (hp) | 9.2 (12.4) | 9.2 (12.4) | 12.0 (16.1) | 12.0 (16.1) |
| $W_f$—kg/h (1b/hr) | 7.62 (16.8) | 7.62 (16.8) | 9.07 (20.0) | 9.03 (19.9) |
| $W_a$—kg/s (1b/sec) | 0.249 (0.548) | 0.249 (0.548) | 0.282 (0.621) | 0.276 (0.608) |
| $R_c$ | 3.523 | 3.523 | 3.961 | 3.904 |
| $T_2$—°C (°F) | 207 (404) | 207 (405) | 229 (445) | 231 (448) |
| $T_5$—°C (°F) | 868 (1594) | 868 (1594) | 857 (1574) | 872 (1601) |
| $T_6$—°C (°F) | 771 (1420) | 785 (1445) | 749 (1380) | 779 (1435) |

# III. COMPRESSOR DEVELOPMENT

## 3.2 COMPRESSOR MECHANICAL DEVELOPMENT

Compressor mechanical development during this period consisted of thinning compressor impeller blades, investigating inlet heating, and evaluating running clearances.

Engine testing has indicated low airflow with respect to compressor rig testing. Two possible explanations for this reduced airflow are (1) heating of the engine inlet air by the inlet guide vanes and aluminum engine air inlet ducting and (2) thick compressor impeller blading.

Limited engine test data have suggested an increase in engine inlet air temperature from test cell ambient to the compressor impeller inlet face. This situation was investigated during testing of BU8 by removing the inlet guide vanes and plugging the resulting holes. In place of one of the plugs, a total temperature rake was installed. The data acquired from this total temperature rake showed an increase in inlet air temperature with respect to test cell ambient of approximately 2.8°C (5°F). This increase in temperature accounts for a decrease in airflow of about 0.5%. The cause of this temperature increase is thought to be heat transfer from the 15 inlet guide vanes and the aluminum inlet duct. The inlet duct is located on top of the gear case, which is heated by engine oil and which may reach temperatures over 93°C (200°F). Possible design modifications are currently under investigation.

Inspection charts of the engine test impeller indicated extra thickness on both the full blades and the splitters. The results of a previous compressor rig test indicated increases in airflow, pressure ratio, and efficiency as a result of thinning compressor blades. It was therefore decided to thin the engine impeller by removing metal from the suction side only of the full blades and splitters, as shown in Figure 12. The impeller was not thinned to the extent the rig test impeller was due to the possibility of damage to engine hardware in the event of a compressor failure. The thinned impeller was tested in engine BU8 with no significant improvement in airflow, pressure ratio, or efficiency. Investigation into other aerodynamic impeller modifications is in process.

Compressor clearance measurements at the time of engine build are acquired by allowing the

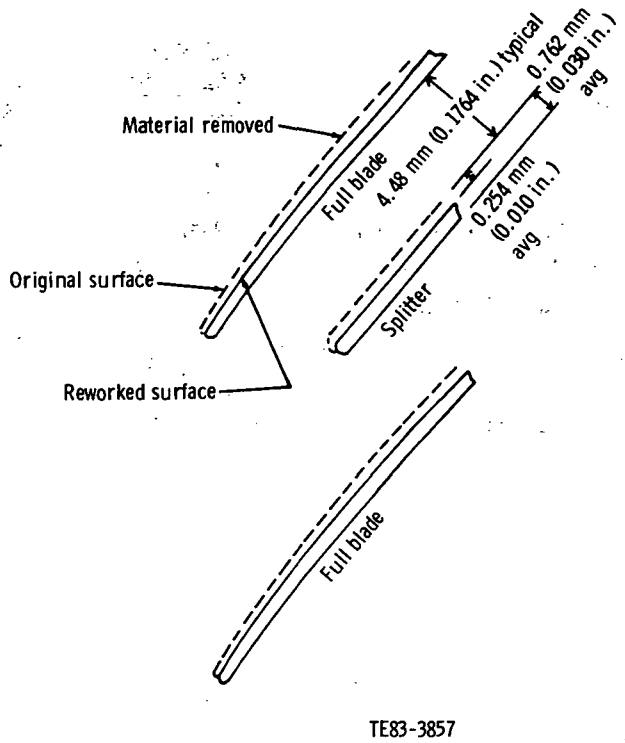


**Figure 12. Compressor impeller thinning.**

compressor impeller to cut small mounds of wax that are added to the shroud in the inducer, knee, and tip areas. The impeller is loaded forward, toward the shroud, to simulate the engine running condition. To measure the minimum clearance between the impeller and shroud during engine running, nine small mounds of epoxy are added to the shroud in groups of three each at the inducer, knee, and tip, as shown in Figure 13. Compressor clearances for engine builds 5 through 8 are shown in Table V. No data are available for TD6 and BU7, since the cold section of the engine was not disassembled at TD6.

In general, the wax measurements made during assembly appear to be consistent from build to build with inducer clearance varying from 0.11 mm to 0.24 mm (0.0045 in. to 0.0095 in.), knee clearance varying from 0.25 mm to 0.37 mm (0.010 in. to 0.0145 in.), and tip clearance varying from 0.25 mm to 0.36 mm (0.010 in. to 0.014 in.). The teardown rub pad measurements show a discrepancy between TD7 and TD8. Since the maximum speed reached during

## Table V.
## Compressor and turbine cold wax and rub pad measurements.

| | BU5, cold wax— mm (in.) | | TD5, rub pads— mm (in.) | | BU6, cold wax— mm (in.) | | TD6, rub pads— mm (in.) | | BU7, cold wax— mm (in.) | | TD7, rub pads— mm (in.) | | BU8, cold wax— mm (in.) | | TD8, rub pads— mm (in.) | |
|---|---|---|---|---|---|---|---|---|---|---|---|---|---|---|---|---|
| | Min | Max | Min | Max | Min | Max | Min | Max | Min | Max | Min | Max | Min | Max | Min | Max |
| Compressor | | | | | | | | | | | | | | | | |
| Inducer | 0.178 (0.007) | 0.178 (0.007) | 0.076* (0.003)* | 0.152* (0.006)* | 0.127 (0.005) | 0.241 (0.0095) | — | | | — | 0.076 (0.003) | 0.102 (0.004) | 0.114 (0.0045) | 0.229 (0.009) | 0.076 (0.003) | 0.127 (0.005) |
| Knee | 0.254 (0.010) | 0.318 (0.0125) | 0.127* (0.005)* | 0.152 (0.006)* | 0.279 (0.011) | 0.330 (0.013) | — | Cold section not disassembled | | — | 0.102 (0.004) | 0.127 (0.005) | 0.305 (0.012) | 0.368 (0.0145) | 0.152* (0.006)* | 0.229* (0.009)* |
| Tip | 0.254 (0.010) | 0.330 (0.013) | 0.102* (0.004)* | 0.127* (0.005)* | 0.279 (0.011) | 0.356 (0.014) | — | | | — | 0.102 (0.004) | 0.102 (0.004) | 0.254 (0.010) | 0.356 (0.014) | 0.178* (0.007)* | 0.229* (0.009)* |
| Gasifier turbine | | | | | | | | | | | | | | | | |
| Tip—clearance to original surface | 0.559 (0.022) | 0.635 (0.025) | 0.318 (0.0125)* | 0.356 (0.014)* | 0.356 (0.014) | 0.381 (0.015) | 0.203 (-0.008) | 0.076 (0.003) | 0.838 (0.033) | 0.914 (0.036) | -0.076 (-0.003) | 0.254 (0.010) | 0.533 (0.021) | 0.610 (0.024) | -0.051 (-0.002) | 0.279 (0.011) |
| Tip—coating erosion | | | | | | | 0.483 (0.019) | 0.559 (0.022) | | | 0.279 (0.011) | 0.584 (0.023) | | | 0.178 (0.007) | 0.457 (0.018) |
| Knee—clearance to original surface | 0.356 (0.014) | 0.610 (0.024) | 0.229R1 (0.009)R1 | 0.241 (0.0095) | 0.279 (0.011) | 0.330 (0.013) | 0.051 (0.002) | 0.102 (0.004) | 0.381 (0.015) | 0.610 (0.024) | -0.025 (-0.001) | 0.152 (0.006) | 0.330 (0.013) | 0.457 (0.018) | 0.178 (0.007) | 0.203 (0.008) |
| Knee—coating erosion | | | | | | | 0.051 (0.002) | 0.330 (0.013) | | | 0.102 (0.004) | 0.254 (0.010) | | | — | — |
| Exducer—clearance to original surface | 0.406 (0.016) | 0.559 (0.022) | 0.165R (0.0065)R | 0.191 (0.0075) | 0.356 (0.014) | 0.432 (0.017) | -0.102 (-0.004) | 0.025 (0.001) | 0.533 (0.021) | 0.559 (0.022) | 0.025 (0.001) | 0.305 (0.012) | 0.279 (0.011) | 0.508 (0.020) | 0 (0) | 0.254 (0.010) |
| Exducer—coating erosion | | | | | | | 0.127 (0.005) | 0.203 (0.008) | | | 0.025 (0.001) | 0.102 (0.004) | | | — | — |
| Backplate—outer diameter—clearance to original surface | 1.067 (0.042) | 1.067 (0.042) | 0.622 (0.0245) | 0.711 (0.028) | 0.508 (0.020) | 0.559 (0.022) | -0.178 (-0.007) | 0 (0) | 0.584 (0.023) | 0.787 (0.031) | 0.254 (-0.010) | 0.076 (0.003) | 0.711 (0.028) | 0.787 (0.031) | LP | LP |
| Backplate—outer diameter—coating erosion | | | | | | | 0.025 (0.001) | 0.254 (0.010) | | | 0.178 (0.007) | 0.305 (0.012) | | | | |
| Backplate—inner diameter—clearance to original surface | 1.295 (0.051) | 1.295 (0.051) | 0.775 (0.0305) | 0.953 (0.0375) | 0.559 (0.022) | 0.610 (0.024) | 0.051 (0.002) | 0.102 (0.004) | 0.584 (0.023) | 0.635 (0.025) | 0.076 (0.003) | 0.127 (0.005) | 0.635 (0.025) | 0.711 (0.028) | LP | LP |
| Backplate—inner diameter—coating erosion | | | | | | | 0 (0) | 0.051 (0.002) | | | 0 (0) | 0 (0) | | | | |
| Power turbine | | | | | | | | | | | | | | | | |
| Tip | 1.194 (0.047) | 1.321 (0.052) | 0.457* (0.018)* | 0.508* (0.020)* | 1.626 (0.064) | 1.727 (0.068) | 0.457* (0.018)* | 0.508* (0.020)* | 1.626 (0.064) | 1.727 (0.068) | * | * | 0.686 (0.027) | 0.889 (0.035) | 0.305 (0.012) | 0.533 (0.021) |
| Knee | 0.419 (0.0165) | 0.737 (0.029) | 0.178* (0.007)* | 0.254* (0.010)* | 0.406 (0.016) | 0.686 (0.027) | 0.457* (0.018)* | 0.254* (0.010)* | 0.406 (0.016) | 0.686 (0.027) | * | * | 0.406 (0.016) | 0.533 (0.021) | 0.330 (0.013) | 0.406 (0.016) |
| Exducer | 0.254 (0.010) | 0.635 (0.025) | 0.165* (0.0065)* | 0.178* (0.007)* | 0.381 (0.015) | 0.508 (0.020) | 0.152* (0.006)* | 0.178* (0.007)* | 0.381 (0.015) | 0.508 (0.020) | * | * | 0.254 (0.010) | 0.533 (0.021) | 0.279 (0.011) | 0.279 (0.011) |
| Backplate outer diameter—clearance to original surface | 1.118 (0.044) | 1.118 (0.044) | 0.495 (0.0195) | 0.635 (0.025) | 0.457 (0.018) | 0.533 (0.021) | 0.203 (0.008) | 0.203 (0.008) | 0.457 (0.018) | 0.610 (0.024) | 0.254 (0.010) | 0.254 (0.010) | 0.356 (0.014) | 0.508 (0.020) | 0.076 (0.003) | 0.076 (0.003) |
| Backplate—outer diameter—coating erosion | | | | | | | 0 (0) | 0.076 (0.003) | | | 0 (0) | 0.025 (0.001) | | | | |
| Backplate—inner diameter—clearance to original surface | 1.067 (0.042) | 1.067 (0.042) | 0.457 (0.018) | 0.508 (0.020) | 0.432 (0.017) | 0.559 (0.022) | LP | LP | 0.432 (0.017) | 0.559 (0.022) | LP | LP | 0.381 (0.015) | 0.483 (0.019) | 0.051 (0.002) | 0.051 (0.002) |
| Backplate—inner diameter—coating erosion | | | | | | | 0.051 (0.002) | 0.051 (0.002) | | | 0 (0) | 0.051 (0.002) | | | | |

LP = Lost rub pad
R = Rub
* = Rub pad not touched
R1 = Rub between pads

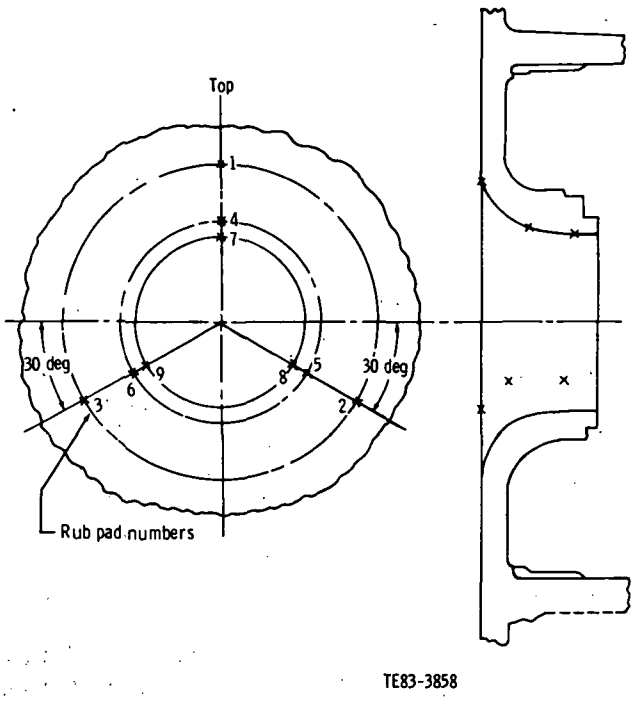


**Figure 13. Compressor rub pad locations.**

BU7 was 90% and the maximum speed reached during BU8 was 100%, one would expect the rub pad heights measured at TD8 to be the same or slightly less than those measured at TD7. Table V indicates that only one rub pad touched during BU8 running even though the rub pad heights were as much as 0.13 mm (0.005 in.) greater than those indicated at TD7. This discrepancy will be investigated during future engine builds in keeping with the goal of defining the proper cold wax measurement values which, when built into the engine, will provide minimum but safe running clearances.

Preceding Page Blank

# IV. GASIFIER TURBINE DEVELOPMENT

## 4.1 GASIFIER TURBINE AERODYNAMIC DEVELOPMENT

Specific areas for improvement of the gasifier turbine have been identified using experimental data to assess losses at various stations through the turbine. This study resulted in a loss breakdown structure, illustrated in Figure 14, and shows the vane to be deficient in performance. The rotor and scroll appear to perform quite satisfactorily. Similar evidence of high vane loss has been provided through detailed vane exit surveys by NASA-Lewis Research Center (Ref 1)*.

On comparing the gasifier vane design with the more successful power turbine vane, significant differences can be noted. First, the gasifier has a vane trailing edge blockage of 10.8% as compared with 9.3% for the power turbine. This additional blockage contributes to increased wake thickness and higher mixing loss. Second, the gasifier vane width of 8.38 mm (0.330 in.) is small in comparison with the 11.04 mm (0.4346 in.) width of the power turbine. This reduced width is responsible for increased secondary flow losses. Third, the vane downstream turning (suction surface camber downstream of the throat) is 10 deg as compared with 5 deg for the power turbine vane. This additional downstream turning can contribute to suction surface separation and corresponding increase in loss. Fourth, the power turbine was not run in the secondary flow field of a scroll.

The approach to achieving design efficiency objectives therefore focuses on improving the vane performance. Each of the previously mentioned deficiencies will be addressed in the design of a new vane, the following being the key elements:

- The trailing edge diameter will be reduced from 0.030 in. to 0.020 in. This action is based on the

*K. L. McLallin and J. E. Haas, "Experimental Performance Analysis of 15.04-Centimeter Tip Diameter, Radial Inflow Turbine with Work Factor of 1.126 and Thick Blading," NASA Technical Paper 1730, October 1980.

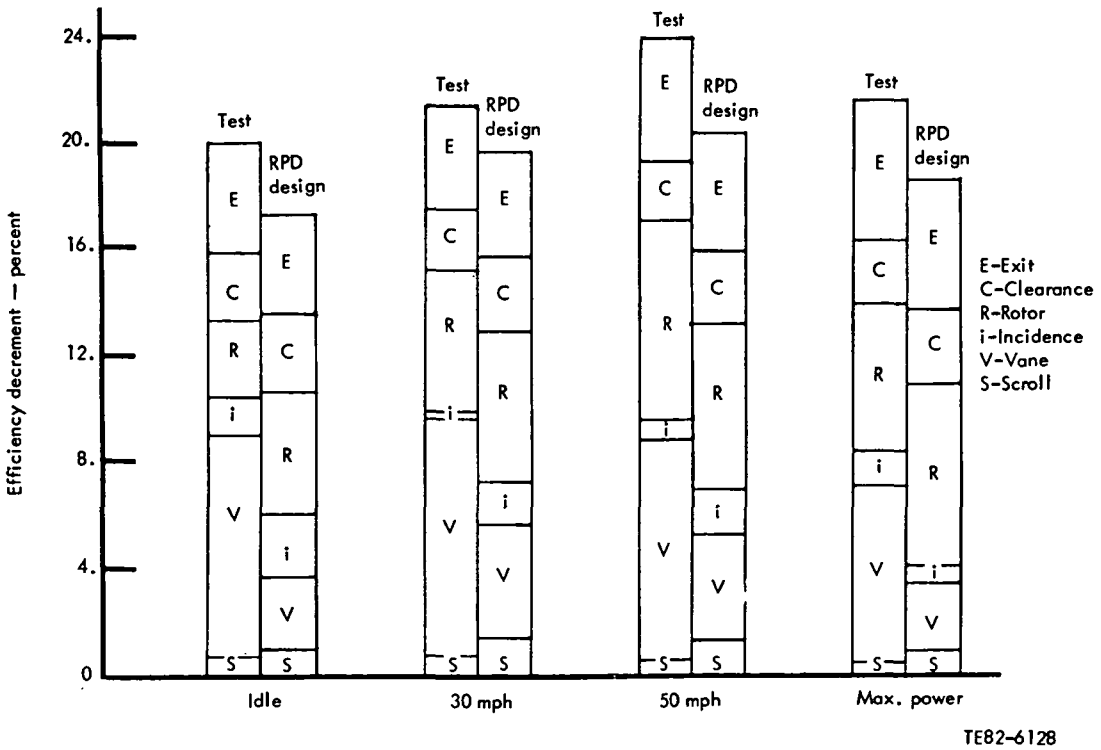


**Figure 14. Loss analysis of gasifier turbine.**

successful development of ceramic axial vanes in the CATE program. Those axial vanes exhibited a trailing edge diameter of 0.020 in.

- The airfoil will be nonsymmetrical and will be constrained to a downstream turning of less than 5 deg.
- The vane width will be increased by 15%-20%.

Increased vane width will be accomplished by increasing the vane exit angle (referenced from radial) by 2 deg or 3 deg. This action becomes more of an attractive trade as a result of reduced trailing edge diameter.

## 4.2 GASIFIER TURBINE MECHANICAL DEVELOPMENT

Gasifier turbine mechanical development during this reporting period included the following items:

- redesigned scroll support system
- analysis of clearance measurements
- design of combustor-to-scroll interface seal system

### Redesigned Scroll Support System

Buildup 6 was the first engine assembly that incorporated a redesigned scroll support system. Prior to this run, a 2-D transient thermal deflection analysis of both the gasifier rotor and scroll was completed. A transient condition that simulates the actual engine starting conditions of 60% rpm, 40% flow, and 1077°C (1970°F) in 18 sec was used. The results of this analysis are shown in Figures 15 through 19. The calculated values of clearance/interference between the rotor and stationary flow-path components at the rub pad locations are shown in these figures. Initial clearances are the cold build (wax) clearances. This analysis includes the effect of the abradable thermal barrier coating on the scroll and inner backplate flow-path surfaces. All figures except Figure 15 show rotor clearance during the transient start period. However, Figure 15 shows a 0.05 mm (0.002 in.) interference between the rotor tip and the inner backplate during the 30 sec to 90 sec time frame.

The following three factors were considered in establishing the BU6 clearances:

- rub pad measurement data from previous builds
- abradable coating of flow-path surfaces
- calculated transient analysis

Therefore, even though the calculations indicated an interference of 0.05 mm (0.002 in.), the decision to run was based on the fact that the flow path surfaces had a 0.30 mm (0.012 in.) thick abradable coating that would wear away if interference occurred.

### Analysis of Clearance Measurements

Assembly wax clearance measurements on the gasifier turbine are acquired in a manner similar to that used on the compressor. The rotor is loaded aft (toward the shroud) when cutting the wax to simulate the engine running condition. A total of 13 platinum weld-wire rub pads are used to measure gasifier turbine running clearances, with 7 mounted on the rotor shroud and 6 on the inner backplate, as shown in Figures 20 and 21, respectively.

TD6 measurements (see Table V) and calculated clearances are in good agreement, except at the shroud tip. At that location, the calculated results (see Figure 17) show that running clearance would be greater than build clearance between the rotor and scroll. However, engine running experience from rub pad measurements shows a decrease in the clearance.

No physical changes were made to the scroll or rotor contours between TD6 and BU7. Therefore, BU7 cold wax clearances are greater than BU6 because of erosion and/or rubbing of the abradable coating during BU6 running.

Significant erosion of the abradable coatings on the shroud and outer backplate was observed at TD7. The decision was made to remove the abradable coatings and restore the surfaces to the original contours by respraying with yttria stabilized zirconia (YSZ) thermal barrier coating only. Previously, the YSZ thermal barrier coating had been between the abradable coating and the metal-to-YSZ bond coating. These changes were incorporated in BU8.

Table V indicates loss of coating during BU8 running. Since the YSZ coating is extremely hard, it is thought that the loss of coating was due to erosion caused by chips from the ceramic combustor, which were produced when the compliant layer separating the combustor and scroll was lost. The gasifier turbine vanes also showed erosion on the pressure surface, as seen in Figure 22.

### Combustor-to-Scroll Interface Seal System

At the beginning of this reporting period, the combustor-to-gasifier turbine compliant layer or interface seal was a 1.524 mm (0.060 in.) thick pad of Nextel fabric. This pad was retained only by the combustor retention loading (13.6 kg [30 lb] from springs, approximately 11.3 kg [25 lb] pressure load,

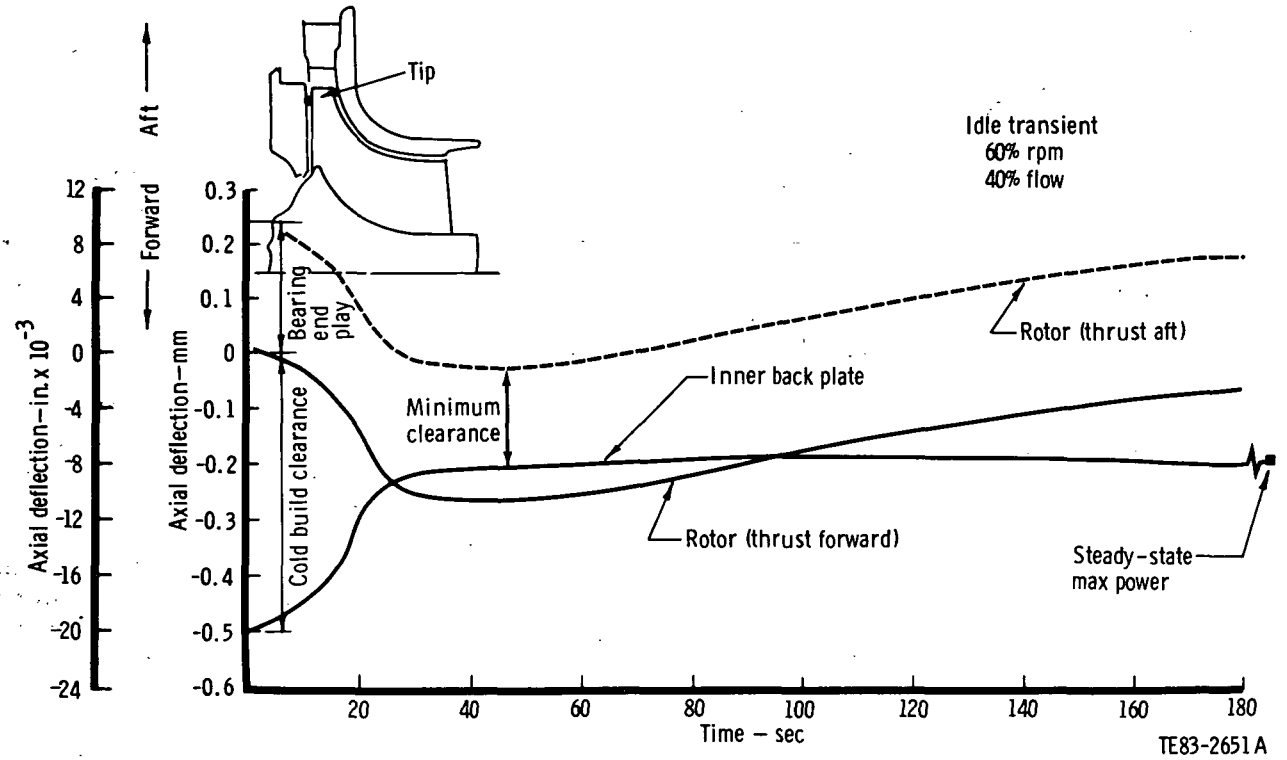


**Figure 15. Build 6 predicted gasifier turbine inner backplate tip deflection.**

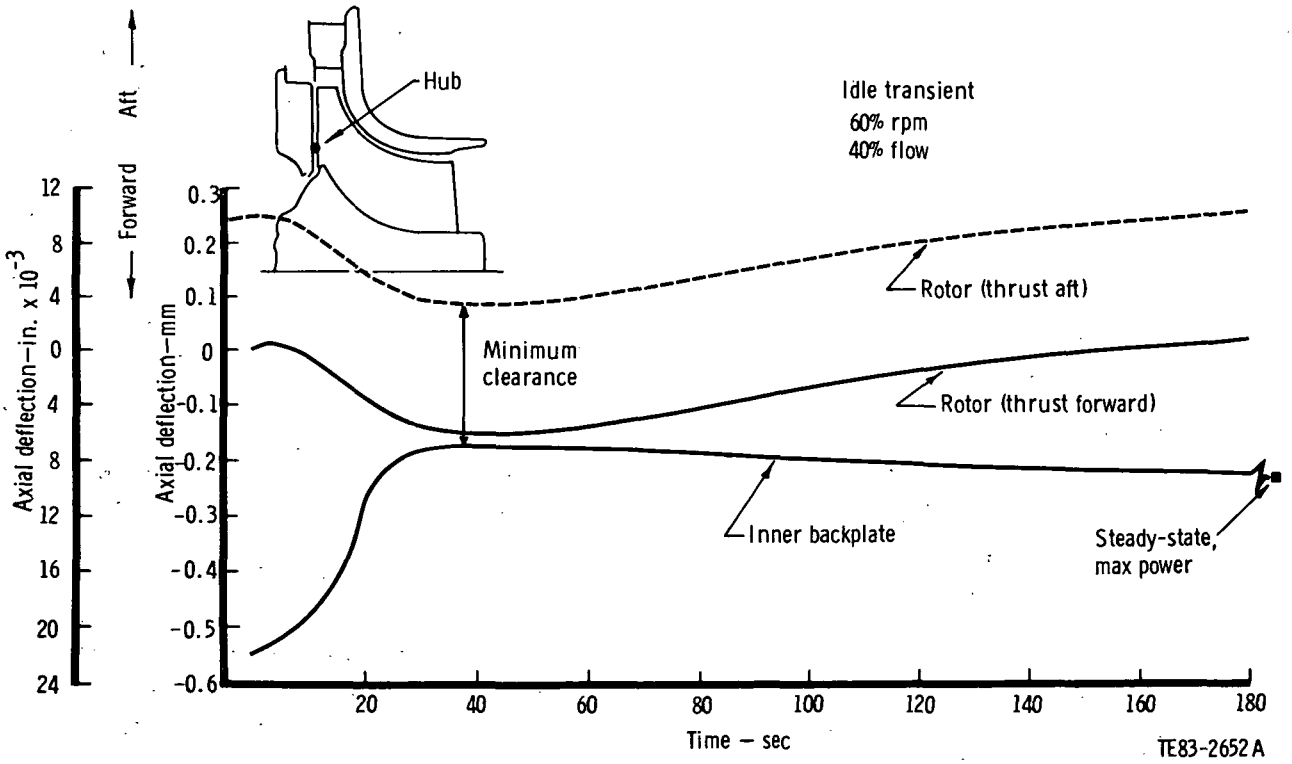


**Figure 16. Gasifier turbine predicted inner backplate hub deflection.**

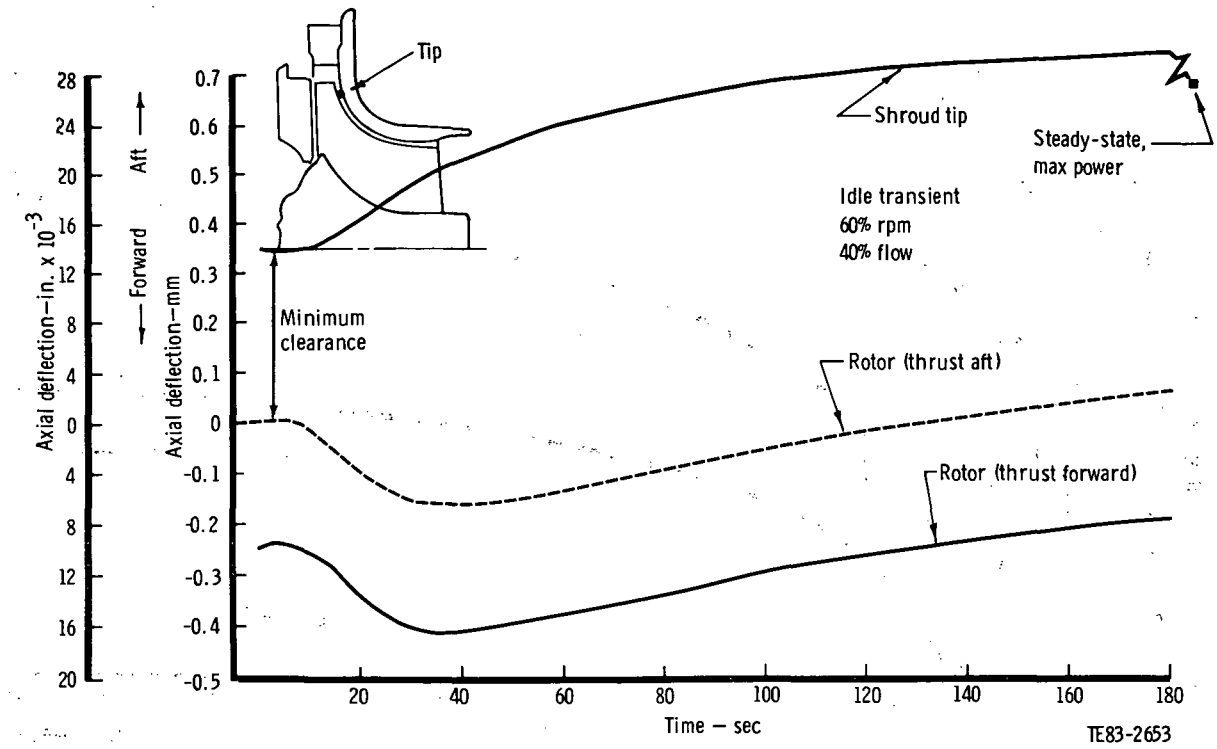


**Figure 17. Gasifier turbine scroll tip deflection.**

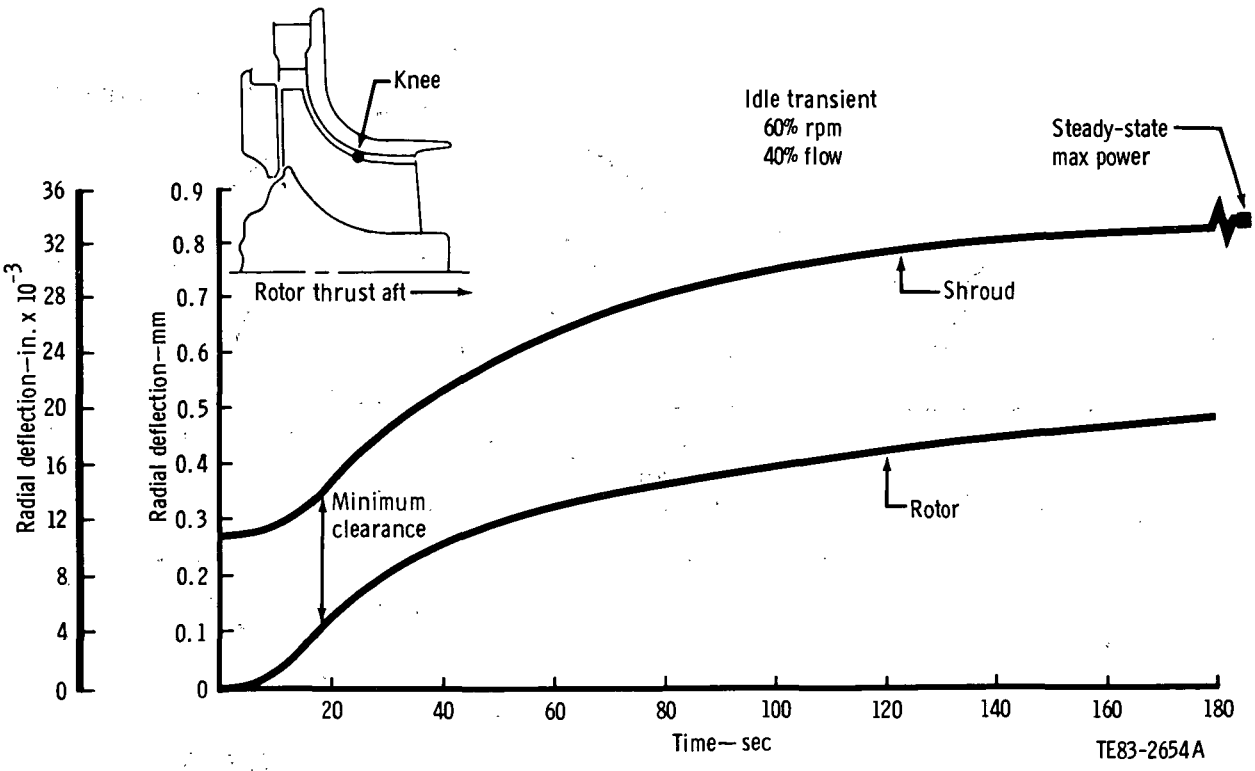


**Figure 18. Gasifier turbine scroll knee deflection.**

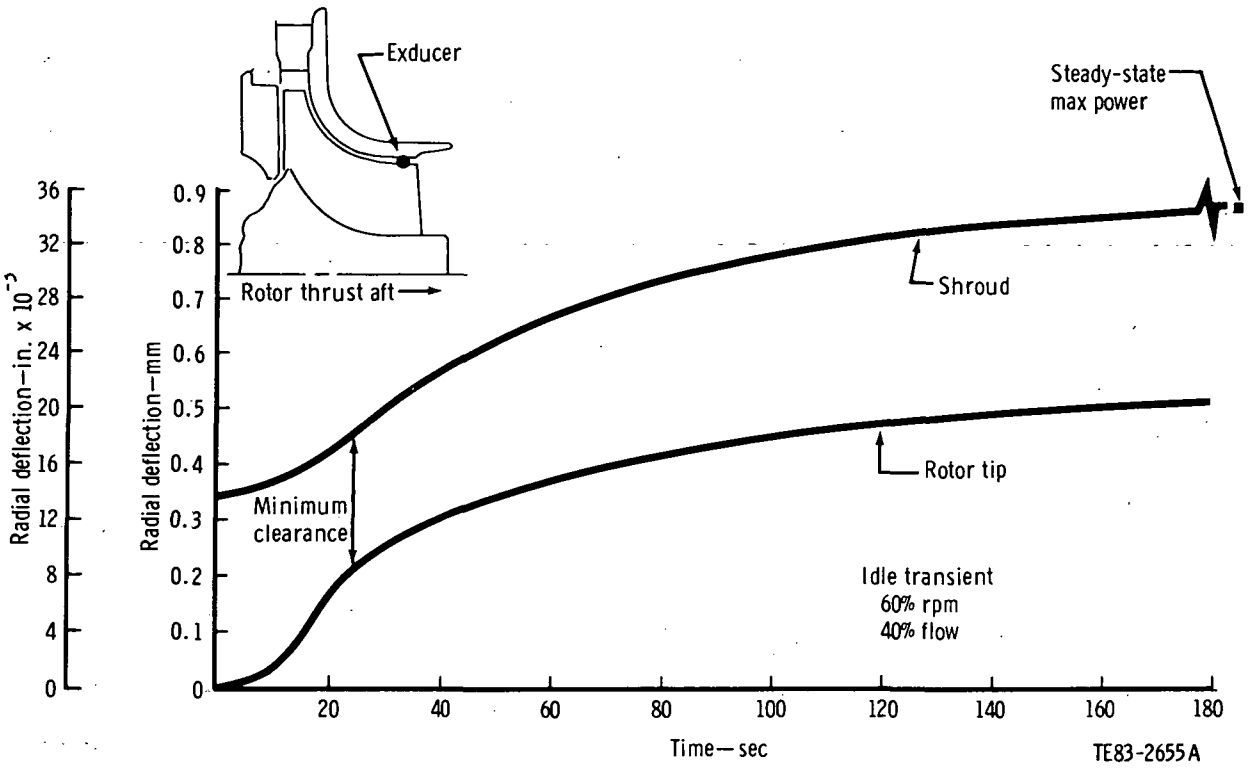


**Figure 19. Gasifier turbine scroll exducer deflection.**

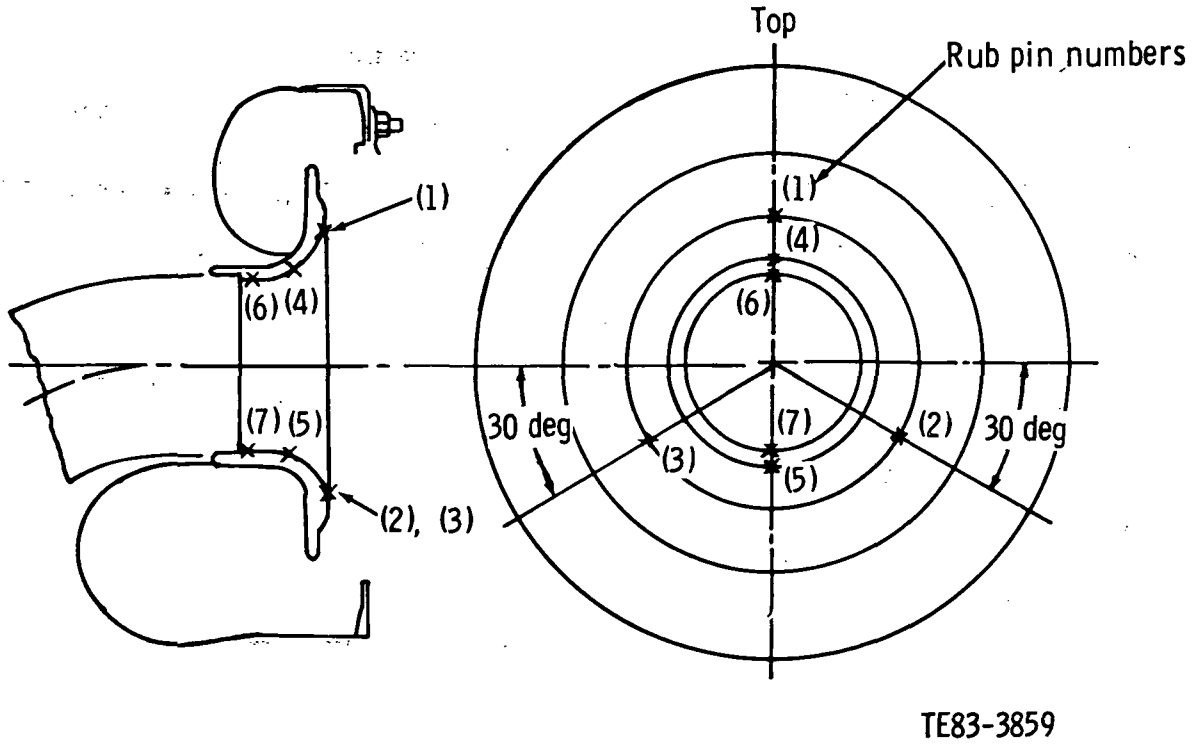


**Figure 20. Gasifier turbine rotor shroud rub pad locations.**

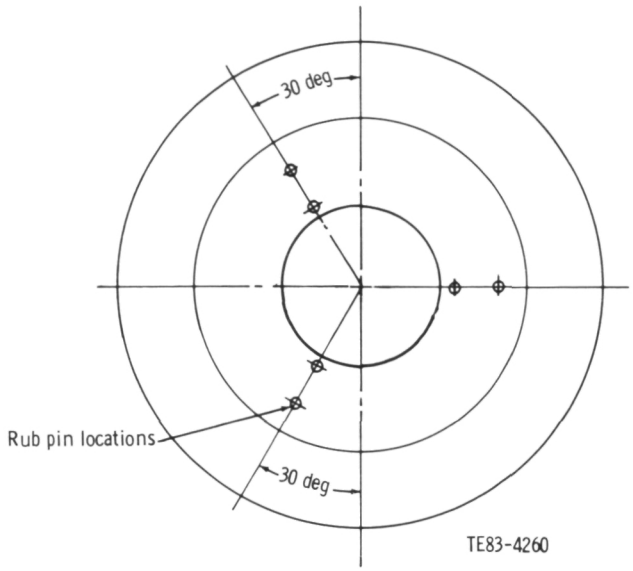


**Figure 21. Gasifier turbine inner backplate rub pad locations.**

and a large combustor assembly load). The free edges of the fabric frayed severely. During BU7 running, a portion of the seal was sucked into the gas path and blocked three gasifier turbine vane passages. While performing a routine inspection of the ceramic combustor body between runs on BU8, it was noticed that approximately one-third of the interface seal had been sucked into the flow path. Since the BU8 interface seal was a one piece (donut-shaped) fabric, it was thought that additional running would cause the entire seal to be sucked into the flow path, which could cause severe mechanical damage. The entire interface seal was removed at that time and additional engine testing accomplished. TD8 revealed chipping of the ceramic combustor where it contacts the gasifier turbine scroll, as shown in Figure 23. These chips, which occurred after removal of the Nextel fabric, are thought to be the primary cause of the erosion of the gasifier turbine vanes and coatings, as mentioned previously.

To relieve this problem for BU9, the interface seal configuration was changed. A retainer was designed to hold the fabric in place and to minimize the tendency of fray. The seal is assembled using eight, 45-deg segments. These segments are cut from the Nextel fabric so that the free edge adjacent to the flow path is the woven edge of the fabric. The opposite side of all segments is clamped between a split retainer and a 360-deg clamp ring. The split ring retainers hook under the scroll inlet, and the assembly is held in place by 16 rivets, as shown in Figure 24.

## 4.3 CERAMIC GASIFIER TURBINE DESIGN

### Gasifier Ceramic Scroll Operating Clearance Analysis

Two-dimensional finite element models were used to define deflections of the ceramic rotor and scroll assembly during a start-up transient. Typical temperature vs time plots for the scroll and rotor are shown in Figures 25 and 26.

Typical plots of deflections for the ceramic scroll and rotor are presented in Figures 27 and 28. The locations are indicated on the plots. Initial build clearances were assumed for the purpose of making the plots and are not necessarily the final recommended values.

To meet recommended goals for build clearances for the reference power-train design (RPD) gasifier turbine, an assessment was made of experimental engine clearance data. Table VI presents total clearance change as indicated from build measurements and rub pad data obtained from BU6 and TD6. Calculated values of clearance change due to thermal deflections for the experimental engine metal configuration are listed. These are subtracted from the total clearance change due to other effects, i.e., whip and shaft deflections. This clearance value is assumed to be equal to or greater than that of the ceramic components and should be somewhat conservative if used to add to the thermal deflection clearance component to arrive at a total clearance change for the RPD. The bottom line of the table is obtained by adding 0.076 mm (0.003 in.) to the total clearance change to provide a minimum operating clearance of 0.076 mm (0.003 in.) for the RPD ceramic turbine.

### Gasifier Turbine Rotor

To maintain a continuity of information, the gasifier turbine rotor development discussion is incorporated into Section IX, "Materials Development." This allows all relevant information pertaining to the component to be presented under a single heading.

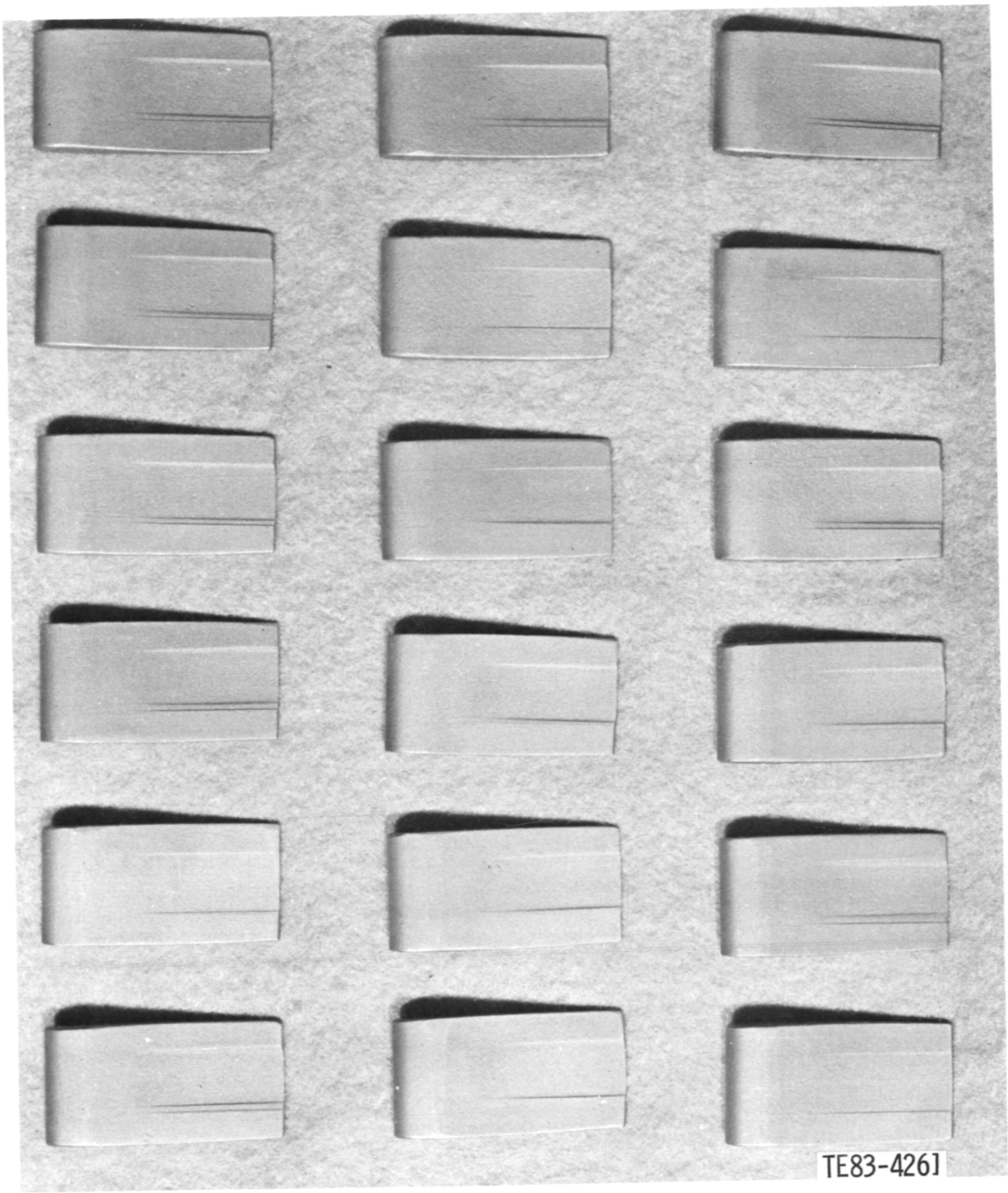


**Figure 22. Gasifier turbine vane pressure surface erosion.**


Figure 23. Chipping of ceramic combustor at gasifier scroll interface.

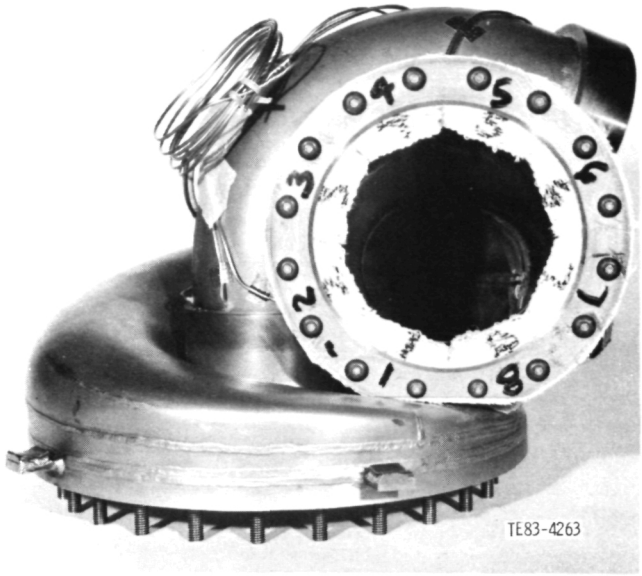


Figure 24. Combustor-to-scroll seal retention feature.

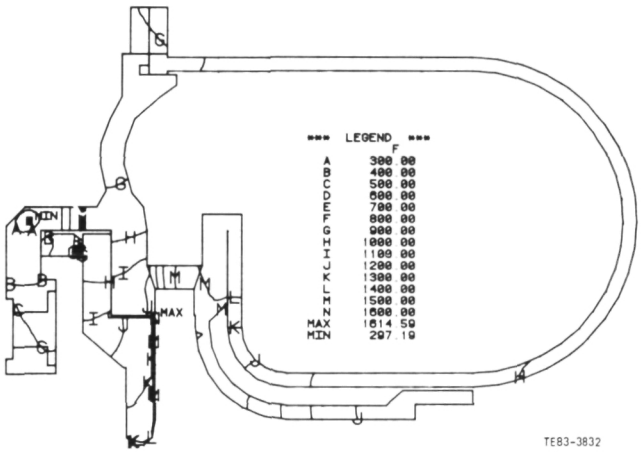


Figure 25. Ceramic scroll RPD temperature distribution.

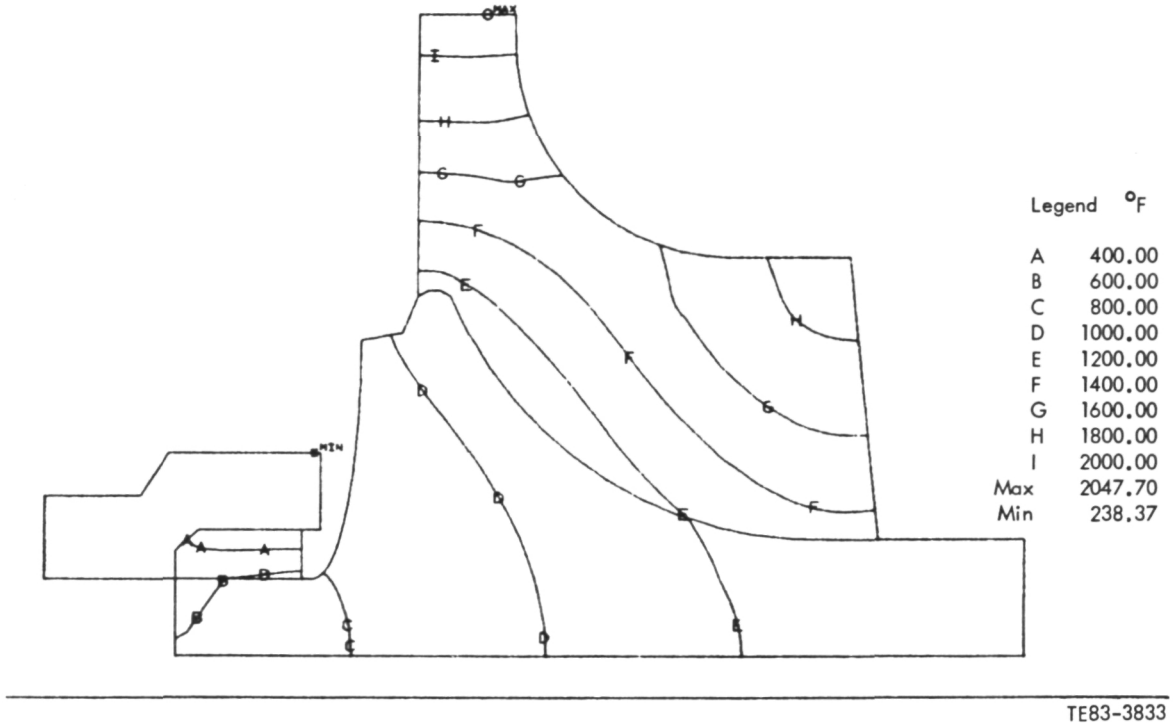


**Figure 26. Ceramic gasifier rotor predicted RPD temperature distribution.**

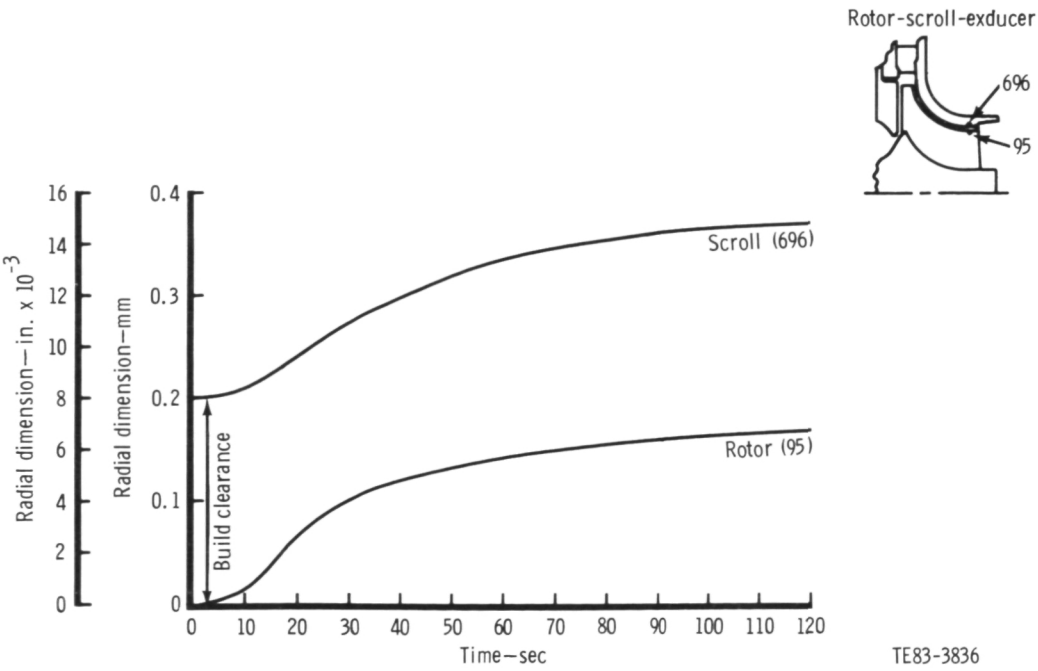


**Figure 27. Predicted ceramic gasifier turbine exducer clearance change vs time.**

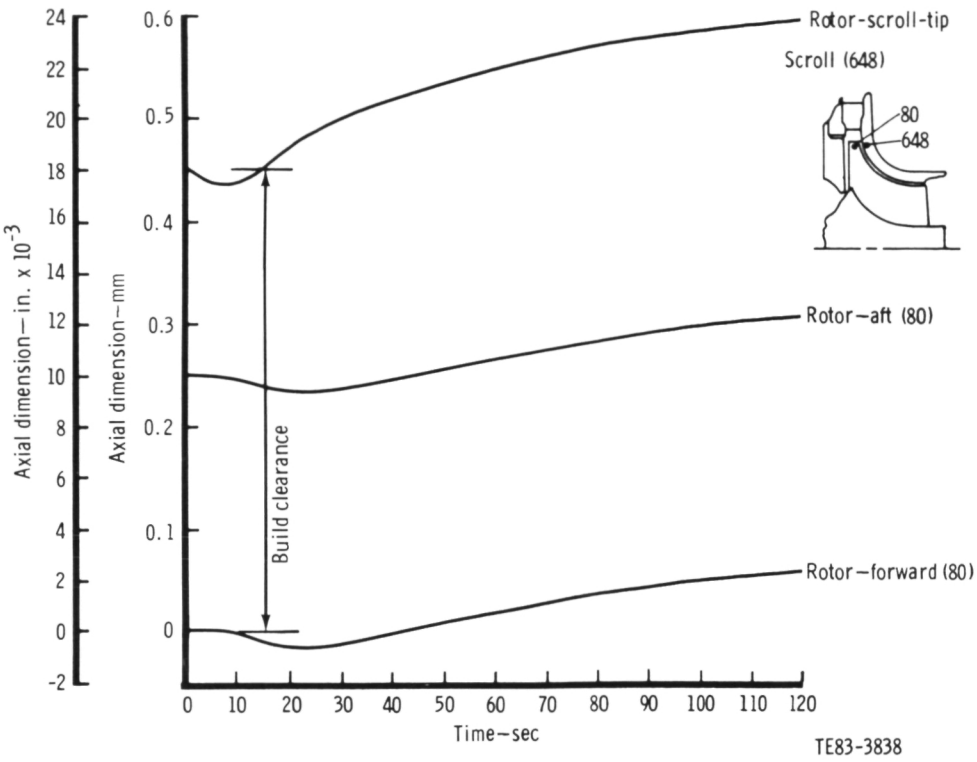


**Figure 28. Predicted ceramic gasifier turbine shroud tip clearance change vs time.**

**Table VI.**
**Total clearance changes.**

| | | Backplate tip— mm (in.) | Backplate hub— mm (in.) | Shroud tip— mm (in.) | Shroud knee— mm (in.) | Shroud exit— mm (in.) |
|---|---|---|---|---|---|---|
| | Build clearance required to provide zero running clearance for experimental engine (BU6) | 0.686 (0.027) | 0.508 (0.020) | 0.559 (0.022) | 0.229 (0.009) | 0.457 (0.018) |
| Minus: | Calculated max relative deflections for experimental engine | 0.584 (0.023) | 0.559 (0.022) | 0 (0) | 0.051 (0.002) | 0.127 (0.005) |
| Equals: | Experimental engine clearance required due to other considerations (whip, shaft deflections, etc) | 0.102 (0.004) | – 0.051 ( – 0.002) | 0.559 (0.022) | 0.178 (0.007) | 0.330 (0.013) |
| Plus: | RPD calculated max relative deflections | 0.178 (0.007) | 0.178 (0.007) | 0 (0) | 0 (0) | 0.025 (0.001) |
| Equals: | Build clearance required to provide zero running clearance for RDP | 0.279 (0.011) | 0.127 (0.005) | 0.559 (0.022) | 0.178 (0.007) | 0.356 (0.014) |
| Plus 0.076 mm (0.003 in.) equals: | Recommended build clearance to provide 0.076 mm (0.003 in.) min running clearance | 0.356 (0.014) | 0.203 (0.008) | 0.635 (0.025) | 0.254 (0.010) | 0.432 (0.017) |

# V. POWER TURBINE DEVELOPMENT

## 5.2 POWER TURBINE MECHANICAL DEVELOPMENT

Power turbine mechanical development during this reporting period included the following items:

- analysis of clearance measurements
- LAS bulkhead failure
- power turbine exhaust coupling piston ring yielding

### Analysis of Clearance Measurements

Cold wax clearance measurements on the power turbine are acquired in a manner similar to that used on the compressor and gasifier turbine. The rotor is loaded forward (toward the shroud) when cutting the wax to simulate the engine running condition. A total of 13 platinum weld wire rub pads are used to measure power turbine running clearances, with 7 mounted on the shroud and 6 mounted on the inner backplate. The power turbine rotor shroud rub pad locations are shown in Figure 29, and the power turbine inner backplate rub pad locations are similar to those of the gasifier turbine inner backplate shown in Figure 21.

The power turbine clearances between the rotor and the shroud were intentionally left open during most of this reporting period. Note in Table V that the rub pads on the power turbine shroud were not touched from BU5 to TD7, and the cold wax build clearances corresponding to these rub pad data are approximately 1.65 mm (0.065 in.) at the tip. The rotor-to-shroud clearance was reduced by approximately 1.02 mm (0.040 in.) between TD7 and BU8, and the TD8 measurements indicated a significant improvement in clearances.

Clearance measurements between the power turbine inner backplate and the rotor were reduced by approximately 0.51 mm (0.020 in.) between TD5 and BU6. A further reduction of approximately 0.10 mm (0.004 in.) was made between TD7 and BU8, resulting in a clearance of 0.05 mm-0.08 mm (0.002 in.-0.003 in.). This value is acceptable for the rotor-to-backplate clearance. Further clearance reduction is required, however, between the rotor and the shroud.

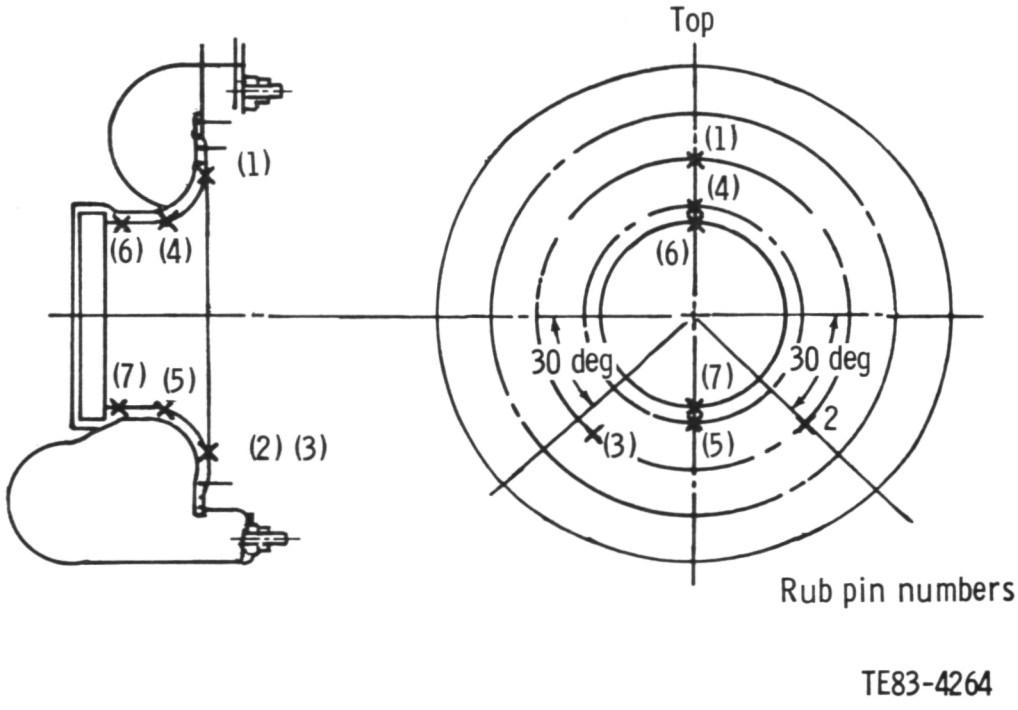


**Figure 29. Power turbine rotor shroud rub pad locations.**

## LAS Bulkhead Failure

Engine disassembly after BU5 running revealed a broken ceramic power turbine exhaust duct/seal platform. This part is also referred to as the bulkhead and is constructed of a lithium alumina silicate (LAS) material. The bulkhead was broken where the power turbine exhaust coupling fits into the bulkhead, as shown in Figure 30. This failure was caused by a difference in thermal expansion between the metal (HAST-X) power turbine exhaust coupling and the ceramic (LAS) bulkhead. The metal coupling, which has a high coefficient of thermal expansion compared with the ceramic bulkhead, was mounted inside the bulkhead, and the greater thermal growth of the coupling caused it to grow into the bulkhead, resulting in the failure.

To prevent recurrence of this problem on BU6, the outside diameter of the end of the coupling that fits into the bulkhead was reduced by 1.02 mm (0.04 in.), and the piston ring that goes into that same end of the coupling was notched, as shown in Figure 31, to permit more thermal expansion of the piston ring.

## Power Turbine Exhaust Coupling Piston Ring Yielding

Inspection of engine hardware after BU8 running revealed a change in free gap of the notched piston ring, which mounts in the bulkhead end of the power turbine exhaust coupling. Figure 32 shows a power turbine exhaust coupling with a yielded notched piston ring on the right and a power turbine exhaust coupling with new piston rings on the left. Subsequent calculations confirm that the notched configuration piston ring will yield when exposed to the hot engine environment. Investigation of this problem and appropriate modifications is in process.

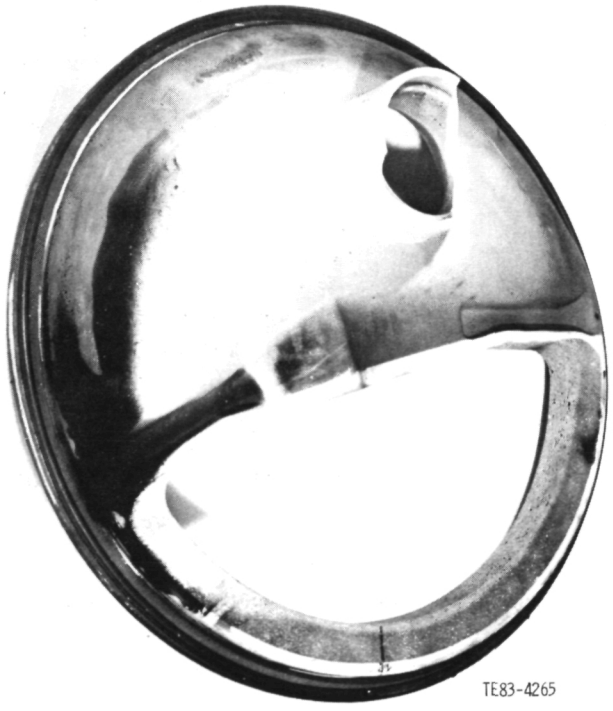


**Figure 30. Failed ceramic bulkhead (TD5).**

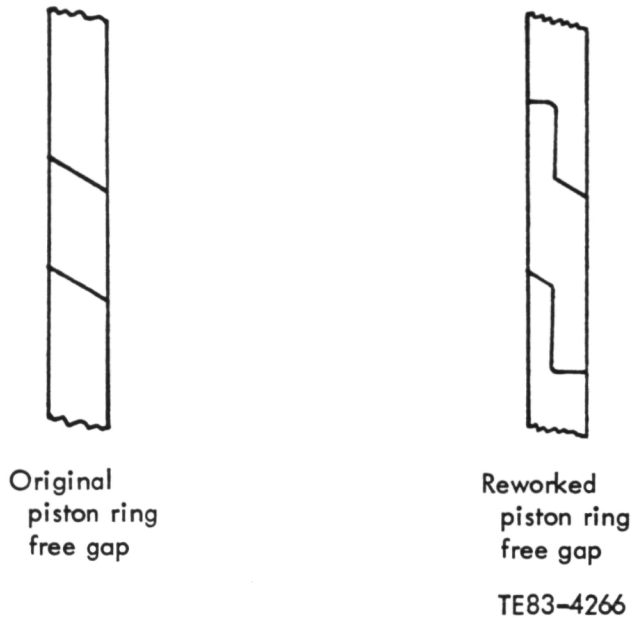


**Figure 31. Power turbine exhaust coupling piston ring rework.**

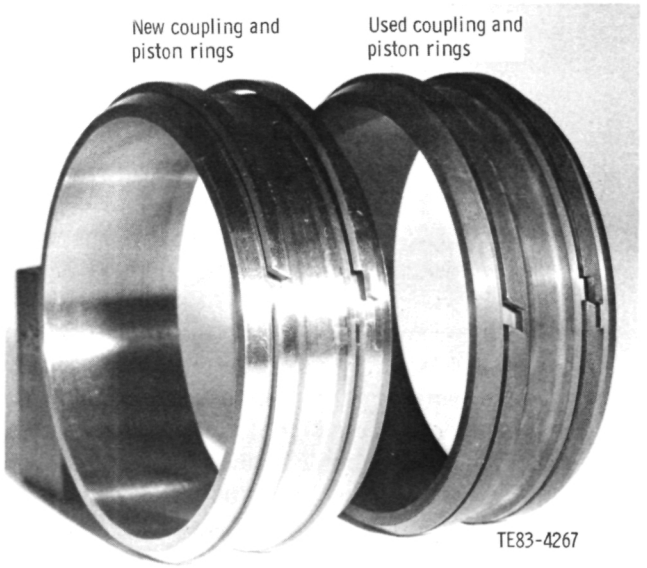


**Figure 32. Power turbine exhaust couplings and piston rings.**

# VI. COMBUSTOR DEVELOPMENT

## TEST FACILITY

As previously reported in the Fifth AGT Semiannual Report, a new combustor rig test section, capable of handling the high temperatures of the RPD cycle, was designed and fabricated. This facility duplicated as much as possible the environment expected in the engine, including flow path, insulating features, combustor orientation, variable geometry control, and fuel systems. A television camera, positioned to look through a periscope in the combustor exhaust, was connected to a color television monitor permitting visual observation of the combustion tests. This arrangement has proved extremely beneficial in analyzing the combustion phenomena during the development of the combustor. A preheater, capable of providing a combustion inlet air temperature of 1024°C (1875°F), was successfully added to the combustor rig.

Pilot, start-nozzle, and main nozzle operation was investigated with emphasis placed primarily on the main nozzle portion of the test effort. Due to a preheater air leak that occurred late in the rig test program, start-nozzle operation at elevated temperatures was limited to approximately half the required engine idle fuel flow.

After completing the testing required for the first engine build, the preheater core was removed and returned to the vendor for evaluation and repair. Following extensive redesign involving both the vendor and Allison personnel, the new heater was reinstalled in the combustor rig. Over 20 hr at high-temperature operation have been accumulated to date with all data indicating that the heater meets or exceeds design specifications.

## TEST RESULTS

Of the two ceramic combustor assemblies used to date in the engine testing, teardown inspection indicated that one of the combustor bodies cracked in the region of the dilution holes. It is believed that this phenomenon initiated during cold start-up conditions, i.e., operation on the start-nozzle diffusion flame injector. As a result of this event, recent combustor development activities have concentrated on the combustor rig testing of new ceramic combustor assemblies under cold start-up conditions. Following the preheater air leak repair, a combustor assembly proof-test procedure was established to rig-simulate those conditions believed necessary to operate the engine combustor during cold start.

During this reporting period, 4.5 hr of burning time were accumulated on the combustion rig. That time was devoted exclusively to proof-testing current engine configuration combustor assemblies. Approximately 2.5 hr were devoted to start-nozzle-only operations, while the remaining 2 hr involved main-nozzle-only operation.

### Start-Nozzle

Since the start-nozzle had been reworked to provide a higher idle fuel flow rate, there was some question as to its flow uniformity. In the combustor region where cracking appears to initiate (dilution hole area), high thermal stresses appear to be present due to potential start-nozzle flow striation, late burning in the region of the dilution holes, and a subsequent buildup of high hoop stress. It is conceivable that in the presence of significant start-nozzle flow maldistribution, portions of the lower end of the combustor may actually be hotter than corresponding regions of the primary zone.

The start-nozzle was removed and tested to recheck the flow distribution profile. The profile was found to be skewed some 35% to 50% (maximum deviation between six sectors), considerably less uniform than the nozzles had been at a lower flow number configuration.

Combustor rig testing at elevated start-nozzle fuel flow rates and cold start-up condition was initiated. Tests with the start-nozzles left with the skewed profile resulted in combustor cracking in the dilution hole region, similar to that experienced on the engine. The start-nozzles were then reworked to a 20% more uniform profile, and subsequent combustor testing at cold start-up conditions has been successful to date. Combustion efficiency during the reworked start-nozzle testing was measured at greater than 99%.

### Main-Nozzle

Proof-testing of the combustor assembly on main-nozzle operation was conducted at a burner inlet temperature of 760°C (1400°F) and a burner outlet temperature greater than 1093°C (2000°F). Fuel flow exceeded 13.6 kg/h (30 lbm/hr). This represented a significant increase in fueling rate, since

the maximum power condition was chosen to be that simulated. No unusual or adverse effects from the nearly 2 hr of snap fuel transients performed were observed.

## Pilotless Operation

Due to the desirability of eliminating the pilot combustor (with its attendant fuel use, air leakage, periodic carbon deposition, and subsequent hot spot formation), new pilotless combustor bodies are also in the design process. These require the placement of an igniter within the present centerbody assembly, and this item is now in fabrication. Extensive open air testing was conducted to optimize the placement of the igniters. A drawing of the new centerbody appears in Figure 33.

## Ceramic Components

Additional early combustor rig testing revealed that the original ceramic dome of the variable geometry combustor could fail during severe test conditions. During this last reporting period, the ceramic dome design was improved by maintaining its basic shape and function while minimizing material thickness, eliminating sharp edges, and reducing the size of the unheated rim. A new ceramic dome, fabricated to meet the specifications of the redesign, has been repeatedly and successfully tested under very severe test conditions, both on the combustor rig and in the engine.

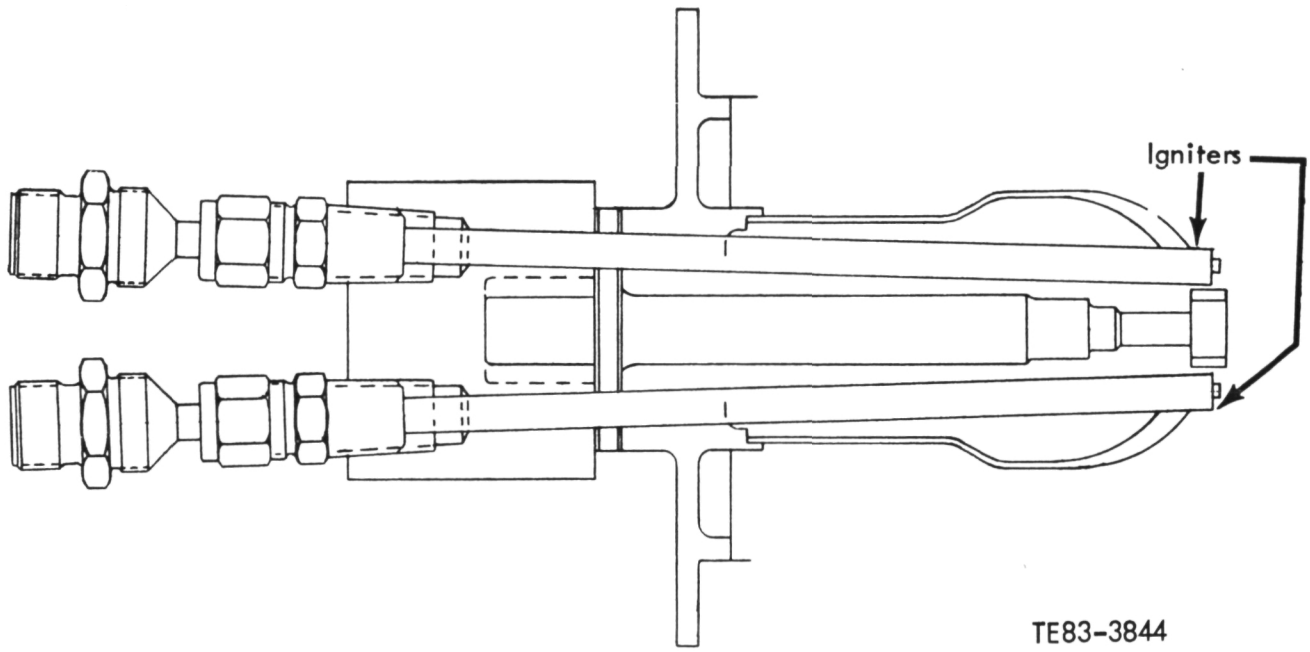


**Figure 33. Schematic showing placement of igniters in centerbody.**

# VII. REGENERATOR DEVELOPMENT

Development of the AGT 100 regenerator system during this period was focused on the reduction of system leakage and the initial steps in raising system temperature capability from its present 982°C (1800°F) level to the 1065°C (1950°F) operational level of the all-ceramic RPD engine. Discussions will center on the design and material developments, the associated rig testing, and the engine test results.

## DESIGN AND MATERIAL DEVELOPMENT

In pursuing the dual goals of lower system leakage and increased $T_6$ regenerator gas inlet temperatures, design and material development effort has been directed toward both the regenerator seals and the disk.

### Outboard Seal

During the last reporting period, the various sources of regenerator system leakage were identified through lab and rig testing, as shown in Figure 34. A series of design changes has been made that is directed toward reducing the leaf and wearface leakage of the outboard seal assembly with the secondary benefits of reduced complexity and lower cost. This sequence is depicted in Figure 35. Temperature measurements in the regenerator hot rig indicated maximum ambient temperatures of 246°C-260°C (475°F-500°F) in the seal leaf environment. A single-piece leaf was designed using high-temperature silicone, which eliminates all leaf joints, a primary source of outboard seal leaf leakage. Leaf rig testing confirmed effectively zero leaf leakage with the design, and hot rig testing (5 hr) of a prototype verified leaf compatibility in the operational environment. Hot rig testing uncovered an attachment problem on the negative crossarm (where disk rotation is from low pressure to high pressure),

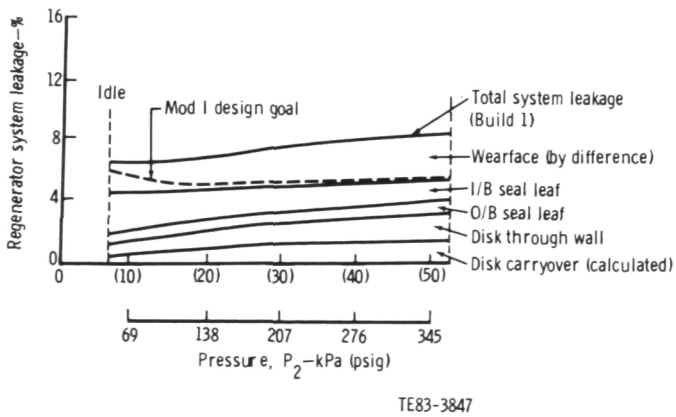


**Figure 34. Breakdown of regenerator leakage losses for AGT 100 BU1.**

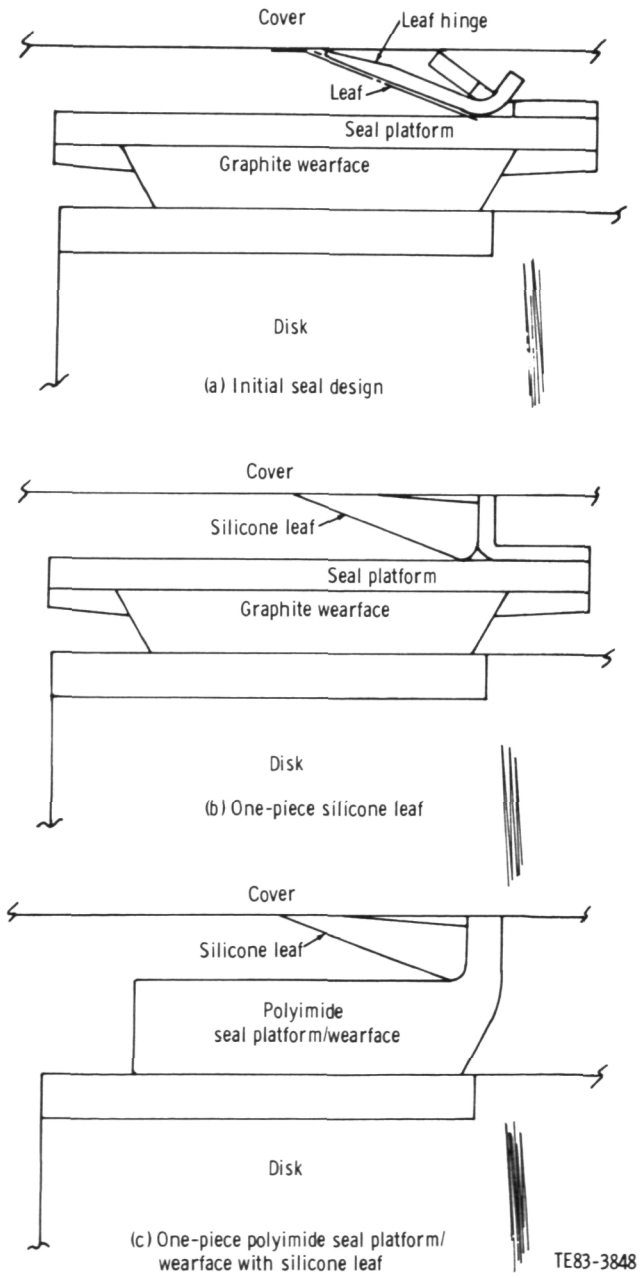


**Figure 35. Outboard seal development sequence.**

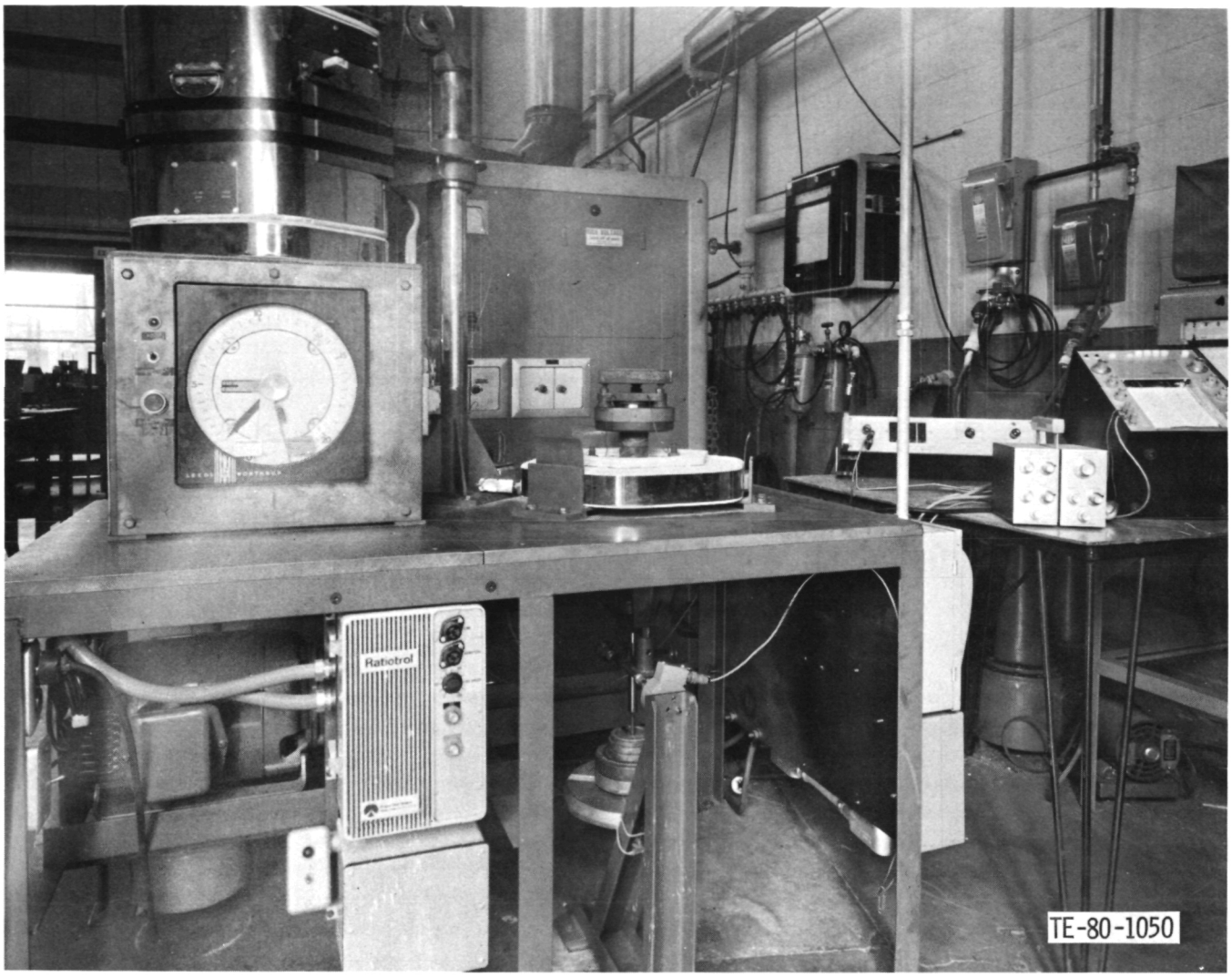


**Figure 36. Friction/wear rig.**

due to the impingement of high-temperature gases. A design change utilizing a thermal barrier is being prepared and will be incorporated into the initial test seals now being fabricated.

The second phase in improving the outboard seal is to utilize a single-piece platform and wearface fabricated from a polyimide-type material. Friction/wear tests of candidate materials were conducted using the friction/wear rig shown in Figure 36.

This rig, used to evaluate friction and wear behavior, uses a 6-in. dia test disk of ceramic regenerator matrix (Corning Glass Works [CGW], code 9461), which is driven by a variable speed electric motor and speed reducer. Testing was conducted at sliding velocities of 0.05, 0.2, and 0.5 m/s (10, 45, and 105 ft/min), equivalent to hub-to-tip crossarm velocities. Candidate seal wearface specimens are held in contact with the rotating disk by a gimballed spider and loaded by a dead weight system. A guide-load-torque (GLT) translator is instrumented to measure the torque loads created by the rubbing interface of the test specimen and the disk. These are then recorded and converted to friction coefficient values.

The screening test consisted of measuring the coefficient of friction at stabilized conditions of room temperature 93°C, 204°C, 316°C (200°F, 400°F, 600°F), and repeating room temperature at sliding velocities of 0.05, 0.2, and 0.5 m/s (10, 45, and 105 ft/min) with a contact pressure of 103 kPa (15 psi). Disk and wearface thicknesses were measured before and after the test for wear characteristics during the 6-hr test. The results of the five materials screened are shown in Table VII. Three of the five exhibited satisfactory performance in the screening tests. Because of availability of material and prior experi-

**Table VII.**
**Friction/wear screening test results (6 hr at 103 kPa [15 lb/in.$^2$] contact pressure).**

| Material | Test conditions: Sliding velocity—m/s (ft/min) | Test conditions: Temperature—°C (°F) | Results: Coefficient of friction, $\mu$ | Results: Wear—mm (in.) |
|---|---|---|---|---|
| DuPont Vespel SP21 | 0.05 (10) | 204/316 (400/600) | 0.12/0.25 | |
| | 0.2 (45) | 204/316 (400/600) | 0.15/0.21 | 0.03 (0.001) |
| | 0.5 (105) | 204/316 (400/600) | 0.08/0.19 | |
| DuPont Vespel SP22 | 0.05 (10) | 204/316 (400/600) | 0.12/0.20 | |
| | 0.2 (45) | 204/316 (400/600) | 0.09/0.19 | 0.03 (0.001) |
| | 0.5 (105) | 204/316 (400/600) | 0.08/0.16 | |
| Amoco Torlon 4275 | 0.05 (10) | 204/316 (400/600) | 0.12/— | |
| | 0.2 (45) | 204/316 (400/600) | 0.14/— | failed at > 260°C (500°F) |
| | 0.5 (105) | 204/316 (400/600) | 0.06/— | |
| Amoco Torlon 4301 | 0.05 (10) | 204/316 (400/600) | 0.14/— | |
| | 0.2 (45) | 204/316 (400/600) | 0.10/— | failed at > 260°C (500°F) |
| | 0.5 (105) | 204/316 (400/600) | 0.09/— | |
| Pure Polybon M (TO454) | 0.05 (10) | 204/316 (400/600) | 0.07/0.12 | |
| | 0.2 (45) | 204/316 (400/600) | 0.07/0.08 | 0.08 (0.003) |
| | 0.5 (105) | 204/316 (400/600) | 0.05/0.07 | |

ence, DuPont Vespel SP22 was tentatively selected for use, and a 100-hr friction/wear test was completed at 260°C (500°F). Total wear was 0.076 mm (0.003 in.), and the friction coefficient varied between 0.05 and 0.07 over the range of sliding velocities tested (0.05 to 0.5 m/s [10 to 105 ft/min]). Work has started to fabricate the first experimental seal from SP22. The seal leaf will be a silicone rubber design, and initial rig testing is planned for the fall of 1983.

## Inboard Seal

Design effort on the inboard seal was limited to friction/wear screening tests of several candidate wearface materials and the initiation of preliminary design of improved leaves and crossarm platforms. The friction/wear testing completed on the rig described earlier included one ceramic-based material that potentially could be used as a monolithic platform and wearface. The remaining four materials were graphite-based, and all were found to be lacking in performance at temperatures above 649°C (1200°F). The results are summarized in Table VIII. This work will continue as derivatives of these materials and several planned plasma spray samples become available.

Design changes planned in the development of the inboard seal include improvements in leaf design, modifications to the wearface, and evolution of a seal platform compatible with 1066°C (1950°F) operation. Preliminary design of leaf and platform changes have been initiated and will continue in the next reporting period, with designs defined and initial test hardware fabricated. An inboard seal assembly utilizing a ZnO/SnO (Ford I-112) plasma-sprayed wearface will be available for hot rig and engine evaluation late in 1983.

## Regenerator Disk

As shown in Figure 34, significant regenerator system leakage could be identified as disk through-wall leakage. Two disks with reduced leakage properties were obtained from Corning Glass Works and were used for both rig and engine testing. A 0.5% to 1% reduction in regenerator system leakage was measured using these disks in rig tests.

The current AGT 100 regenerator disk matrix material (CGW Alumino-Silicate [AS] code 9461) is thermally stable to 1100°C (2012°F), which is satisfactory for the steady-state design goal of 1066°C (1950°F) regenerator inlet temperature but is questionable for the projected engine acceleration transient temperatures up to 1221°C (2230°F). As a result, Allison has developed a laboratory cyclic thermal exposure (CTE) test procedure to evaluate simulated acceleration temperature transients effects on disk samples to define the limiting capabilities of the current AS material as well as the alternate materials.

Previous work at Allison (reported under Ceramic Applications in Turbine Engines [CATE] Program) established that the critical mode of operation for a ceramic regenerator matrix is the combination of the maximum power acceleration

**Table VIII.**
**Friction/wear screening test results.**

| Material | Test conditions | | Results | |
|---|---|---|---|---|
| | Sliding velocity—m/s (ft/min) | Temperature °C (°F) | Coefficient of friction, $\mu$ | Wear—mm (in.) |
| Ceramic (SGC-1) | 0.05 (10) | 427 (800) | 0.12† | After 6 hr |
| (34 kPa [5 lb/in.$^2$] | | 760 (1400)* | 0.50 | 0.064 (0.0025)—wearface |
| contact pressure) | | 1038 (1900)* | 0.94 | 0.14 (0.0055)—disk |
| | 0.2 (45) | 427 (800) | 0.11 | |
| | | 760 (1400)* | 0.20† | |
| | | 1038 (1900)* | 0.83‡ | |
| Graphite composite | 0.2 (45) | 93 (200) | 0.05 | After 8 hr |
| (H/CCD/009-10) | | 316 (600) | 0.19 | 0.043 (0.0017)—wearface |
| (138 kPa | | 538 (1000) | 0.16 | 0.005 (0.0002)—disk |
| [20 lb/in.$^2$] | | 649 (1200) | 0.33 | |
| contact pressure) | | 760 (1400) | ** | |

* high vibration
** excessive vibration
† max velocity possible—0.1 m/s (22 ft/min)
‡ max velocity—0.09 m/s (17 ft/min)

transient followed by stabilized maximum braking. Two matrices, an AS-wrapped monolithic structure, marketed by CGW, and magnesium-alumino-silicate (MAS) extruded and cemented disks, furnished by NGK of Japan, were evaluated in the CATE program and used as a data base for the AGT 100 program. Because of the increase in temperature level, a new candidate proprietary material—MAT, furnished by CGW—was added to the materials under test.

The approach followed in the laboratory rig for the AS matrix has been to increase the peak transient temperature to 1232°C (2250°F), extend the maximum number of cycles to 20,000, and assess the effect of disk-to-disk variability on the resistance to CTE to define the useful limits of AS under AGT operating conditions. The new MAT material is in the early development stage. As a consequence, a simple extruded sample matrix form is being utilized as a vehicle to develop the optimum physical and chemical material properties. Both as-received and thermally exposed specimens are being tested. The early NGK MAS matrix, a 1200°C (2192°F) material, offered a superior processing-fabrication technique but proved to be weak and porous. An impregnated MAS with improved strength and reduced leakage is under development and will be evaluated in the AGT 100 program.

The outstanding result of the preceding six months is the 1177°C (2150°F) peak temperature, 20,000 cycle CTE test of an 1100°C (2012°F) AS specimen, as shown in Figure 37. The mean residual hot face strength of 1979 kPa (287 lb/in.$^2$) is 600 kPa (87 lb/in.$^2$) higher than the tentative acceptable low mean of 1379 kPa (200 lb/in.$^2$) used in the CATE project, while the lower 95% confidence limit is 1289 kPa (187 lb/in.$^2$), as shown by the lower dotted line in the plot. Further, the aluminous keatite material of the hot face spent a total time of 13 hr above the nominal temperature limit of 1100°C (2012°F) for this material, which is well into the time and temperature regime where the phase transformation from keatite to mullite is well advanced without accelerating the CTE damage rate in any way. (The appearance of mullite will still increase the large-scale [disk-size] stresses due to the overall increase in coefficient of expansion.) The striking effect of disk-to-disk variability can be seen by comparing this result from disk 1, a very high strength disk, with the CTE test of a sample from disk 4, which closely fits the mean in the disk population tested during the CATE program. A sample from disk 4 was subjected to the same CTE cycle for 10,000 cycles, which resulted in a residual hot face strength of 1393 kPa (202 lb/in.$^2$)—some 586 kPa (85 lb/in.$^2$) lower in mean strength. It is clearly shown that potentially major increases in ceramic matrix performance can be achieved by process control and reproducibility from disk to disk.

The effect of number of cycles was investigated for 1000 and 100 cycles, all samples from disk 1, and the results are shown in Figures 38 and 39. The corresponding mean hot face strengths are 2344 kPa (340 lb/in.$^2$) and 2303 kPa (334 lb/in.$^2$) for the two samples. It is not known at this time whether

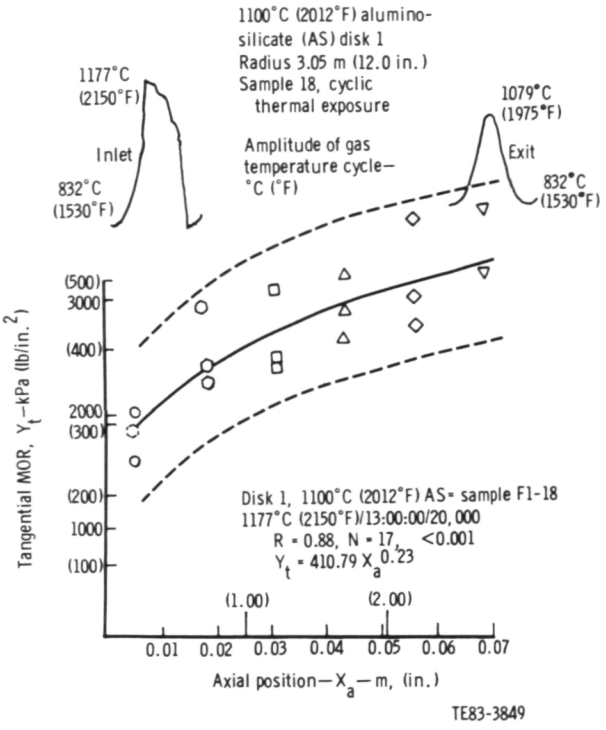


**Figure 37. CTE results of AS matrix after 20,000 cycles to 1177°C (2150°F).**

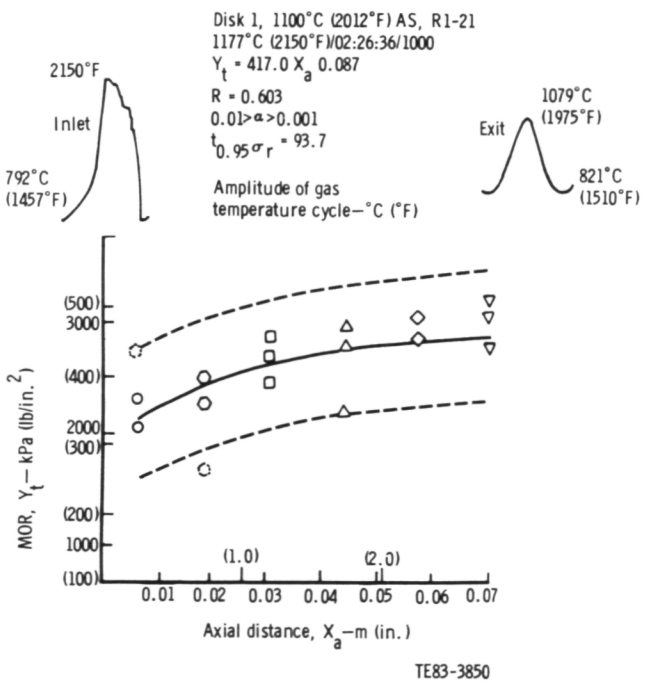


**Figure 38. CTE results of AS matrix after 1000 cycles to 1177°C (2150°F).**

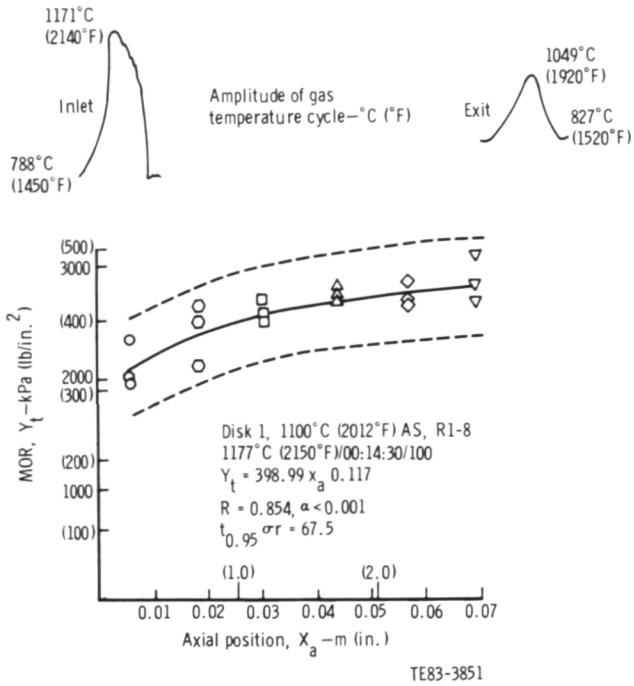


**Figure 39. CTE results of AS matrix after 100 cycles to 1177°C (2150°F).**

the very close agreement in hot face strength between the 100 and 1000 cycle samples is due to a flattening of the curve or variation between samples. The increase in hot face strength from the 20,000 cycle specimen to the 1000 cycle test looks about right; the expected further increase in strength at 100 cycles does not show up.

Two groups of samples of the MAT ceramic matrix material have been received from CGW and tests have been started. This part of the Allison-CGW effort is focused on a new very high temperature candidate material for ceramic regenerators, and the initial investigation is limited to selecting the most promising formulation from a range of MAT materials.

To simplify and expedite this screening operation, an extruded rectangular channel configuration and nonoptimized process are being used, which results in lower than expected strength levels throughout in a fully mature system such as the 1100°C (2012°F) AS matrix. (For example the triangular channel configuration is 37% stronger than the square channel of identical wall thickness and material.) Figure 40 presents the as-received axial modulus of rupture (MOR) distribution for MAT sample group 1. (Two groups of samples are represented—those with 10 and those with 11 walls per sample.) As can be seen, the strength distribution is very nar-

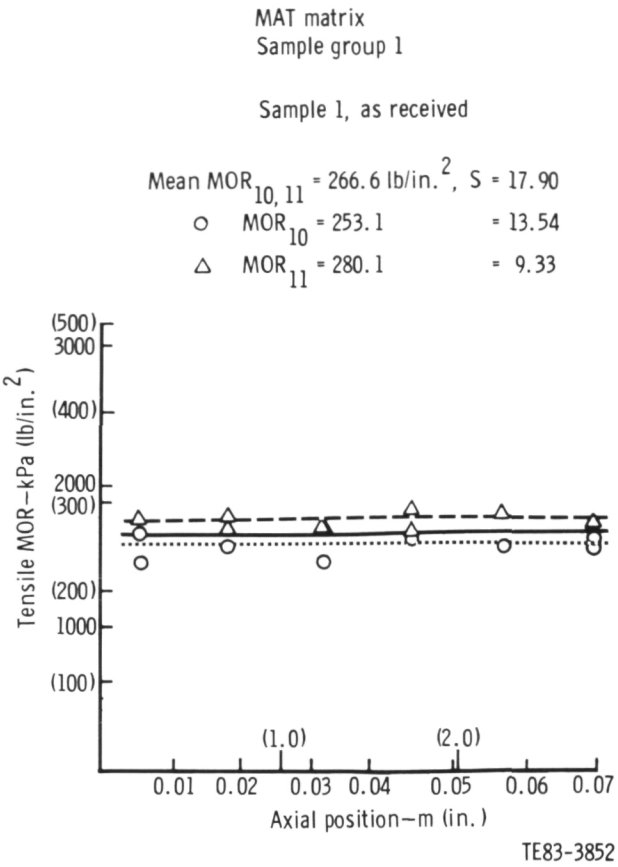


**Figure 40. As-received strength of first MAT sample.**

row and the level is lower than the AS system. Figure 41 presents the axial distribution of the first CTE sample run.

There is a loss in hot face strength similar to that seen for the AS matrix in spite of the change in shape of the strength distribution curve. Comparison of the amplitude of the exit plane gas temperature cycle for the AS and MAT samples (Figures 39 and 41) shows that the axial penetration of the temperature wave is sharply reduced in the MAT due to thicker walls, which limits the damage to the hot face slice. In the AS matrix, the temperature wave penetrates to the exit plane reduced in amplitude by less than half, causing detectable damage to at least the fourth slice (~0.045 m [~1.8 in.]).

Comparison of the CTE damage with a typical 1100°C (2012°F) AS disk sample (disk 4 sample was considered close to the mean for the disk population tested), a sample group 1 MAT piece, and a typical MAS sample is shown in Figure 42. In each case the mean strength distribution is plotted and the lower 95% (-2S) confidence limit is shown to allow an estimate of the effect of variability to be made.

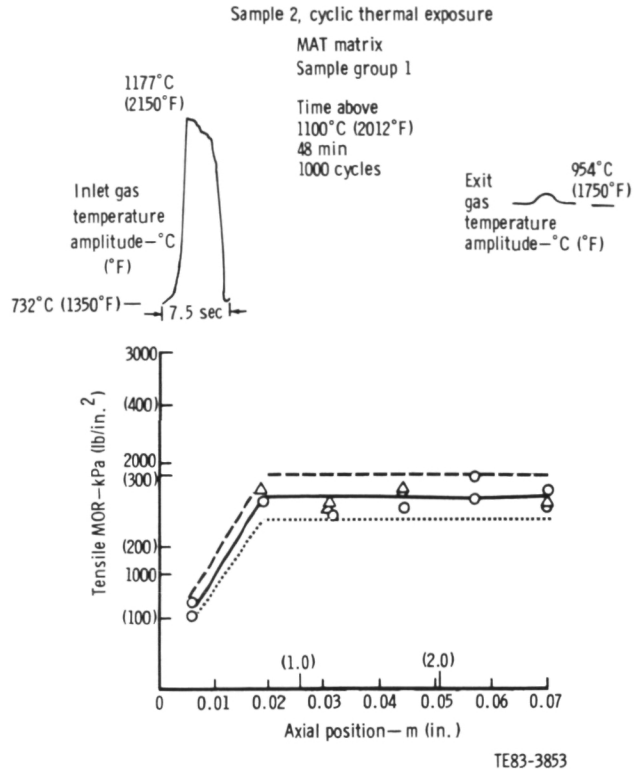


**Figure 41. CTE results of MAT matrix after 1000 cycles to 1000°C (1200°F).**

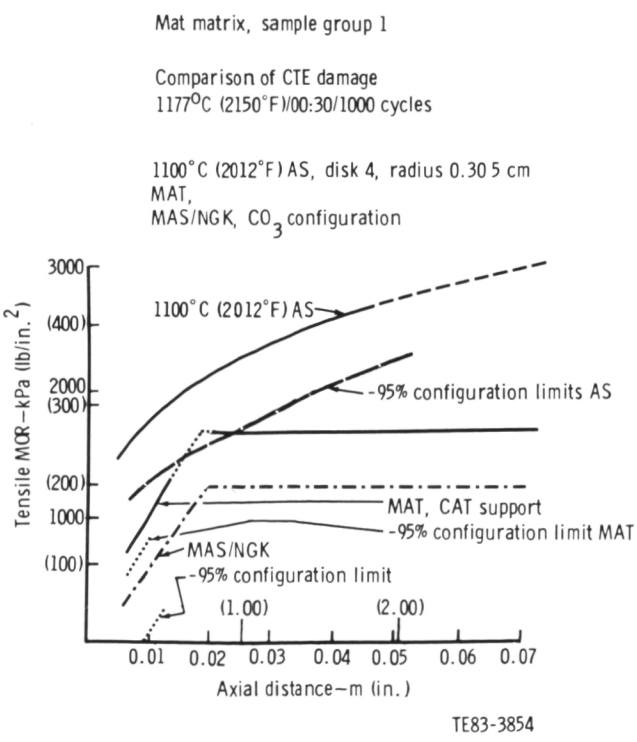


**Figure 42. Comparison of CTE results for AS, MAS, and MAT matrices.**

The 1100°C (2012°F) AS matrix shows significant, but surprisingly small, physical and chemical instability penalties to 1177°C (2150°F) and 20,000 cycles in a selected disk. However, the wrapping process used in fabrication of the disks causes a highly variable disk-to-disk population. This variability, coupled with a peak temperature limit below the current best estimate of the requirements of the AGT engine, establishes the need for a higher temperature disk material.

The initial tests of the new MAT material show an as-received strength level intermediate between the AS and MAS materials. Cyclic thermal exposure results in damage to the hot face strength in the first formulation tested, and work will continue to try to improve the CTE performance to take advantage of the excellent high-temperature potential of this new material.

The results of these laboratory tests of disk samples indicate potential use of the current AS (code 9461) material if the fabrication process can be controlled to match the properties of the best samples tested. However, testing is planned to continue with both the impregnated MAS matrix and the MAT design as a backup to the current disk.

In support of the NGK/MAS development effort, four full-sized test disks are being fabricated for hot rig and engine evaluations. The extruded NGK matrix offers the potential of improved heat transfer characteristics with a rectangular flow passage if the fabrication, strength, and leakage characteristics can be mastered. Because of limitations in extrusion size, the test disks will be of a mosaic design, as shown in Figure 43. Both triangular and rectangular configurations (two disks each) of the impregnated MAS material will be tested during the fall of 1983.

### Parts Fabrication

During this period a new vendor (Tri-Industries, Terre Haute, Indiana) has been selected to replace the original source of regenerator hardware (Harrison Radiator Division, GMC). Orders for engine and development parts have been placed and the first regenerator disk assembly has been received at Allison. All parts will be inspected at Allison, and selected rig testing will be used to ensure the quality of parts completed at Tri-Industries. Hardware condition will be reviewed as test time is accumulated to monitor fabrication and/or design factors that would affect parts reliability.

## RIG DEVELOPMENT TESTING

The AGT 100 regenerator development effort is highly dependent on rig testing to investigate problem areas and to evaluate design changes. The seal leaf leakage rig was used to evaluate the silicone outboard seal leaf discussed earlier and also to study the leaf characteristics of two inboard seal assemblies being qualified for engine use.

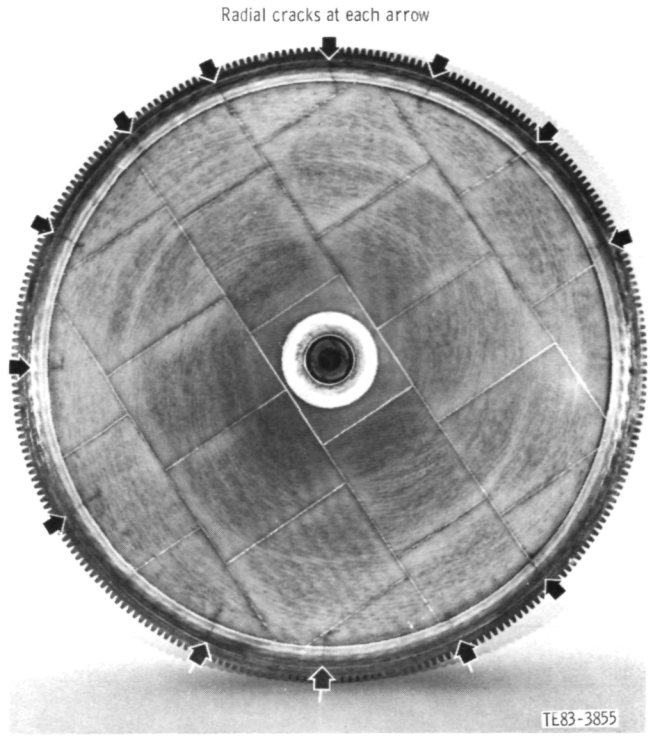


**Figure 43. Mosaic regenerator disk assembly.**

The regenerator hot rig accumulated an additional 115 hr of test time (355 hr total) during the six-month period as 20 seal/disk configurations were tested. Highlights of these tests include the following:

- initial testing of the reduced through-wall leakage regenerator disks
- demonstration of system leakage levels that match the Mod I engine design goals (See Figure 44)
- qualified sets of regenerator hardware for both engines S/N-1 and S/N-2
- initial testing of a prototype silicone leaf seal

Hot rig testing will continue as required to support both the design/development efforts and qualifications of engine hardware.

A key part in achieving a design compatible with the 1066°C (1950°F) operational temperature goal is upgrading the hot test rig. These changes are to (1) incorporate a simulated ceramic exhaust duct to match engine gas flow into the regenerator, (2) use the engine regenerator cover/housing to provide actual air inlet flow conditions to the regenerator disk, and (3) upgrade rig operating temperatures

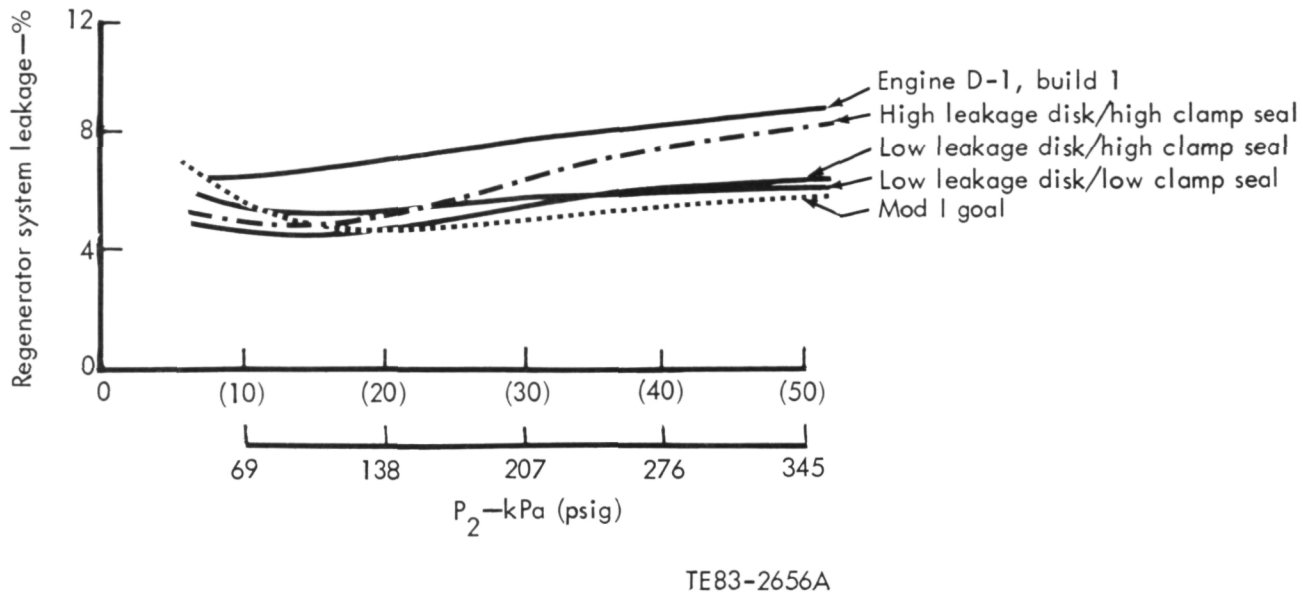


**Figure 44. Regenerator system leakage hot rig test results for AGT 100.**

from the current 982°C (1800°F) to 1066°C (1950°F) at part-power conditions. These and other changes are summarized in Figure 45. Item 2 will permit the rig testing of a complete engine regenerator subassembly (disk, seals, and cover) to substantially eliminate rig-to-engine differences in the evaluation of leakage, effectiveness, and friction-torque characteristics. The design effort has been completed and parts fabrication initiated in preparation for rebuilding the hot rig at approximately the year's end.

## ENGINE TESTING

The regenerator hardware for the AGT 100 has satisfactorily met the engine operational requirements through the first eight engine builds and approximately 9 hr of test time. Testing has included demonstrations of 100% engine speed and regenerator gas inlet temperatures to ~910°C (~1670°F)—the first experience with the ceramic bulkhead and transition duct to operate at full pressure and at elevated temperature. One failure of the bulkhead occurred on Buildup 5, shown in Figure 46. This was caused by the thermal growth of the metal power turbine coupling/piston ring into the ceramic bulkhead, shown in Figure 47, and occurred on the first sustained engine test at elevated temperatures. Design changes of the coupling/piston ring corrected this problem, and three subsequent engine builds (~6 hr testing) showed no recurrence of the problem.

No operational problems with the seals or disk have been evident in testing thus far. The bulkhead O-ring support (see Figure 47) is fabricated from high-temperature silicone and has shown evidence of locally excessive temperatures where it is adjacent to the combustor. A material change and/or a local radiation shield is being evaluated.

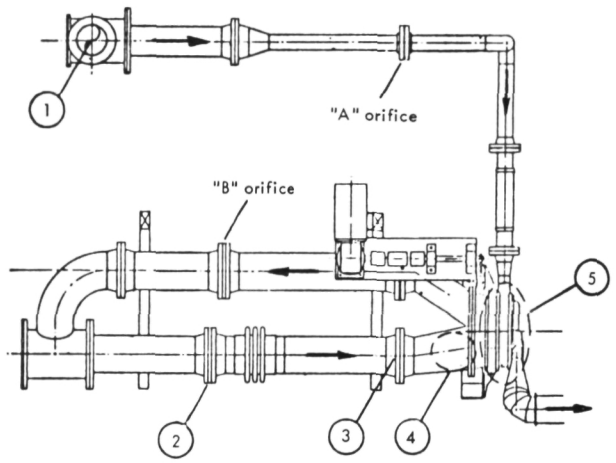


**Figure 45. AGT 100 regenerator hot rig modifications.**

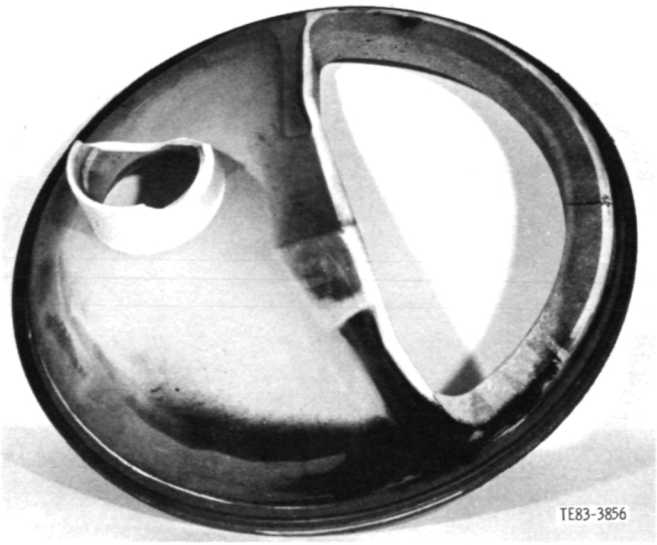


**Figure 46. Ceramic bulkhead failure on TD.**

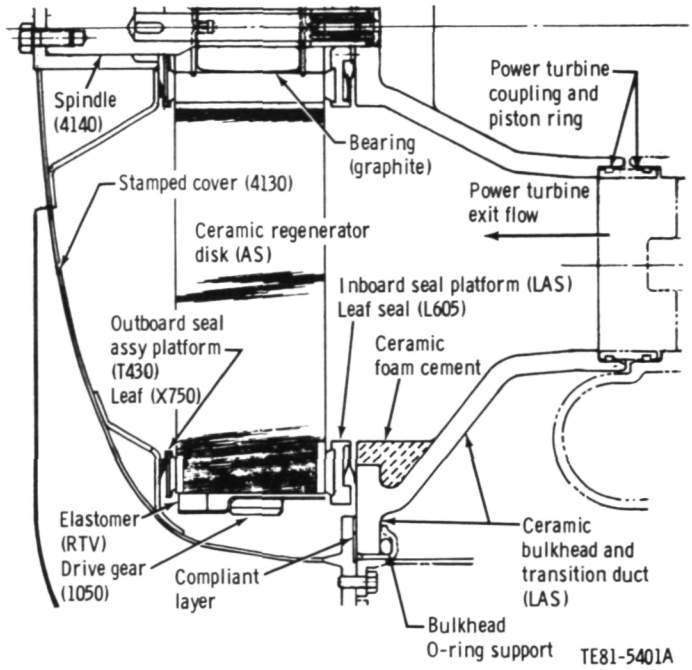


**Figure 47. Regenerator seal platform/exhaust duct installation.**

# VIII. SECONDARY SYSTEMS

## 8.2 POWER TRANSFER CLUTCH

The power transfer clutch has been rig developed and is now available for engine use. It had been reported earlier (July-December 1982 Semiannual Report) that this clutch lacked sufficient torque capacity and that a dual-piston clutch was being developed. However, the problem was found to be insufficient drainage of a circuit designed to equalize oil flow. This lack of drainage caused pressure to develop on the drainage side, eliminating the pressure differential needed to develop torque. Increasing the drainage area eliminated the back pressure and thereby increased the torque capability of this clutch to an acceptable level. Consequently, the original, single-piston configuration was retained.

## 8.3 BEARINGS/SEALS

A redesign was completed to provide positive retention of the two turbine carbon main-shaft seals. A difference in thermal expansion existed between the seal housings and the bearing supports into which the seal housing fits. Thus, as the engine came up to operating temperature, the seal housings expanded more than the bore in which they were mounted. This caused the seal housing to yield. On cooling, the seal became loose in the support and, in the case of the power turbine, came out of the bore far enough to rub the rotor.

The following design changes have been made to change this situation:

- addition of spiral retaining rings to seals
- reduction of seal-to-housing fit from 0.079 mm (0.0031 in.) tight (diametral) to 0.058 mm (0.0023 in.) tight (diametral)
- increase seal-to-shaft clearance from 0.020 mm (0.0008 in.) minimum to 0.076 mm (0.003 in.) minimum diametral
- procure seal housings with a thermal coefficient to match the bearing supports

## 8.4 SECONDARY AIRFLOW SYSTEM

The secondary airflow system for the AGT 100 engine is concerned with minimizing leakage flow, isolating the bearing compartments from hot gas, and determining thrust balance loading to ensure proper selection and operation of bearings.

As part of pre-and post-test analysis, an assessment was made of the leakage flows based on buildup and/or teardown measurements. Each build produced additional information about the leakage flows. The present status of the understanding of the secondary flow system is summarized in Table IX, which represents the post-test analysis of BU8. Based on measured hardware, measured pressure, and performance synthesis, the indicated breakdown of leakage flows was deduced. Regenerator seal leakage is discussed in Section VII, "Regenerator Development," of this report. This summary is consistent with the engine performance analysis for Record 11163, BU8, discussed in Section II, subsection 2.2 of this report.

Design goals and BU8 values are shown in Table X. Turbine backplate leakage represents an appreciable percentage of the increased leakage. This leakage results from the tolerance stack of engine parts and the allowance for thermal growth due to differential metal temperature.

During the next reporting period, turbine nozzle flow calibration for both gasifier and power turbines will be experimentally acquired to further validate the deduced secondary flow network. Attention will be directed toward proposing design modifications to reduce leakage paths, particularly those with the ceramic hardware.

## Table IX.
## Leakage analysis

| | | Design max power—% | BU8 Rec 11163—% |
|---|---|---|---|
| R1 | Pressure vessel flange leakage at gasifier | 0.19 | 0.39 |
| R2 | De-oiler | 0.52 | 1.36 |
| R4 | Power turbine scroll splitline | 0.11 | 0.12 |
| R5 | Pressure vessel flange leakage at power turbine | 0.01 | 0.01 |
| R6 | Leakage from pressure vessel to block corner cavity | 0.07 | 0.17 |
| R7 | Face seal at power turbine backplate | 0.07 | 0.75 |
| R8 | Front compressor shaft ring seal | 0.0 | 0.0 |
| R9 | Compressor scroll splitline leakage | 0.10 | 0.21 |
| R10 | Gearbox ring seal at power turbine | 0.13 | 0.47 |
| R11 | Power turbine ring seal | 0.13 | 0.88 |
| R12 | Pressure vessel flange leakage at regenerator | 0.26 | 0.29 |
| R13 | Power turbine discharge ring seals | 0.25 | 1.06 |
| R14 | Power turbine feed passage | 0.26 | 1.36 |
| R15 | Front compressor block corner ring seal | 0.09 | 0.26 |
| R16 | Front compressor flow-path ring seal | 0.07 | 0.28 |
| R17 | Rear compressor flow off-take | 0.81 | 1.43 |
| R18 | Gasifier bearing vent | 0.29 | 0.63 |
| R19 | Gasifier bearing ring seal—compressor side | 0.13 | 0.17 |
| R20 | Gasifier bearing cross flow passage | 0.26 | 0.73 |
| R21 | Compressor shaft supply holes | 0.16 | 0.54 |
| R22 | Gasifier ring seal | 0.10 | 0.27 |
| R23 | Gasifier bearing ring seal—turbine side | 0.16 | 0.46 |
| R24 | Face seal at gasifier turbine backplate | 0.04 | 0.46 |
| R25 | Gasifier exit ring seals | 0.25 | 0.82 |
| R26 | Gasifier turbine scroll splitline | 0.04 | 0.02 |
| R27 | Transfer tube flange leakages | 0.15 | 0.11 |
| R28 | Gasifier backplate | — | 1.29 |
| R29 | Power turbine backplate | — | 1.78 |
| R30 | Gasifier leakage by thermal isolator | — | 0.04 |
| R31 | Power turbine leakage by thermal isolator | — | 0.06 |

Note: Flows are in % of compressor inlet flow.

## Table X.
## BU8 leakage summary.

| | Sink | Design max power—% | BU8 Rec 11163—% |
|---|---|---|---|
| A | Before gasifier turbine | 0.08 | 0.48 |
| B | Between turbines | 0.53 | 3.25 |
| C | After power turbine | 0.38 | 3.72 |
| D | Overboard leakage | 0.66 | 1.16 |
| E | Gearbox | 0.51 | 1.36 |
| | **Source** | | |
| F | Compressor discharge | 0.96 | 2.90 |
| G | Regenerator discharge | 1.20 | 7.07 |
| | Total | 2.16 | 9.97 |

# IX. MATERIALS DEVELOPMENT

## 9.1 THERMAL BARRIER DEVELOPMENT

### CBO Mullite Material Development

Production of thermal barrier materials in the mullite-cordierite system has continued at Carborundum (CBO). These materials, which are 59/41 mullite to cordierite, are produced using sol-gel derived powders and pressureless sintering techniques. Work during this period has focused on batch-to-batch consistency in microstructure and material shrinkage variability.

Sixteen consecutive batches have been prepared with the same microprocessor-controlled firing treatment. X-ray diffraction analysis (XRD), coefficient of thermal expansion (CTE), modulus of rupture (MOR), and percent shrinkage have been completed for 10 of the 16 batches. In all cases, XRD showed that mullite was the major phase and cordierite the minor. Table XI lists the results according to batch number.

### Zircon Material Development

Effort this period has centered on a scaling-up of the powder process and characterization of microstructures. A 3.6-kg (8-lb) lot of spray-dried powder was procured, and studies to determine the best steps for pressing the powder are underway.

The spray-dried powder in Figure 48, nominally characterized with the scanning electron microscope (SEM), shows that the granules are spherical with dimple-like depressions. Nominal sieve analysis has shown the lot to be 93% by weight less than 60 mesh (0.250 mm). Granules greater than 60 mesh were removed prior to pressing.

In the studies performed, it was shown that the best microstructures are obtained after the granules have been stored in a humid environment. In this case, the granules were stored for 48 hr in a desiccator partially filled with water. Test plugs were then isopressed with and without storage in the humid environment. The preforms were uniaxially pressed into a die at 55.2 MPa (8 ksi), followed by isopressing at 206.8 MPa (30 ksi). All test plugs were fired for 4 hr in the same furnace at 1425°C (2597°F), and the percent diametral shrinkage was recorded for each.

A significant variation in microstructure was noted between the surface and central bulk region of some of the test plugs. For minus 60 mesh as-sprayed granules, there was a greater amount of porosity observed near the surface of the plugs, as can be seen in Figure 48a. Figure 48b shows far less porosity at the center. The same two plug locations after storage in a humid environment are shown in Figure 49. There was a marked improvement in the microstructure near the surface (shown in Figure 49a), clearly supporting the need to store the granules in a humid environment. The percent of diametral shrinkage was recorded for both the as-sprayed

**Table XI.**
**CBO mullite material properties.**

| Batch No. | CTE at 1300°C (2372°F) Mean — in./in./°C (in./in./°F) | CTE at 1300°C (2372°F) Std dev— in./in./°C (in./in./°F) | Four-pt MOR Mean — MPa (ksi) | Four-pt MOR Std dev— MPa (ksi) | Sample size | Density— g/cm³ | Shrinkage—% |
|---|---|---|---|---|---|---|---|
| 83-0 | 4.96 (2.75) | 0.110 (0.061) | 85.08 (12.34) | 9.24 (1.34) | 8 | 2.73 | 27.5 |
| 83-1 | 4.88 (2.71) | 0.150 (0.083) | 109.21 (15.84) | 7.93 (1.15) | 10 | 2.75 | 29.8 |
| 83-2 | 4.94 (2.74) | 0.050 (0.027) | 101.08 (14.66) | 13.86 (2.01) | 11 | 2.74 | 27.9 |
| 83-3 | 5.15 (2.86) | 0.062 (0.034) | 94.46 (13.70) | 9.79 (1.42) | 13 | 2.71 | 28.6 |
| 83-4 | 5.69 (3.16) | 0.000 (0.000) | 87.70 (12.72) | 7.38 (1.07) | 11 | 2.72 | 27.5 |
| 83-5 | 4.92 (2.73) | 0.075 (0.042) | 121.97 (17.69) | 7.03 (1.02) | 12 | 2.76 | 25.2 |
| 83-6 | 4.92 (2.73) | 0.086 (0.048) | 105.01 (15.23) | 9.10 (1.32) | 7 | 2.70 | 24.04 |
| 83-7 | 4.94 (2.74) | 0.130 (0.072) | 93.84 (13.61) | 9.38 (1.36) | 8 | 2.77 | 25.42 |
| 83-8 | 4.83 (2.68) | 0.072 (0.040) | 110.25 (15.99) | 8.48 (1.23) | 10 | 2.81 | 24.71 |
| 83-9 | 4.94 (2.74) | 0.168 (0.093) | 94.80 (13.75) | 11.31 (1.64) | 8 | 2.77 | 24.34 |

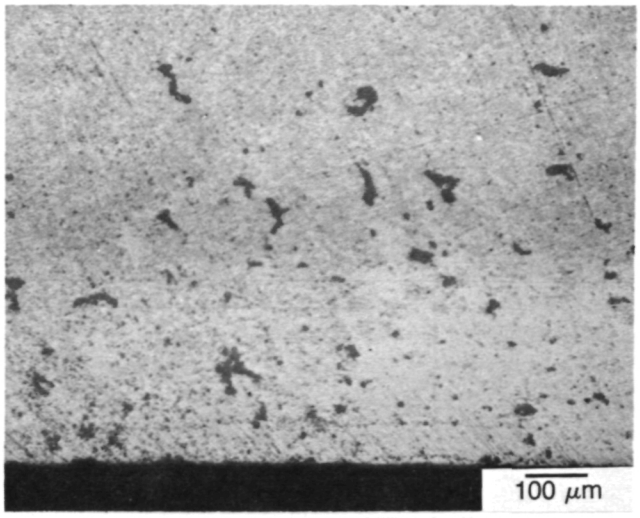


(A) SURFACE

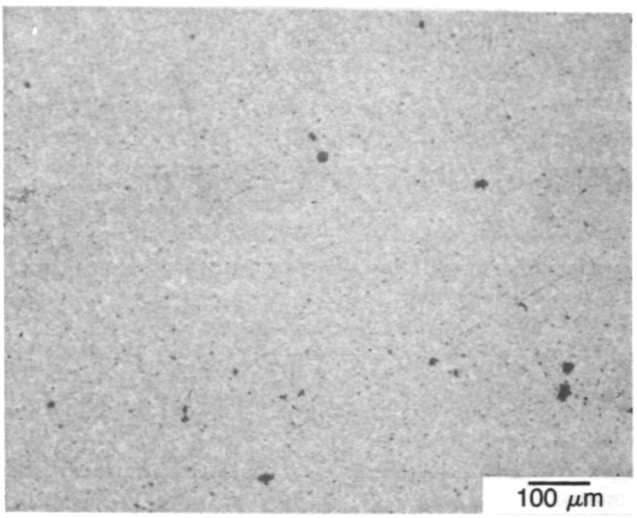


(B) BULK

TE83-3845

**Figure 48. As-sprayed minus 60 mesh granules.**

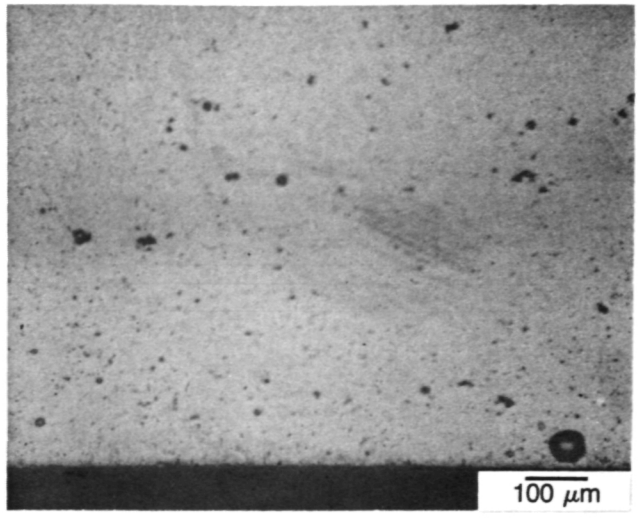


(A) SURFACE

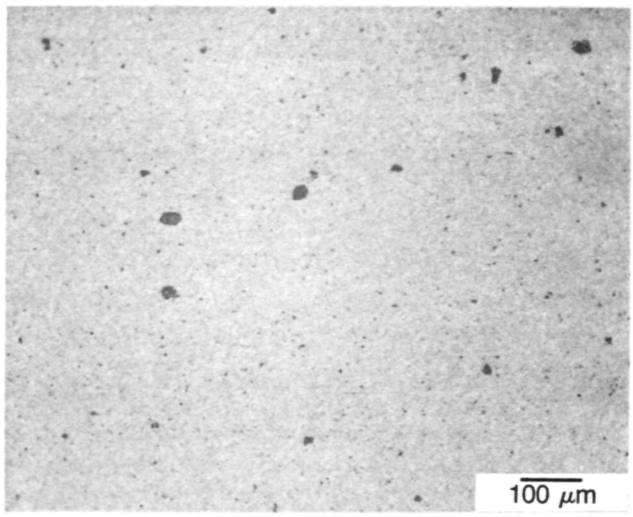


(B) BULK

TE83-3846

**Figure 49. Humid environment minus 60 mesh granules.**

and minus 60 mesh-sized granules. Table XII shows the effect of granule size and humidity on the percent of diametral shrinkage.

In summary, the powder process can be scaled-up by utilizing spray-drying to prepare the granules for pressing. Controlled forming procedures were observed to yield more uniform microstructures with little effect on shrinkage. Future work will continue to focus on assessments of batch-to-batch variability.

**Table XII.**
**Percent diametral shrinkage.**

| | As-sprayed— % | -60 mesh— % |
|---|---|---|
| As-sprayed | 16.72 | 16.54 |
| Stored in high humidity | 16.12 | 16.12 |

## 9.2 SILICON CARBIDE COMPONENT DEVELOPMENT, CHARACTERIZATION, AND QUALIFICATION

Efforts during this reporting period continued to focus on the fabrication, characterization, and qualification of silicon carbide and silicon nitride components. Development activities at CBO on the gasifier rotor concentrated on injection molding trials of engine configuration rotors (ECRs) free of surface indications. These trials were divided into three groups:

1. process routing based on the prototype rotor process,
2. experimental processing with various combinations of sprue bushings and injection nozzles, and
3. optimum bushing/nozzle combination with and without thermal control of the mold base (rotor backface).

Characterization of the initial group of ECRs (48 total) progressed with spin-to-failure tests of eight rotors. Processing of combustors and scroll assemblies continued, including delivery of four combustors. Development of reaction-bonded SiC material progressed with the forming of rotors, scroll bodies, and other components.

### Gasifier Rotor

**Sintered Alpha SiC.** The sixth semiannual report (1 July 1982-31 December 1982) reported receipt of 47 ECRs. Subsequent accounting showed receipt of 48 rotors with one used for display purposes. The rotors were produced following a process routing established for the prototype rotors. A total of 17 spin tests are planned. A tabular summary of the eight spin tests thus far completed is shown in Table XIII. Note the comments that orbiting of the rotor (whip) on the quill drive shaft and multiple balancing was frequently required (test Nos. 4 through 8). Test numbers 6, 7, and 8 were invalid, and this prompted an investigation into the dynamic stability of the rig. The investigation was initiated in July 1983 and will be subsequently reported.

The overall disposition of the 48 ECRs is summarized as follows:

| | |
|---|---|
| Sectioned | |
| NDE | 13 |
| Strength (rings and disks) | 3 |
| Spin | |
| Completed | 8 |
| Pending | 9 |
| Machining | 2 |
| Display | 1 |
| Scrap | 12 |
| Total | 48 |

The disposition is explained as follows:

- NDE—visual and FPI
- strength
  - rings—internal pressure load strength samples sectioned from rotors (see Figure 50)
  - disks—biaxial strength determination
- spin—spin tests to burst for strength characterization
- machining—samples for trial machining of the blade tip contour
- display—visual aid
- scrap—rotors not suitable for additional tests because of surface flow lines, porosity, and FPI indications

A serialized accounting of the 48 rotors is shown in Table XIV. The visual and FPI examination revealed the rotors were B and C quality. B quality is by definition a rotor that can be upgraded by minor blending of a surface indication; C quality is a nonsalvageable rotor. All but the following four exceptions were judged C quality (not engine candidates): serial numbers FX30550, FX31553, FX31558, and FX31569.

Early in this reporting period, rotor processing trials were initiated addressing the goal of ECRs free of surface indications (flow lines, porosity, and FPI indications). These trials were divided into the following three groups:

1. optimized process routing with microprocessor control based on the prototype rotor process
2. experimental processing with various combinations of sprue bushings and injection nozzles
3. optimum bushing/nozzle combination with and without thermal control of the mold base (rotor backface)

The trials are listed by group in Table XV. As can be seen, 132 rotors were molded with a net yield

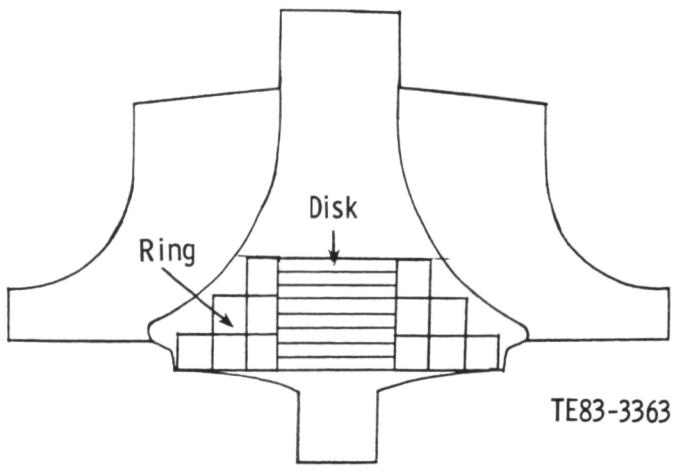


**Figure 50. Internal pressure load strength samples (sectioned from rotors).**

## Table XIII.
## Spin test, ECR samples (first 100).

| No. | S/N | Surface quality (visual/FPI)* | Test date | Configuration | | | Rig configuration | Failure | Comment | Valid test |
|---|---|---|---|---|---|---|---|---|---|---|
| | | | | Attach | Nose | Pitch/ Polar | | | | |
| 1 | 31572 | C<br>Severe flow lines and porosity | 10/22/82 | Test adapter | Trimmed | 0.95 | String, 3/16 dia quill | Burst at 48,500 rpm | | Yes |
| 2 | 30549 | C<br>Cracks and flow lines | 10/22/82 | Test adapter | Trimmed | 0.95 | String, 3/16 dia quill | Burst at 75,000 rpm | S/N 31,551 originally scheduled, blades broken in handling | Yes |
| 3 | 31566 | C | 11/24/82 | Shaft simul Zircon insul | Trimmed | 1.94 | String, 3/16 dia quill | Rotor release at 33,500 rpm | Shaft stub fracture | No |
| 4 | 31559 | B<br>Flow lines | 4/29/83 | Shaft simul Mullite ins | Trimmed | 1.94 | String, 3/16 dia quill | Burst at 95,200 rpm | Instability (large whip) at 38,000 rpm drove through it; retraced, whip repeated | Yes |
| 5 | 30542 | B/C<br>Bent and broken airfoils | 5/13/83 | Test adapter | Trimmed | 0.95 | String, 3/16 dia quill | Burst at 93,250 rpm | Two balance attempts; Second was successful | Yes |
| 6 | 30557 | C<br>Broken airfoils | 6/8/83 | Test adapter | Trimmed | 0.991 | String (1) & (2)<br>Support bearing (3) | Rotor release at 77,000 rpm | (1) Severe whip at 77,600 rpm; quill loose in adapter; classic out of balance<br>(2) Refit quill and rebalance; achieved 81,500 rpm; severe whip; bent shaft<br>(3) Stagnation at 77,000 rpm; fatigued and failed shaft; rotor released | No |
| 7 | 31563 | C<br>Bent vane | 6/10/83 | Test adapter | Full | 1.07 | String, 3/16 dia quill | Rotor release at 56,000 rpm | Severe whip at 42,500 rpm; drove through it, shaft failed at 56,000 rpm | No |
| 8 | 31553 | C<br>Bent vane | 6/24/83 | Test adapter | Full | 1.07 | Support bearing | Rotor release at 65,500 rpm | At 75,000 rpm; stagnation against support bearing on deceleration shaft failed at 65,500 rpm | No |

*B = B/B
C = C/C

## Table XIV.
## Disposition—48 engine configuration rotors.

| No. | S/N | Visual | FPI | Dimensional | Disposition | Spin date |
|---|---|---|---|---|---|---|
| 1 | FX 30533 | N—FL | N—FL | N—DV | Sectioned | |
| 2 | 30534 | A—LP | A—FL,LP | N—DV,BV | Rings and disks | |
| 3 | 30535 | A—FL | A—FL | N—DV | Reserve | |
| 4 | 30536 | A—FL | A—FL | N—DV,BV | Reserve | |
| 5 | 30537 | A—FL | A—FL | N—DV | Sectioned | |
| 6 | 30538 | N—FL,C,B | N—FL,C,B | N—DV | Sectioned | |
| 7 | 30539 | A—FL | A—FL | N—DV | Reserve | |
| 8 | 30540 | A—FL | A—FL | N—DV,BV | Rings and disks | |
| 9 | 30541 | A—FL | A—FL | N—DV | Sectioned | |
| 10 | 30542 | A—LP | A—LP | N—DV,BV | Spin test—93,250 | 5/13/83 |
| 11 | 30543 | A—B | A—B | N—DV | Sectioned | |
| 12 | 30544 | A—FL | A—FL | N—DV | Sectioned | |
| 13 | 30545 | A—FL | A—FL | N—DV,BV | Sectioned | |
| 14 | 30546 | A—LP | A—LP | N—DV,BV | Sectioned | |
| 15 | 30547 | A—LP | A—LP | N—DV | Sectioned | |
| 16 | 30548 | A—FL | A—FL | N—DV | Sectioned | |
| 17 | 30549 | N—FL,C | N—FL,C | A— | Spin test—75,000 | 10/22/82 |
| 18 | 30550 | A—FL | A—FL | A— | Sectioned | |
| 19 | 30551 | A—FL | A—FL | A—BV | Spin test—68,000 | 7/29/83 |
| 20 | 30552 | A—FL | A—FL | N—BV | Rings and disks | |
| 21 | 30554 | A—FL,LP | A—FL,LP | N—BV | Reserve | |
| 22 | 30555 | A—FL | A—FL | A— | Spin test—110,300 | 7/15/83 |
| 23 | 30557 | A—FL,LP | A—FL,LP | N—BV | Spin test—77,000* | 6/8/83 |
| 24 | 31541 | A—LP | A—LP | N—BV | Reserve | |
| 25 | 31542 | A—LP | A—LP | N—BV | Machining trials | |
| 26 | 31544 | A—LP | A—LP | N—BV | Spin test—104,000 | 7/19/83 |
| 27 | 31545 | N—HP | N—HP | A— | Sectioned | |
| 28 | 31546 | A— | A—LP | N—BV | Spin test—88,000 | 7/20/83 |
| 29 | 31547 | N—FL | N—FL | A— | Sectioned | |
| 30 | 31549 | A—FL | A—FL | N—BV | Spin test—88,300 | 8/24/83 |
| 31 | 31550 | A—FL,LP | A—FL,LP | N—BV | Reserve | |
| 32 | 31551 | N—HP | N—HP | N—BV | Reserve | |
| 33 | 31552 | A—FL | A—FL | N—BV | Display | |
| 34 | 31553 | N—LP | N—LP | A— | Spin test—65,500* | 6/24/83 |
| 35 | 31554 | N—HP | N—HP | A— | Spin test—88,600 | 8/5/83 |
| 36 | 31556 | N—FL,LP | N—FL,LP | N—BV | Reserve | |
| 37 | 31557 | N—FL,LP | N—FL,LP | A— | Reserve | |
| 38 | 31558 | A—LP | A—LP | A— | Spin test—58,000* | 7/12/83 |
| 39 | 31559 | A—FL | A—FL | A— | Spin test—95,200 | 4/29/83 |
| 40 | 31560 | N—FL,HP | N—FL,HP | A— | Reserve | |
| 41 | 31563 | A—FL | A—FL | N—DV | Spin test—56,000* | 6/10/83 |
| 42 | 31565 | N—HP | N—HP | A— | Reserve | |
| 43 | 31566 | N—FL | N—FL | A— | Spin test—33,500* | 11/24/83 |
| 44 | 31567 | N—FL | N—FL | A— | Reserve | |
| 45 | 31568 | N—FL,HP | N—FL,HP | A— | Spin test—90,550 | 8/9/83 |
| 46 | 31569 | A—LP | A—LP | A— | Spin test—86,200 | 8/9/83 |
| 47 | 31571 | N—FL,HP | N—FL,HP | A— | Machining trials | |
| 48 | 31572 | N—HP | N—HP | A— | Spin test—48,500 | 10/22/82 |

A = acceptable
N = not acceptable
FL = flow lines
LP = light porosity
HP = heavy porosity
B = blister
C = crack
DV = distorted vane
BV = broken vane
* = invalid test (excessive whip)

of 29 sintered rotors (22%). The rotors were NDE inspected and allocated for subsequent tests. The results of the inspection and the disposition of the rotors are summarized in Table XVI.

The dimensional data presented in Table XVI revealed that the exducer throat was typically closed by approximately 1 mm (0.040 in.) at the outside diameter. Review of the rotor processing identified a slumping of the exducer blade tip during the sinter operation. Design and manufacture of a blade tip support insert were initiated, and trials are planned during the next reporting period (July-December 1983).

The six rotors identified with a large grain structure (surface and internal) were the result of a sinter furnace temperature control malfunction. The control governed to a 25°C (45°F) change over the required temperature during the sinter operation. This resulted in excessive grain growth. However, these rotors are being strength evaluated (spin), as the surface quality is generally good.

The remaining groups of ECRs (groups 2 and 3) are progressing through the processing sequence with deliveries anticipated during the next six months. Evaluation and disposition similar to that shown in Table XVI for group 1 will be accomplished with the additional goal of identification of candidate engine rotors.

**Reaction-Bonded SiC.** The development of a reaction-bonded SiC material for use in injection-molded gasifier rotors is currently being addressed at CBO. During the current reporting period, a total of 26 rotors was molded using the prototype configuration tool. Visual inspection of the rotors showed the surfaces were generally free of indications. Sectioning of representative rotors indicated complete siliconization throughout the entire rotor hub. Further processing of this group of rotors is proceeding, with anticipated delivery in late 1984.

## Gasifier Scroll Assembly

Efforts at CBO during this period focused on the fabrication of gasifier scroll assembly components. Substantiated progress has been realized in the development of slip casting procedures for silicon carbide components, most notably for the gasifier scroll assembly. The previous difficulties

**Table XV.**
**Process development, gasifier turbines.**

| P/N | No. molded | CBO S/N | As-molded B- or better | Sintered rotors Quantity | Sintered rotors Date | Condition | |
|---|---|---|---|---|---|---|---|
| | | | | Actual↓ | | | |
| AA100395 | 42 | 486 to 527 | 14 | 9 | 6/3 | Reed + microprocessor | Group 1 |
| (oval shaft) | 90 | 528 to 617 | 21 | 20 | 6/8 | Reed + microprocessor | |
| | 110 | 618 to 727 | 33 | 29 | 7/18 | Reed (65.09 mm [2.5625 in.] shot) | |
| | 16 | 728 to 743 | 0 | | | Reed (66.68 mm [2.6250 in.] shot) | |
| AA100932 | 138 | 744 to 881 | 16 | 12 | 8/9 | SB-1, N-1 experimental | |
| (round shaft) | 15 | 882 to 896 | 7 | 6 | 8/22 | SB-1, N-1 (15) | Group 2 |
| | 20 | 897 to 916 | 5 | 4 | 8/31 | SB-2, N-2 (20—same as 15) | |
| | 33 | 917 to 949 | 13 | 10 | 9/9 | SB-2, N-2 experimental | |
| | 15 | 950 to 964 | 10 | 8 | 9/16 | SB-2, N-2 (15) | |
| | 15 | 965 to 979 | 7 | | | SB-3, N-1 experimental | |
| | 20 | 980 to 999 | 8 | 12 | 9/22 | SB-3, N-1 (20) | |
| | 100 | 1000 to 1099 | 17 | 14 | 10/1 | SB-2, N-2 (100) without heat | Group 3 |
| | 100 | 1100 to 1199 | 29 | 23 | 10/15 | SB-2, N-2 (100) with heat | |
| | 76 | 1200 to 1275 | 0 | 0 | | Variable conditions | |
| | 100 | 1276 to 1375 | 27 | 22 | 10/31 | SB-2, N-2 (100) with heat | |
| | | | | Estimated↑ | | | |

169 deliverable rotors (estimated)

Code:
Reed = type of compounder
SB-1, -2, -3 = three sizes for the injection mold sprue bushing
N-1, -2 = two sizes for the injection mold nozzle

## Table XVI.
## Summary, development ECRs.

**Group 1 (reed + microprocessor)**

| CBO S/N | Allison S/N | Visual | FPI | Dimensional* rotor/throat—mm | Comment | Disposition |
|---|---|---|---|---|---|---|
| 508 | FX 34138 | C | C | 8.15 | Exducer curled | Reserve |
| 510 | 34129 | C | C | not measured | Handling damage | Scrapped |
| 511 | 34130 | B | B | 5.64 | — | MOR |
| 512 | 34131 | C | C | 7.11 | — | Trial spin at Balco |
| 515 | 34134 | B | B | 6.78 | Broken exducer tip | Section |
| 516 | 34135 | B | B | 6.60 | — | MOR |
| 517 | 34136 | C | C | 5.11 | Exducer drop | Section |
| 519 | 34137 | B | B | 6.60 | Broken blade | Section |
| 527 | 34139 | C | C | 6.61 | — | Trial spin at Balco |
| 528 | 34140 | C | C | 7.49 | — | Shaft attach |
| 529 | 34141 | B | C | 7.42 | — | Spin |
| 530 | 34142 | C | C | 7.44 | — | Shaft attach |
| 531 | 34143 | C | C | 7.34 | — | MOR |
| 532 | 34144 | B | C | 7.54 | — | Section |
| 533 | 34145 | C | C | 7.77 | Large grain | Spin |
| 534 | 34146 | C | C | 7.62 | — | Shaft attach |
| 536 | 34147 | B | C | 7.65 | Large grain | Proof spin at Allison |
| 538 | 34149 | C | C | 7.65 | — | Reserve |
| 543 | 34150 | C | C | 7.65 | — | Machine |
| 545 | 34151 | C | C | 7.67 | — | Thermal shock |
| 549 | 34152 | B | C | 7.70 | — | Spin |
| 550 | 34153 | B | A | 7.95 | Large grain | Trial spin at Balco |
| 554 | 34154 | B | A | 7.77 | Large grain | Proof spin at Allison |
| 561 | 34155 | B | C | 7.87 | Large grain | MOR |
| 562 | 34156 | B | B | 7.96 | Large grain | Section |
| 563 | 34157 | B | A | 7.54 | — | Spin |
| 572 | 34158 | C | C | 7.67 | — | Thermal shock |
| 574 | 34159 | B | C | 7.75 | — | Spin |
| 581 | 34160 | B | C | 7.47 | — | MOR |

Note: 29 rotors received during reporting period

*Nominal throat dimension at exducer outer diameter = 8.33 mm (0.328 in.)

encountered with the slip cast scroll assembly have been alleviated through refinements in the starting powder, slurry composition, and mold design.

Twelve gasifier scroll bodies fabricated of sintered alpha SiC were recently cast, with a net yield of 10 components currently being processed through green machining. Thirteen sintered SiC connecting ducts were also slip cast with nine ducts judged to be of acceptable quality. In addition, two complete sintered SiC gasifier scroll assemblies are currently being finish-machined at an outside vendor, with the first scheduled for shipment the second week of July 1983 and the second in September 1983.

Developmental activities addressing the use of siliconized SiC for the scroll assembly to minimize warpage and dimensional deviations are proceeding on schedule, with five scroll bodies and six connecting ducts currently in green machining. The first siliconized scroll assembly is scheduled to be machined in October 1983.

## 9.3 SILICON NITRIDE COMPONENT DEVELOPMENT, CHARACTERIZATION, AND QUALIFICATION

The Sixth Semiannual Report (1 July 1982-31 December 1982) explained the development effort on injection-molded silicon nitride rotors at GTE Laboratories. The rotors are the prototype configuration, and a sample of nine was spin-test evaluated during the current reporting period. These nine represent the initial development effort. The spin-to-burst test results are summarized in Table XVII. The cracks on the backface, illustrated in Figures 51 and 52, are representative of the general nature of this sample of rotors. The burst tests were consistent with the observed structure of the rotors. Continued development of the process was active at GTE, addressing the goal of 30 structurally sound rotors. Delivery of the 30 rotors is anticipated during the next six months.

**Table XVII.**
**Spin-burst tests, silicon nitride rotors.**

| No. | GTE serial No. | Burst speed*—rpm | Comments |
|---|---|---|---|
| 1 | 263 (Ref Figure 51) | 63,300 | Airfoil release at 48,750 rpm; rebalance and core burst at 63,300 rpm; remnants revealed a very porous core region |
| 2 | 264 (Ref Figure 52) | 51,000 | Reached 62,500 rpm; failed on decel at 51,000 rpm concurrent with whip and rub on the whip pickup; remnants revealed a failure origin at a blade root (see Figures 53, 54, and 55) |
| 3 | 291 | 66,600 | Airfoil release at 38,500 rpm; rebalance and core burst at 66,600 rpm; failure origin not clear |
| 4 | 330 | | Erratic behavior on balance machine—rotor scrapped |
| 5 | 463 | | Erratic behavior on balance machine—rotor scrapped |
| 6 | 475 | 41,400 | Core region burst on first accel to speed—no prior blade release or rebalance required |
| 7 | 478 | 38,800 | Core region burst on first accel to speed—no prior blade release or rebalance required |
| 8 | 494 | 48,500 | Core region burst on first accel to speed—no prior blade release or rebalance required |
| 9 | 518 | 43,000 | Core region burst on first accel to speed—no prior blade release or rebalance required |

*100% speed = 86,240 rpm

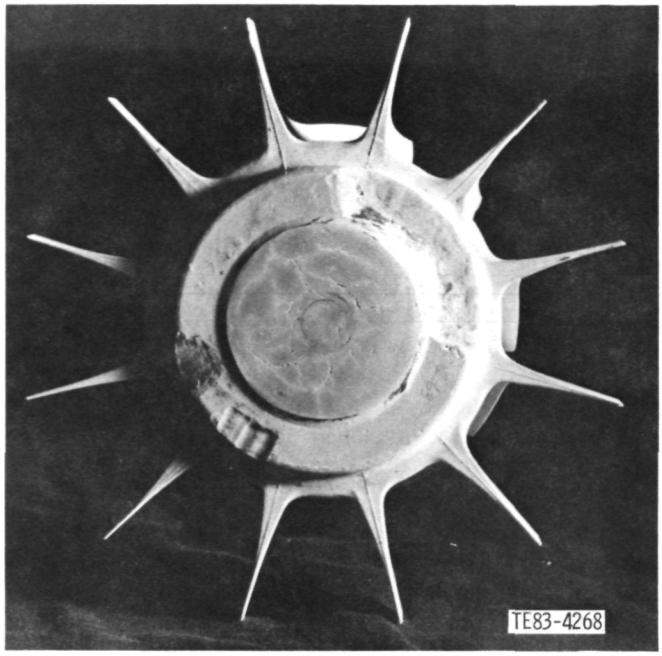


Figure 51. Silicon nitride rotor, S/N 263, surface cracks.

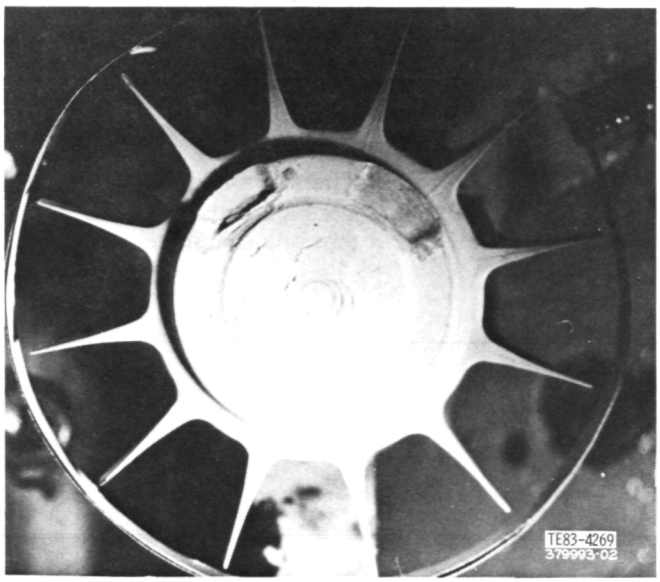


Figure 52. Silicon nitride rotor, S/N 264, surface cracks.

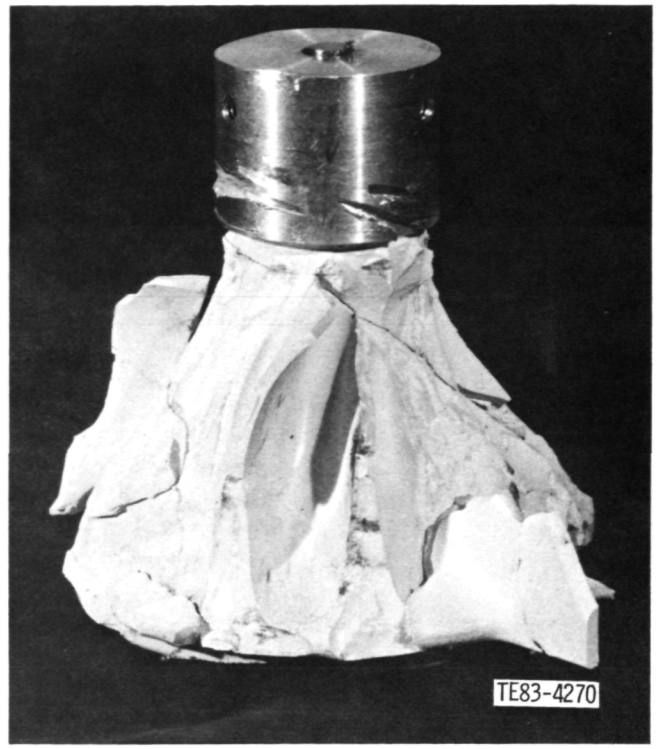


Figure 53. Postburst failure reconstruction, silicon nitride rotor, S/N 264.


**Figure 54. Burst failure remnants, silicon nitride rotor, S/N 264.**

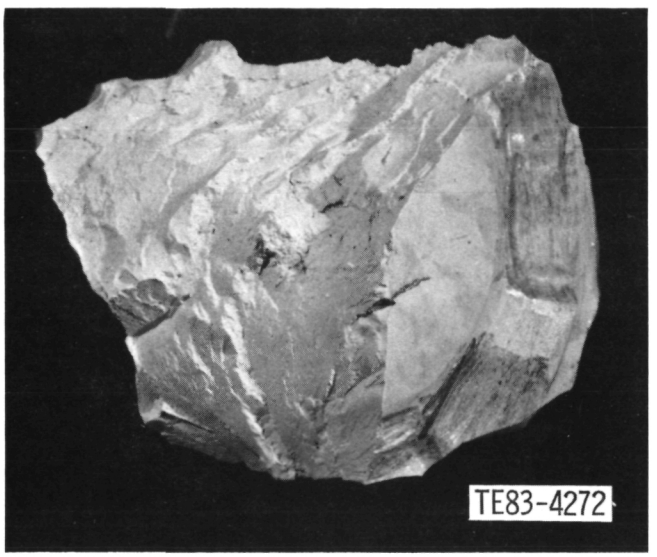


**Figure 55. Internal porosity, postfailure remnant, silicon nitride rotor, S/N 264.**

# X. CONTROLS DEVELOPMENT

The controls effort during this period has been concentrated in three areas: (1) to adapt the control logic based on engine performance and test conditions, as required, (2) to correct controls-related problems, and (3) to investigate new hardware for the fuel pump and metering valve.

## SUPPORT ENGINE TESTING

Software changes continued to be the major activity of control system support. The flexibility of the digital controller and the availability of an in-house software development system allowed software changes to be made with a minimal amount of down time. Many of the changes were made as a result of different engine configurations or test conditions. One example was the software change required to accommodate a hydraulic starter that replaced the original electric starter. Other modifications included turbine inlet temperature (TIT) control, burner variable geometry (BVG) position, transition time from the start fuel nozzle to the main fuel nozzle, and adjustments in the fuel flow scheduling during starts.

In an attempt to more accurately control TIT, one of the four thermocouple channels was dedicated to measuring TIT. The AGT 100 engine was designed to include a ceramic turbine capable of sustaining a TIT of 1288°C (2350°F). Because thermocouples cannot survive in this temperature range, TIT was not intended to be measured directly. Instead, turbine outlet temperature (TOT) will be used to control TIT. The engine testing during this period, however, used a metal turbine and a TIT of 1080°C (1976°F). This allowed TIT to be measured directly with thermocouples and helped define an accurate relationship between TIT and TOT for future control applications using TOT. A TIT limit schedule was then programmed into the logic, and provisions were made to manually adjust this schedule by means of a bias potentiometer located on the electronic control unit (ECU). Fuel flow is now capable of controlling to either a gasifier rotor speed or a TIT.

Closed-loop control of BVG position was implemented, replacing manual selection by the operator. The computer now calculates the desired BVG position as a function of fuel/air ratio and burner inlet temperature. This position is then compared with actual BVG position, sensed by a potentiometer, and actuator current is adjusted until the two agree.

The BVG position is now determined by the existing engine conditions, namely fuel/air ratio and burner inlet temperature. Using these two parameters, the required BVG position is calculated from a schedule that was programmed into the control logic. Having the ECU determine where BVG should be, rather than operator input, provides a more accurate control, especially during start-to-main nozzle transitions.

Start-to-main-fuel-nozzle transition occurs when a manual switch is selected and burner inlet temperature is greater than 482°C (900°F). Fuel does not instantaneously flow from the main nozzle because the manifold volume must first be filled. Previously, the ECU calculated this fill time based on a predetermined fuel flow at which the transition occurred. If a transition were attempted at a different fuel flow, the engine might experience significant fuel flow fluctuations during the transition. In an attempt to widen the fuel flow range at which a transition can occur, the main manifold volume was integrated in the software to determine the manifold fill time. With this new feature, successful transitions have consistently been made at numerous fuel flows.

During the engine testing, fuel flow schedules were adjusted to provide cooler starts and to avoid thermal shocks that could damage the ceramic combustor. With these new schedules, both cold and warm engines have demonstrated safe, successful starts.

These software changes have been made to the control logic as a result of the engine testing. As the engine undergoes further testing, modifications will be made accordingly.

## SUPPORT CONTROL SYSTEM

During the engine testing, two changes were made to correct controls-related problems. The first correction addressed the possibility of failure in a critical component in the ECU computer hardware, which would affect the engine performance. The critical component might be either the central processing unit or a memory device. To protect the engine, a hardware shut down logic circuit was built into the ECU. If a failure occurs, the ECU will be shut down and all outputs will be depowered. The second correction involved the two variable geometry actuators. During engine starts, the actuators were not

operating consistently. Therefore, pressure previously supplied by the engine is now provided by a separate hydraulic oil system, resulting in a sufficient and consistent pressure. A three-micron, absolute filter was also added to the actuator inlet to prevent contaminants from damaging the actuators.

## INVESTIGATE NEW HARDWARE

New developments in control system techniques have been limited. One of the areas under consideration, however, is the fuel pump and control valve assemblies. The new system will meter engine fuel flow directly rather than control the amount through a bypass throttling valve. The physical size of the pump will be substantially reduced as will be the software required to operate the fuel system. Parts for this new system have been ordered along with other control system components that are needed for a second AGT 100 engine. The new fuel system configuration will be subjected to bench tests starting in September 1983. If the system performs as expected, it will be incorporated into the fuel system for the second engine.

# XII. SUPPORTIVE MANUFACTURING, COST, AND MARKETABILITY

## 12.1 MANUFACTURING FEASIBILITY

The effort at Pontiac during this reporting period has primarily been focused on planning and implementing an experimental die development program for several major components of the engine. Objectives of the die development program are as follows:

- verify manufacturability of components incorporating design revisions that have been proposed to Allison for high-volume manufacture
- develop and verify new cost reduction proposals for incorporation in the RPD design
- gain experience with the draw and forming characteristics of SAE 4130 steel
- determine and/or confirm the downstream machining operations required based on the experience gained from the experimental die development program

The components selected for this program are the combustion case assembly housing and bulkhead and the regenerator housing assembly.

The combustion case assembly housing was selected to gain experience with the expansion-forming technique proposed for production. The housing redesign proposed for the RPD engine utilizes this process to roll the mounting flanges and also to form the combustor support area. The experimental die program will be used to determine the formability of these surfaces and any downstream machining operations required to qualify them for flatness.

The combustion case assembly bulkhead was selected to verify the formability of a proposed redesign. The initial design had several deep-drawn areas that were not acceptable for high-volume production, and the experimental die development program will verify manufacturability of the proposed redesign for incorporation in the RPD engine.

The regenerator housing assembly was selected to determine whether there is potential for cost reduction in the RPD engine. The current design utilizes three large stampings welded to the exterior of the main housing.

Significant savings due to elimination of extensive welding are possible by forming these pockets into the base housing.

The experimental die development program will encompass all three parts. However, initial effort has been directed towards the bulkhead and regenerator cover. The plaster draw die development models for both the bulkhead and regenerator cover have been completed, evaluated by Pontiac's Die Engineering Department, and are currently being revised to incorporate suggestions made to improve the drawability of the parts. Both models were ready for final approval at the end of this reporting period. The prototype tooling shop has been selected, and tooling will start as soon as the models have been approved. The SAE 4130 steel has been ordered and is scheduled to be received this week. The steel will undergo a series of laboratory tests on receipt to determine mechanical properties and suitability for draw.

# APPENDIX A. TERMS AND DEFINITIONS

| | |
|---|---|
| AGT | advanced gas turbine |
| AGT 100 | the AGT model being developed by Allison |
| AS | aluminum silicate |
| BU | buildup number |
| BVG | burner variable geometry |
| °C | degrees Celsius |
| CBO | Carborundum Company |
| CGW | Corning Glass Works |
| cm | centimeter |
| CTE | cyclic thermal evaluation |
| CTE | coefficient of thermal expansion |
| CY | calendar year |
| DOE | U.S. Department of Energy |
| DuPont Vespel SP 21, SP 22 | polyimide materials |
| E | Young's modulus |
| ECR | engine configuration rotor |
| ECU | electronic control unit |
| EDR | Engineering Development Report (of Allison) |
| EMI | electromagnetic inspection |
| EMTL | Energy Materials Testing Laboratory |
| °F | degrees Fahrenheit |
| ft | foot |
| G | shear mode |
| GLT | guide-load-torque |
| GM | General Motors Corporation |
| GTE | General Telephone and Electronics Corporation |
| green machining | machining a ceramic before it is fired |
| h or hr | hour |
| I/B | inboard |
| IGV | inlet guide vane |
| in. | inch |
| kg | kilogram |
| kPa | kilopascal |
| ksi | thousand pounds per square inch |
| L | liter |
| LAS | lithium aluminum silicate |
| lb | pound |
| lbm | pound mass |
| m | meter |
| mA | milliampere |
| MAS | magnesium-alumino-silicate |
| Mg | megagram |
| min | minutes |
| mm | millimeter |
| Mod I | the first design of AGT 100 using some ceramic hot section components |
| Mod II | the second AGT 100 design with ceramic hot section |
| MOR | modulus of rupture |
| MPa | megapascal |
| N | force (Newton) or speed of rotation (rpm) |
| $N_1$ | gasifier speed of rotation |
| $N_2$ | power turbine speed of rotation |
| NASA | National Aeronautics and Space Administration |
| NDE | nondestructive evaluation |
| NGK | manufacturing company in Japan |
| O/B | outboard |
| PMD | Pontiac Motor Division of General Motors |
| psig | pounds per square inch gage |
| RBSiC | reaction-bonded silicon carbide |
| Ref | reference |
| RPD | reference power-train design |
| RTV | room temperature vulcanizing |
| s or sec | second |
| SAE 4130 | moly steel containing 39% C and 51% Mg, along with P, S, Si, Cr, and Mo |
| S/N | serial number |
| S/N-1 | the first experimental AGT 100 engine |
| S/N-2 | the second experimental AGT 100 engine |
| TD | teardown |
| TIT | turbine inlet temperature |
| TOT | turbine outlet temperature |
| XRD | x-ray diffraction analysis |
| YSZ | yttria stabilized zirconia |
| $\overline{\alpha}$ | Average coefficient of thermal expansion |
| $\Delta$ | difference between two measurements, e.g., $\Delta T$ |
| $\eta$ | efficiency |
| $\nu$ | Poisson's ratio, E/2G-1 |

| 1. Report No. | 2. Government Accession No. | 3. Recipient's Catalog No. |
|---|---|---|
| NASA CR-174629 | | |

| 4. Title and Subtitle | 5. Report Date |
|---|---|
| ADVANCED GAS TURBINE (AGT) TECHNOLOGY PROJECT | November 1983 |
| | 6. Performing Organization Code |
| 7. Author(s) | 8. Performing Organization Report No. |
| Engineering Department, Allison Gas Turbine Operations | EDR 11577 |
| | 10. Work Unit No. |
| 9. Performing Organization Name and Address<br>Allison Gas Turbine Operations, Division of General Motors Corp<br>P.O. Box 420<br>Indianapolis, IN 46206-0420 | 11. Contract or Grant No.<br>DEN 3-168 |
| | 13. Type of Report and Period Covered<br>Contractor Report |
| 12. Sponsoring Agency Name and Address<br>U.S. Department of Energy<br>Office of Vehicle and Engine Research Development<br>Washington, D.C. 20545 | 14. Sponsoring Agency Code<br>DOE/NASA |

15. Supplementary Notes

Semiannual report, prepared under Interagency Agreement DE-AI01-77CS51040.
Project Manager P. T. Kerwin, Transportation Propulsion Division,
NASA Lewis Research Center, Cleveland, OH 44135

16. Abstract

Technical work on the design and effort leading to the testing of a 74.5 kW (100 hp) automotive gas turbine is described for the period January through June 1983. This is the seventh semiannual report. The goal of the first year of engine testing is to accomplish engine familiarization, shakedown of mechanical systems, and reach design speed (100%, 86,000 rpm). This period completes the first year of engine testing. During the previous period five engine buildups were evaluated and 2 hr 45 min of engine testing were completed. During the current period, three engine buildups (6, 7, and 8) were evaluated and 6 hr 13 min of engine testing were accomplished. Total test time on the engine stands at 8 hr 58 min. Testing of BU8 included successful operation at 100% gasifier rotor speed. Engine testing was accomplished with realistic heat-up rates, and with a 1080°C (1976°F) steady-state limit on turbine inlet temperature. Ceramic components included the combustor (SiC), regenerator disk (AS) and bulkhead (LAS), and zirconia insulators and spacers. An improved method of retaining the turbine scroll assemblies was successfully tested. The control system was modified, and successfully tested, to add automatic limiting of measured turbine inlet temperature and automatic shceduling of combustor variable geometry (BVG). Analysis indicated that gasifier turbine efficiency could be improved with a new vane design that incorporates thinned trailing edge, cambered airfoil with reduced downstream turning, and increased vane width. Analysis also indicated that the power turbine, although meeting the FPD efficiency goal, is not optimally matched to the 1080°C (1976°F) experimental engine. Reducing its flow capacity and operating rpm provides significant efficiency at the engine operating point. Combustor development addressed the isopressed SiC dome, which had previously cracked during hot proof-tests conducted on the combustor rig. A design modification was translated into parts which completed rig proof-tests and engine testing. Regenerator development was active in several areas. Highlights of rig testing included evaluation of ceramic disks with low through-wall leakage, implementation of seal improvements, and initial testing of a silicone outboard seal. Rotor attachment/thermal barrier development continued at Carborundum (CBO) with mullite and and Allison with zircon. Rotor development was conducted at CBO (SiC) and GTE ($Si_3N_4$). The CBO effort concentrated on developing the injection molding process and parameters. Allison spin-tested 8 SiC rotors. GTE continued molding experiments and Allison spin-tested 9 $Si_3N_4$ rotors. CBO produced and delivered 4 SiC combustors.

| 17. Key Words (Suggested by Author(s)) | 18. Distribution Statement |
|---|---|
| Automotive gas turbine<br>Ceramic components<br>Engine configuration rotors<br>Alternate propulsion systems<br>Improved fuel economy | Unclassified--unlimited |

| 19. Security Classif. (of this report) | 20. Security Classif. (of this page) | 21. No. of Pages | 22. Price* |
|---|---|---|---|
| Unclassified | Unclassified | | |

* For sale by the National Technical Information Service, Springfield, Virginia 22151